The relationship between primate distal fibula trabecular architecture and arboreality, phylogeny and size

Alfieri F.[1,2,3,4], Veneziano A.[5], Panetta D.[6], Salvadori P.A.[6], Amson E.[7], Marchi D.[8,9]

1. Institute of Ecology and Evolution, Universität Bern, Bern, Switzerland
2. Department of Earth Sciences, University of Cambridge, Cambridge, UK
3. Institut für Biologie, Humboldt Universität zu Berlin, Berlin, Germany
4. Museum Für Naturkunde, Leibniz-Institut Für Evolutions- Und Biodiversitätsforschung, Berlin, Germany
5. Departament d'Enginyeria Mecànica, Universitat Rovira i Virgili, Tarragona, Spain.
6. Institute of Clinical Physiology, IFC-CNR, Pisa, Italy,
7. Staatliches Museum für Naturkunde, Stuttgart, Germany.
8. Department of Biology, Università di Pisa, Pisa, Italy.
9. Centre for the Exploration of the Deep Human Journey, University of the Witwatersrand, Johannesburg, South Africa.

Corresponding author: Fabio Alfieri, email: fabio.alfieri@unibe.ch and fabio_alfieri@yahoo.it

ORCID:

Fabio Alfieri: 0000-0001-8241-7309

Alessio Veneziano: 0000-0002-2543-5188

Daniele Panetta: 0000-0002-4184-0175

Piero A. Salvadori: 0000-0001-6114-1059

Eli Amson: 0000-0003-1474-9613

Damiano Marchi: 0000-0002-6331-8783

Abstract

The fibula, despite being traditionally overlooked compared to the femur and the tibia, has recently received attention in primate functional morphology due to its correlation with the degree of arboreality. Highlighting further fibular features that are associated with arboreal habits would be key to improving palaeobiological inferences in fossil specimens. Here we present the first investigation on the trabecular bone structure of the primate fibula, focusing on the distal epiphysis, across a vast array of species. We collected µCT data on the distal fibula for 21 species of primates, with representatives from most of the order, and we employed a recently developed approach implemented in the R package 'indianaBones' to isolate the entire trabecular bone underlying an epiphysis or articular facet. After extracting both traditional trabecular parameters and novel topological indices, we tested for the posited relationship between trabecular bone and degree of arboreality. To disentangle this effect from others related to body size and phylogenetic relationship, we included a body mass proxy as covariate and employed phylogenetic comparative methods. We ran univariate/multivariate and exploratory/inferential statistical analyses. The trabecular structure of the fibular distal epiphysis in primates does not appear to be associated with the degree of arboreality. Instead, it is strongly affected by body mass and phylogenetic relationships. Although we identified some minor trends related to human bipedalism, our findings overall discourage, at this stage, the study of distal fibula trabecular bone to infer arboreal behaviors in extinct primates. We further found that body size distribution is strongly related to phylogeny, an issue preventing us from unravelling the influence of the two factors and that we believe can potentially affect future comparative analyses of primates. Overall, our results add to previous evidence of how trabecular traits show variable correlation with locomotor aspects, size and phylogenetic history across the primate skeleton, thus outlining a complex scenario in which a network of interconnected factors affects the morphological evolution of primates. This work may represent a starting point for future studies, e.g. focusing on the effect of human bipedalism on distal fibula trabecular bone, or aiming to better understand the effects of body size and phylogenetic history on primate morphological evolution.

Keywords: cancellous bone; ankle joint; substrate preference; body size; phylogenetic signal

1. Introduction

The study of mammal limb long bones offers compelling evidence of the disparate factors related to anatomical diversity, such as ecology, body size and/or shared phylogenetic history (e.g. Alfieri et al., 2021, 2022, 2023; Cooper, 2019; Kilbourne and Hutchinson, 2019; Polly, 2007; Tarquini, 2021). Among mammalian clades, primate long bone functional morphology has been widely investigated (e.g. Chiu and Hamrick, 2002; Gebo, 1989, 2014; Ruff, 2003; Swartz, 1989) with special focus on adaptations to biomechanical loadings deriving from different locomotor specializations (e.g. Burr et al., 1981; Demes and Jungers, 1993; Kimura, 1995, 2003; Marchi et al., 2016; Ruff, 2002; Ruff et al., 2019; Ruff and Runestad, 1992; Runestad, 1997; Schaffler et al., 1985; Schaffler and Burr, 1984). In primates, hindlimb morphology is key to some of the most distinctive primate locomotor adaptations, such as vertical clinging and leaping in strepsirrhines (Gebo, 2011; Napier and Walker, 1967a) or bipedalism in hominins (O'Neill et al., 2015; Tardieu, 2010). Hence, the long bones of the primate hindlimbs represent an optimal context in which understand if anatomical traits are more related to the locomotor environment (Berles et al., 2024; Georgiou et al., 2018; Harmon, 2007; Marchi, 2007; Marchi et al., 2022; Ruff, 2002; Ryan and Ketcham, 2002a; Sylvester, 2013) or to other factors (e.g. allometric relationships, Ruff, 1987; Ryan and Shaw, 2013, or phylogenetic signal, O'Neill and Dobson, 2008; Ryan and Shaw, 2013). In primates, the femur and tibia have been by far the most studied hindlimb long bones, with the aim of identifying locomotor correlates through analyses involving different approaches and anatomical levels, as external joint proportions/shape (e.g. Godfrey, 1988; Harmon, 2007; Jungers et al., 2002; Marchi et al., 2016; Sylvester, 2013), diaphyseal cross-sectional geometry, (CSG; e.g. Carlson, 2005; Demes and Jungers, 1993; Kimura, 2002; Marchi et al., 2016; Polk et al., 2000; Ruff, 2002) and epiphyseal trabecular architecture (e.g. Barak et al., 2013a; Fajardo and Müller, 2001; Georgiou et al., 2019, 2018; MacLatchy and Müller, 2002; Scherf, 2008). This trend is possibly explained by the fact that the femur and tibia are the two main elements of the hindlimb and, thus, are expected to have a prominent role in sustaining the hindlimb mechanical loads. Moreover,

compared to other skeletal elements, the two bones are relatively abundant in the fossil record (e.g. Anemone and Covert, 2000; DeSilva et al., 2010; Ford and Morgan, 1986; MacLatchy and Bossert, 1996; Rafferty et al., 1995; Ryan and Ketcham, 2002b). These aspects are not independent, since the identification of anatomical features associated with specific locomotor behaviors in extant taxa can be leveraged, in turn, to infer locomotor habits in extinct primates for which fossil specimens are available.

1. 1. Primate fibula functional morphology

For the fibula, the other hindlimb long bone, a close relationship between fibular anatomy and the prehensile power of the foot has long been hypothesized (Owen, 1866), and some early analyses addressed the functional morphology of the fibula in mammals (Barnett and Napier, 1953; Carleton, 1941; Walmsley, 1918). Importantly, although these works have highlighted several fibular traits possibly related to locomotor behaviors, many of those features (e.g. degree of distal tibia-fibula fusion, fibular robusticity relative to the tibia) can be assessed only in association with the tibia (Barnett and Napier, 1953). This may explain why the fibula has long been overlooked in primate comparative anatomical studies (and even defined as 'the forgotten bone', Rittweger et al., 2018), being considered only the lateral strut of the ankle with almost no role in load bearing (White et al., 2011) or even vestigial (Moore and Dalley, 2006). Moreover, it explains why a renewed attention to the fibular functional morphology initially led to the study of this bone only in association with the tibia. Indeed, it has been highlighted that the relative (to the tibia) fibular diaphyseal robusticity ('relative robusticity' hereafter) relates to a specific aspect of locomotor behavior: substrate preference. Specifically, fibular relative robusticity is higher in primates with higher degree of arboreality (DOA) (Marchi, 2015a, 2007; Marchi and Borgognini-Tarli, 2004). As further detailed below, DOA is here and hereafter meant as a discrete grouping, e.g. splitting 'arboreal', 'semi-arboreal' and 'terrestrial' primates, defined according to the relative amount of time spent in trees (Table 1). Importantly, it should be kept in mind that all non-human primates, however, show a minimum exploitation of arboreal substrates/superstrates. Hence, the effects of arboreality on fibular morphology have been assumed to be caused by frequent and repeated arboreal locomotion, not by the simple capability of performing arboreal

behaviors. The relationship between fibular relative robusticity and DOA is possibly explained by the fact that the distal portion of the hindlimb of arboreal species is subject to relatively more frequent laterally oriented loadings, compared to terrestrial ones (Carlson et al. 2005, see also below) and considering that the fibula is laterally located at this anatomical level. Moreover, a higher relative fibular diaphyseal robusticity has been found in humans performing activities involving frequent laterally oriented loadings in the distal segment of the hindlimb (Auerbach et al., 2017; Carlson and Marchi, 2014; Hagihara and Nara, 2016; Marchi et al., 2011; Marchi and Shaw, 2011; Sparacello et al., 2014). These results suggest that the fibula may not cover a negligible role in transmitting hindlimb loadings in primates, corroborating previous observations (e.g. Funk et al., 2004; Goh et al., 1992; Lambert, 1971; Takebe et al., 1984). However, the need to study the tibia-fibula system limits the design of comparative analyses (e.g. more demanding data collection) and the quantification of correlates for DOA on primate fossil specimens, due to the extreme rarity of complete associated tibiae and fibulae (Marchi et al., 2019). Thus, it appears advantageous to identify functional traits quantifiable on the primate fibula alone. In this regard, human individuals subject to frequent laterally oriented loadings in the distal portion of the hindlimb have been shown to exhibit a higher fibular diaphyseal absolute (i.e., regardless of tibial measures) robusticity (Marchi and Shaw, 2011), suggesting that a similar pattern may be present in arboreal primates. Moreover, the external morphology of the primate fibula has been recently linked to DOA through traditional morphometrics (Marchi, 2015b) and 3D geometric morphometrics (3D GM; Marchi et al., 2022). As of today, no interspecific comparisons across primate fibulae have been performed based on epiphyseal internal bone structure, i.e. trabecular architecture. This gap in the literature is surprising if we consider the potential of the trabecular architecture of the hindlimb long bones to exhibit functional signals (e.g. Barak et al., 2013a; Fajardo and Müller, 2001; Georgiou et al., 2018; MacLatchy and Müller, 2002 and see below).

1. 2. Trabecular bone architecture

It has been suggested that internal bone, both cortical and trabecular, may record bone usage and behaviors performed during an individual's life and that it may respond to the functional constraints set by

a species' ecology and environment more directly than external morphology (Kivell, 2016). Indeed, internal bone, despite its largely genetically determined morphology at birth, is responsive to mechanical loadings (Carter and Beaupré, 2007; Currey, 2002) acting through differential strains that in turn depend on bone actual usage (Ruff et al., 2006). Trabecular bone, being more porous and typically remodeling more frequently than cortical bone (Eriksen, 1986, 2010), likely involves a larger amount of functionally responsive cells (also due to greater surface area) (Currey, 2002; Huiskes et al., 2000). Ultimately, trabecular bone is expected to be even more plastic than cortical bone in responding to differential loadings that reflect distinct locomotor habits (Currey, 2002; Jacobs, 2000; Kivell, 2016).

Several experimental works performed *in vivo*, e.g. applying controlled strains and measuring the trabecular bone response, highlighted that specific trabecular properties result from certain mechanical loads. For instance, the trabecular alignment tends to follow strain orientations, i.e. trabecular struts orient along the main loading vectors (e.g. Biewener et al., 1996; Pontzer et al., 2006). Although not yielding the specific direction (e.g. in degrees of arc) along which trabeculae orient, a commonly used parameter in this regard is the degree of anisotropy (DA). This parameter informs on a more general but more straightforwardly interpreted property, i.e. the extent to which the trabeculae tend to align toward a uniform direction. Indeed, the more homogeneous the orientation is in the studied region, the more the latter is anisotropic, the higher DA (as defined here) will be (Harrigan and Mann, 1984). DA is one of the most structurally informative trabecular properties, measuring the fabric orientation, which is in turn closely associated with the mechanical main direction (Odgaard, 1997) (i.e. the direction, if any, along which biomechanical loadings are mainly applied), and explains 10% of trabecular stiffness (Maquer et al., 2015). Accordingly, DA proved an informative parameter in primate interspecific analyses related to behavior, in that species with locomotor habits involving more directionally stereotyped loadings yielded more anisotropic trabecular structure, i.e. higher DA (e.g. leaping taxa discriminated from non-leaping ones in strepsirrhines, Ryan and Ketcham, 2002a).

Properties directly related to bone density are other suitable predictors of bone strength: i.e. regions characterized by increased strength show increased density and, hence, larger values for these traits. Although increased strength in a given anatomical region is often considered the direct consequence of increased magnitude of the load, this specific aspect of loading patterns (e.g. measured in terms of strain magnitude, in mm/mm) is only one of the factors contributing to trabecular remodeling. Indeed, besides load magnitudes, one should also consider how trabecular remodeling is affected by the duration (e.g. Barak et al. 2011; Lambers et al. 2013; Skerry and Lanyon, 1995) and frequency (e.g. Barak et al. 2011; Bassey and Ramsdale, 1994; Pontzer et al. 2006; Simkin et al. 1989) of loadings (Kivell, 2016). Importantly, concerning load frequency, Rubin et al. (2001; 2002) showed that even extremely low loadings when exerted with high frequency may cause a substantial (34.2%) increase in trabecular bone density (Rubin et al. 2001; 2002). This outcome suggests that, besides or even instead of the magnitude, other characteristics of the loading pattern acting on a specific joint, as the frequency, may be crucial in determining density related trabecular parameters. For this reason, here and throughout (see below and Table 2), we will refer to 'increased loadings' (keeping in mind that they may derive from increased loading magnitude and/or frequency and/or duration) as the factor to which some trabecular parameters may respond. Instances of density-related traits are bone volume fraction (BV/TV) (Barak et al., 2011; Chang et al., 2008; Mittra et al., 2005) and trabecular thickness (Tb.Th) (Barak et al., 2011; Mittra et al., 2005), with the former being particularly informative from a biomechanical point of view (besides DA, see above), accounting for the 88% of trabecular stiffness (Stauber et al., 2006). Both BV/TV. and Tb.Th, similarly to DA, proved suitable to discriminate locomotor categories in human and non-human primate samples (e.g. Ryan and Shaw, 2015; Sukhdeo et al., 2020).

The computation of parameters related to density (e.g. BV/TV and Tb.Th) and orientation (e.g. DA) is often combined with the characterization of additional features of the trabecular network, as the overall shape. A way to quantify the latter is through measures of trabecular bone surface, as the bone surface to total volume fraction (BS/TV, also termed 'bone surface density', Scherf et al., 2013). This parameter informs on the shape complexity of the intertrabecular spaces (in life filled with marrow that, in turn, directly

contacts the inner epiphysis bony parts through the surface of the trabeculae). Hence, a larger BS/TV corresponds to larger trabecular surface exposed to marrow in life and to more complex trabecular shape (Scherf et al., 2013). BS/TV has been proposed as correlated to ecological factors including locomotor adaptations, in recent interspecific evolutionary analyses of mammals. Specifically, low BS/TV is associated with low and/or infrequent loadings deriving from slow cautious arboreal lifestyle (Alfieri 2022) and hence we can assume that increased loadings would be associated with higher BS/TV.

The aforementioned properties and the related parameters were abundantly employed in the last decades, often computed on subsamples of trabecular bone virtually extracted from epiphyses of skeletal elements represented by μCT scans (e.g. Barak et al., 2013a; DeSilva and Devlin, 2012; Fajardo and Müller, 2001; Hébert et al., 2012; MacLatchy and Müller, 2002; Maga et al., 2006; Ryan and Ketcham, 2002a; Ryan and Shaw, 2015, 2012; Scherf, 2008; Scherf et al., 2013). Due to their well-established use, we can now consider this to be the traditional approach to trabecular structure quantification and we can refer to these traits as 'traditional parameters.' However, alternative approaches have been developed, as the one proposed by Veneziano et al. (2021), based on the study of trabecular bone from entire epiphyses/articulations, instead of subsamples, and, importantly, representing the studied trabecular regions as morphological skeletons. In other words, through a skeletonization procedure, the anatomical information is reduced to only nodes (deriving from the trabeculae connection regions) linked by branches (deriving from the trabeculae themselves). This minimized information provides researchers the advantage to focus only on topological properties of the studied inner epiphysis, i.e. only the spatial arrangement of trabecular struts (through the computation of 'topological indices', detailed below) (Veneziano et al. 2021), hence the skeletonized region is termed 'topological skeleton' hereafter.

Despite the recent work of Veneziano et al. (2021), the trabecular generalisation by means of a topological skeleton is not new and has been previously adopted, for example for the computation of trabecular thickness (Garrahan et al., 1987), and for some of the traditional parameters computed with the BoneJ plugin (Doube et al., 2010) of the FIJI software package (Schneider et al., 2012, see also below).

Wang et al. (2013) compared skeletonized and voxel-based finite element models and found that the former accurately preserves Young's modulus and yield strength of the latter (Wang et al. 2013). Furthermore, skeletonization-derived indices could provide additional information about material properties, besides those already available through bone volume fraction. For instance, Pothuaud et al. (2002) showed that combining topological indices with bone volume fraction leads to better predictions of trabecular material properties than using bone volume fraction alone (Pothuaud et al. 2002). This result suggests that skeletonization-derived indices could contribute to explain part of the material properties' variance not addressed by bone volume fraction. This idea is supported by Liu et al. (2006), who found that the trabecular network topology affects the cancellous mechanical properties regardless of bone volume fraction (Liu et al. 2006). These studies suggest that, because of their topological nature, skeletonization-derived indices could extend the mechanical significance of indices standardly adopted in the study of cancellous architecture.

The topological skeleton of the trabecular lattice allows the computation of either geometric traits on single trabecular elements or indices devoid of geometric features other than the topology itself. Both these aspects are involved in the computation of the trabecular density, here intended as the number of trabecular elements per unit volume. Trabecular density can be interpreted as a generalisation of BV/TV, and this relationship is exemplified by a recent study: Tsegai et al., (2018) did not directly measure trabecular density but computed BV/TV over a grid enclosing the bone, and used an interpolation to obtain a virtually continuous map of BV/TV. When TV is expressed as a unit of volume (grid size) rather than the full volume, then BV/TV becomes a density. Skeletonization allows to extend this generalisation further to include only topological information in the computation of trabecular density via the computation of "node density" (NodDen hereafter), or the number of nodes of the topological skeleton per unit volume. Veneziano et al. (2021) have computed this density using a kernel-density estimation over a 3D grid: here, the grid size constitutes the volume over which the trabecular bone is counted (i.e., TV). In other words, it extends the computation of BV/TV over a virtually continuous resolution (dependent on the grid size). Considering that NodDen can be thought of as a generalisation of BV/TV, its mechanical significance could be equivalent:

i.e. increased loadings, as those deriving from specific bone uses, joint positions and loads borne during gait and stance, are expected to cause higher NodDen. NodDen results from the preliminary analysis of Veneziano et al. (2021) go in this direction, i.e. the femoral heads of *Gorilla*, *Pan* and *Homo* show higher NodDen compared to quadrupeds and brachiators, compatibly with a prevalent load-bearing use of the hip (Veneziano et al. 2021). Supporting this perspective, Cendre et al. (1999) used a similar index (i.e. node density over total volume) and found it to correlate positively with maximum compressive strength.

Another property whose calculation is simplified by skeletonization is the trabecular length (TrabLen hereafter), measured at each individual branch of the topological skeleton as the geodesic (or arc) length of the branch between the nodes it contacts. Longer trabecular elements are expected within poorly dense structures and – apart from allometric patterns highlighted in mammals (Swartz, 1989) – the length *per se* is suggested to bear a relevance in terms of bone strength (Parkinson et al., 2012). Hence, we can expect TrabLen to decrease with increased loadings, i.e. the latter cause shorter trabeculae, in association with a denser skeleton (i.e. higher NodDen). The role of TrabLen in the stiffness-elasticity spectrum is better quantified by trabecular tortuosity (TrabTort hereafter). This property is computed dividing the TrabLen (measured as arc length) by the euclidean end-to-end length of each trabecular element, i.e. here being the linear distance between two nodes delimiting one branch. TrabTort provides an intuitive way to describe variations from straight (low tortuosity) to curved/sinuous (high tortuosity) trabeculae. Measures of tortuosity were found to recapitulate bone mechanical properties (Fyhrie and Zauel, 2015), since tortuosity measures the trabecular flexibility under biomechanical load. Specifically, studying the mechanical competence of trabecular architecture, higher tortuosity was found in association with lower stiffness – i.e. higher elasticity (Roque et al., 2012; Roque and Alberich-Bayarri, 2015). Decreased stiffness in a more tortuous and flexible trabecular structure suggests an adaptation to increased loads. Indeed, for a given stress exerted within a joint, a less stiff material is able to sustain higher strains derived from increased loadings.

Another index that can be computed from the topological skeleton is Fractal Dimension (FD hereafter), a measure of structural complexity based on the concept of statistical self-similarity, i.e. an ideal fractal

structure is similar to itself at any degree of magnification (Feder, 1988; Pornprasertsuk et al., 2001). FD measures change in detail across changing scales (Falconer, 2004). The application of FD to trabecular bone has been common, e.g. in studies of fracture risk level and human bone pathology (Feltrin et al., 2004; Messent et al., 2005a, 2005b) thus suggesting a mechanical relevance. Specifically, evidence of the mechanical significance of FD may come from studies highlighting its correlation with bone mineral density, a proxy for bone strength (Ammann and Rizzoli, 2003), or density-related traits in general (in turn related to biomechanical strains, see above). While the correlation between density-related variables and FD seems well supported, it is not easy to establish if it is generally positive or negative, since both the former (Cichański et al., 2010; Feltrin et al., 2001; Uchiyama et al., 1999) and the latter (García-Vilana et al., 2023, Pornprasertsuk et al., 2001) arose. A positive relationship between density-related traits and FD would be theoretically supported by the fact that FD has been shown to be inversely related to Young's Modulus, that in turn positively co-varies with stiffness (Sanchez-Molina et al. 2013). Accordingly, FD would be expected to be inversely related to stiffness and, following what we suggested above for TrabTort, one should expect a direct relationship between FD and bone strength (i.e. the higher the FD, the lower the stiffness, the more the trabeculae can withstand the loadings). However, this framework seems overly simplistic if one considers the many indirect and complex relationships among different variables, and, also, that the potential relationship between FD and Young's Modulus has been highlighted studying the cortical bone (Sanchez-Molina et al. 2013). In this work, we instead preferred to focus on direct evidence showing that bones experimentally subject to inactivity yield high FD combined with low density (Pornprasertsuk et al., 2001). Indeed, FD also proved useful in studies focusing on mammals to predict mechanically relevant properties or trabecular bone loss (e.g. Chappard et al., 2001). Following this interpretation, we expected higher FD in regions subject to decreased biomechanical loadings. For both the traditional trabecular parameters and the topological indices, the traits that we treated (above) and computed (in this work) (summarized in Table 2) are only some of the available ones. For additional traits, see Kivell (2016), Veneziano et al. (2021) and references therein.

The potential relationships between the trabecular properties mentioned above and locomotor habits have long been considered as adaptations occurring only during lifetime due to the high ontogenetic plasticity of bone internal structure, i.e. a relationship traditionally known as 'Wolff's Law' or, more recently, 'bone functional adaptation' (Kivell, 2016; Ruff et al., 2006 and references). While this paradigm remains a key tenet in functional morphology, it is also noticeable that recent works studying ecologically-related trabecular bone diversity in wide phylogenetic contexts highlighted that disentangling ontogenetic adaptations from evolutionary acquisitions is challenging, e.g. the studies of Alfieri et al. (2023) and Amson and Bibi (2021), with the former addressing how much internal structure tends to vary following ecological adaptations across generations and through evolutionary processes, a property termed evolvability, instead of adaptations occurring during ontogeny. In other words, if distantly related taxa with similar locomotor ecology show the same trabecular properties, it is challenging to discriminate ontogenetic bone functional adaptation from repeated evolutionary acquisition of the same phenotype (i.e. convergent evolution), also considering that developmental patterns are subject to both evolutionary and environmental pressures (Wund, 2012). Trabecular analyses studying specimens at different ontogenetic stages from diverse taxonomic samples may contribute to clarify the extent to which some similarities are phylogenetically fixed. Thus far, trabecular studies with an ontogenetic dimension have only focused on few isolated taxa (e.g. Saers, 2023; Saers et al., 2022; Tsegai et al., 2018). This issue is strictly related to the phylogenetic signal, potentially involved in determining trabecular bone across primates and that, when studied, has yielded contrasting results, e.g. minor phylogenetic effects (Doube et al., 2011; Ryan and Shaw, 2012a), or complex anatomically and taxonomically variable phylogenetic influence (Ryan and Shaw, 2013). Thus, despite the potential of studying trabecular bone to highlight locomotion-related features (see above), one should also consider other influencing aspects, such as phylogeny. It indicates that, overall, the locomotion of different species cannot be expected as the only factor affecting trabecular bone (as also suggested by experimental studies not yielding the expected trabecular response, e.g. Carlson et al., 2008).

Another major non-locomotor effect potentially at the base of trabecular bone diversity is size, with different allometric patterns found for different parameters (e.g. Barak et al., 2013b; Doube et al., 2011;

Ryan and Shaw, 2013; Swartz et al., 1998). Further elements of complexity should be accounted for when interspecific trabecular bone analyses are undertaken (additional details in Kivell, 2016 and references), e.g. uncertainty on the prevalent types of loadings affecting trabecular bone (contractile forces from muscles *vs.* gravitational loads from substrate reaction forces, Judex and Carlson, 2009; Robling, 2009), presence of a loading threshold to trigger trabecular remodelling (Frost, 1987), influence on the trabecular response of genetic (Cunningham and Black, 2009a,b), hormonal (Karlsson et al., 2001; Yeni et al., 2011) and vascular factors (Cunningham and Black, 2010).

1. 3. Distal fibula trabecular bone, DOA and functional hypotheses

As detailed above, some studies on primate fibular external morphology yielded a relationship with the DOA (Marchi, 2015b; Marchi et al., 2022). These works focused on the distal epiphysis. This region conceivably bears a functional signal because it articulates with the foot, which is one of the most informative skeletal regions in primates concerning locomotor adaptations (Su and Zeininger, 2022 and references therein), as substrate preference. The distal fibula, together with the distal tibia and the talus, makes up the ankle joint complex (Ding and Song, 2002; Libotte et al., 1982; Seiler, 1986). While for the tibia and talus interspecific trabecular analyses of primates were performed (for the talus, e.g. DeSilva and Devlin, 2012; Hébert et al., 2012; Su et al., 2013; Su and Carlson, 2017; for the distal tibia, e.g. Barak et al., 2013a; Saers et al., 2016; Tsegai et al., 2018) no such studies addressed the fibula. This scenario, together with evidence of a relationship between fibular morphology and locomotor activities, specifically DOA when dealing with non-human primates (e.g. Marchi, 2007; Marchi and Borgognini-Tarli, 2004; Marchi and Shaw, 2011), encouraged us to investigate the primate distal fibular trabecular architecture. Besides these aspects, further investigations of the distal fibula aiming to detect features related to substrate preference, are particularly important because fossil preservation issues concern not only the associated tibiae and fibulae, as mentioned above, but also complete fibulae alone. Indeed, probably due to their extremely slender proportions, fibulae are often found as fragmentary specimens in fossil contexts (even compared to other elongate bones such as the femur and the tibia, the fibula evidently stands out in being

particularly thin in primates, a condition that reasonably makes it more fragile and less able to be preserved without being broken along the diaphysis). Accordingly, distal fibular segments are present in the fossil record (e.g. Anemone and Covert, 2000; Gebo et al., 2015; Heaton et al., 2019; Marchi et al., 2017, 2022 and references therein, Ni et al., 2013; Rodríguez et al., 2018). Hence, we considered the distal epiphysis as the most suitable region to conduct this study, based on its expected functional role and presence in the fossil record. Identifying novel primate fibular traits diagnostic of specific locomotor habits and quantifiable on isolated distal epiphyses, can contribute crucially to palaeobiological inference. More specifically, identifying fibular features related to DOA may contribute to long-standing debates in palaeoanthropology, e.g. the extent to which *Australopithecus afarensis* was an arboreal species (Marchi et al. 2022 and references therein).

This being the first analysis of the internal structure of the distal fibula, we based our experimental hypotheses on previous results from functional morphological analyses of this bone, i.e. we tested DOA as the main locomotor factor influencing fibular anatomy (see above). Thus, we studied a set of primate species split in three discrete categories outlining a cline from arboreal to terrestrial taxa, with semi-arboreal ones in between (Table 1, Fig. 1). Apart from the aforementioned previous works on fibular functional morphology in primates, the approach of categorizing primates according to their DOA in these same three discrete categories has been used by Henderson et al. (2017). Moreover, DOA meant as the relative amount of time spent on trees (although not formalized in discrete categories) arose as a major factor able to explain morphological variation in the primate bone postcranial features studied in Carlson (2005).

Arboreal species are generally characterized by abducted and flexed limbs during quadrupedal locomotion, allowing them to control the center of gravity and to grasp supports of small diameters. The presence of small diameter supports also involves the need for supinated (i.e. inverted, adducted and plantarflexed) foot postures. Moreover, the irregular, highly variable and discontinuous substrates represented by the arboreal environment cause a pronounced joint mobility and range of motion in arboreal species (Carlson, 2005). The arboreal configuration neatly contrasts with the adducted and extended limbs

with a more everted foot posture of terrestrial taxa (Meldrum, 1991 and references therein). From these broad differences between arboreal and terrestrial primates, it can be inferred that the ankle joint of an arboreal primate is likely extremely mobile, especially in mediolateral (ML) direction, with associated higher mobility of the fibula and large dorsi-plantarflexion range of the foot (Barnett and Napier, 1952). As suggested by studies on both forelimbs and hindlimbs of lemurids, in arboreal environments primate limbs likely exert forces that are more frequently medially directed, while during terrestrial locomotion the side-to-side more frequent component is towards the lateral direction (Carlson et al., 2005). Substrate reaction forces (SRFs, in their vertical, fore-aft and side-to-side components) are opposite in direction compared to forces (in the respective component) primarily exerted by an animal's limb. Thus, we can expect that in the arboreal environment SRFs will be more frequently directed laterally, compared to what occurs on the ground, since arboreal primates mainly exert medially directed forces (see above). While this pattern was highlighted for lemurids, similar results arose for anthropoids too (although this is based on a study restricted to the forelimb; Schmitt, 2003). Hence, since the fibula is located on the lateral side of the ankle joint, we here hypothesize that the likely more frequent lateral SRFs in arboreal environments result in increased loadings on the distal fibula of arboreal primates compared to terrestrial taxa. Moreover, due to the highly variably directed loadings involved in the arboreal environment (e.g. Demes et al. 2001; Carlson, 2005) and the extremely mobile ankle joint of arboreal primates (see above), we expect that the range of directional variation of biomechanical loadings to which the distal fibula is subject, is larger for arboreal taxa compared to terrestrial species. For both the hypotheses related to increased/decreased loadings and more/less variable orientation, along the DOA range going from arboreal to terrestrial (see Table 1 and above), semi-arboreal taxa should be characterized by intermediate conditions.

It should be noted that our functional hypothesis, based on more frequent lateral SRFs in the ankle of arboreal compared to terrestrial primates (see above), refers to ML SRFs deriving from linear locomotion (Carlson et al. 2005). Besides them, ML SRFs caused by turning behaviors (i.e. deriving from changes of direction) are substantial in the primate ankle and the medial SRFs are higher than the lateral SRFs in terms of magnitude, both on the ground and on the trees (Demes et al., 2006). It is not surprising if one considers

the evidently higher robustness of the tibia (medially located) compared to the fibula (laterally located), a condition that is widespread in primates and consistent with the fact that, in general and regardless of substrate, medial SRFs are higher than lateral SRFs. However, we base our hypothesis (detailed above) on a comparison of the SRFs on the lateral side of the ankle in arboreal *vs.* terrestrial environments (regardless of SRFs acting on the tibia) and, importantly, our hypothesis is based on ankle lateral loadings that are more frequent (and not with higher magnitude) for arboreal primates. If we consider that turning behaviors are expected to be more frequent during arboreal locomotion (as Demes et al. 2006 suggest), it is possible that in the resulting forces the ankle lateral SRFs in arboreal environment would be relatively more frequent (consistent with the results of Carlson et al. [2005] on linear locomotion), even if, just as the ankle lateral SRFs in terrestrial environment, they are characterized by relatively low magnitude. In other words, we expect that the low magnitude but frequent loadings experienced by the fibula of arboreal mammals can differentially affect trabecular remodeling compared to the low magnitude, but less frequent loadings, experienced by the fibula of terrestrial species (see above and Rubin et al. 2001, 2002). Although Demes et al. (2006) did not detect any lateral SRFs in arboreal environment, their work did not focus on SRF frequency (which is an aspect not tested, indeed) (Demes et al. 2006) and it may be possible that the absence of measured lateral SRFs during the arboreal behavior depends on the specific experimental setting and/or study system (the capuchin monkey *Cebus apella*). Apart from this, Demes and Carlson (2009) showed that both on arboreal and terrestrial substrates the SRF vectors are oriented medially to the segment of the distal portion of the hindlimb. However, if we consider the extremely abducted condition of arboreal primate limbs, the resultant SRFs in an arboreal environment tend to be relatively more laterally oriented than on the ground (Demes and Carlson, 2009). It supports our hypothesis and the expected increased loadings on the fibula in an arboreal environment, not only in terms of frequency but also in terms of direction. Hence, although we recognize that the loading pattern in the primate ankle is probably more complex than how we modeled it, we will follow the hypotheses of previous functional morphological analyses of the primate fibula (e.g. Marchi, 2007; Marchi and Borgognini-Tarli, 2004; Marchi and Shaw, 2011).

In summary, considering the expected functional patterns for the trabecular parameters mentioned above and in Table 2, our hypotheses predict that, due to the expected more frequent loadings on the lateral side of their ankle, arboreal primates should have a distal fibula trabecular structure ideally characterized by higher values for density-related traits (i.e. BV/TV, Tb.Th, NodDen), higher BS/TV, with trabeculae that are shorter (i.e. lower TrabLen), more curved and convoluted (higher TrabTort) and yielding lower FD. Furthermore, the largely multidirectional nature of loadings involved in the arboreal environment should result in lower DA for arboreal primates. For all these variables, the opposite configuration is expected for terrestrial primates, with semi-arboreal taxa showing intermediate values, e.g. significantly higher than those arboreal taxa but significantly lower than those of terrestrial taxa (depending on the expected pattern of co-variation with DOA, see above).

2. Materials and Methods

2. 1. Sample

The analyzed sample is represented by µCT scans from 28 fibulae, representing 21 primate species and including representatives of Strepsirrhini, Platyrrhini and Catarrhini (Fig. 1, Table 1). These µCT data stem from new acquisitions (performed at the National Research Council, CNR, Pisa, Italy) on samples from University of Florence, Italy (Florence Museal System, section La Specola and section of Anthropology and Ethnology) or downloading from MorphoSource (https://www.morphosource.org/). Details on the analyzed fibulae and µCT scans (e.g. resolution, museum collection from which the specimens were sampled, catalogue numbers) are provided in Table S1. All non-human primate data derive from bones of wild-caught individuals, with the exception of *Leontocebus fuscicollis* FMNH 122268 and *Saguinus imperator* FMNH 121551. All fibulae come from adult non-pathological individuals, with adulthood determined by evaluating the degree of fusion of long bone epiphyses. Only one fibula, i.e. *Propithecus diadema* UniFl-SPEC 1505, may belong to a sub-adult individual since the femur, present in the same collection where the fibula was collected, shows incomplete fusion of the epiphysis. Right and left fibulae were pooled together, since

bilateral asymmetry is regarded as a negligible factor in primate adult hindlimb analyses (Ruff and Jones, 1981, see also Auerbach and Ruff, 2006). After parameter extraction (see below), for each µCT scan we computed the relative resolution (i.e. Tb.Th divided by the voxel size, the former computed with the Bone J plugin, see below), yielding an average value of 8.91. We found a relative resolution ranging from 5.4 to 13.22, hence above the minimum recommended limit (i.e. 5, Kivell et al., 2011; Sode et al., 2008), with the only exception of the µCT scan of *Otolemur crassicaudatus* AMNH 80801 (3.47) (Table S1). However, the latter was visually validated, evaluating resolution and contrast.

2. 2. Data collection

2. 2. 1. Anatomical region

We focused on the fibulotalar articulation of the distal fibula. In this region, it is possible to identify a proximal and a distal part, termed PAF (proximal articular facet) and DAF (distal articular facet), respectively (Marchi et al., 2022 and fig. 2 therein, Fig. 2). Both are involved in important functions, e.g. PAF/DAF surface ratio is possibly a fibula load-bearing indicator (Marchi, 2015b; Preuschoft, 1970). Across the studied primates, we expected to find PAF and DAF as quite regular-shaped (in medial view), i.e. PAF as approximately rectangular-elliptical and DAF as approximately triangular, based on previous observations on hominids (Marchi, 2015b). However, DAF, albeit being approximately triangular, showed large variation in size and proportions, preventing a repeatable extraction of anatomically homologous trabecular bone (see below). We hence only analyzed PAF.

2. 2. 2. Orientation and crop

The orientation in standard position and the subsequent crop of the distal fibula region corresponding to PAF were performed in VG Studio Max 3.3 (Volume Graphics, Heidelberg, Germany). First, we positioned PAF in the coronal plane (Fig. 2A, B). Then, we positioned the major and minor sizes of the quasi-elliptical/rectangular PAF in the sagittal and transverse plane (Fig. 2C). From oriented µCT stacks,

we exported sub-stacks of images (16-bits in TIFF format) that in the following steps allowed us to isolate only the trabecular structure underlying PAF (see below) but at this stage are still including both cortical and trabecular bone (Fig. 2D, Fig. 3A). To do so, we cropped the volume between the proximal and the distal limit of PAF. The sub-stacks were subsequently imported in FIJI, binarized and purified employing BoneJ (through the 'Optimise Threshold > Threshold Only' and 'Purify' routines) and then re-exported. The purifying step (https://bonej.org/purify) acts on binarized stacks, identifying and removing all the foreground particles (recognized as 'bone' by the binarizing algorithm) except for the largest one (i.e. the studied anatomical element, in this case). To be recognized as not belonging to the largest particle, a foreground voxel should not be connected (in 3D) at any point to the cortical or trabecular bone, i.e. it should be a particle that is isolated ('floating') in 3D (either within the intertrabecular voids or outside the bone). Due to the nature of trabecular bone, i.e. the material is always connected to other bone regions, such floating particles necessarily represent an artifact (i.e. isolated voxels outside the bone fraction that are erroneously recognized as bone) that, if not removed, may bias some trabecular parameters (e.g. they artificially increase BV/TV). Hence, by purifying we corrected for the potential presence of small isolated particles erroneously recognized as 'bone' that may derive from the binarizing algorithm and depending on the µCT scan grey values.

2. 2. 3. Trabecular bone isolation

We imported the oriented, binarized and purified sub-stacks in R (R Core Team, 2022) ('readTiffStack' function, 'indianaBones' package, Veneziano et al., 2021, https://zenodo.org/record/7615165). To isolate Regions of Interest representing the entire trabecular bone underlying PAF (Fig. 2D, Fig. 3B) (referred to as 'ROI' hereafter), we used the 'makeBrush' ('size'=11; 'EBImage' package, Pau et al., 2010) and the 'splitBone' functions ('indianaBones'). On each specimen, we iterated the isolation procedure calibrating the value of the 'iterFill' argument of 'splitBone', i.e. increasing it and decreasing it. We visually evaluated, for each iteration, the quality of trabecular isolation by comparing the result of the automatic procedure (hence, the ROIs, as shown in Fig. 3B) with the trabecular network visible in the stack representing both

compact and trabecular bone (Fig. 3A). When we considered the isolation to be optimal, we used the corresponding 'iterFill' value of 'splitBone for that specimen (values used for all the specimens are listed in Table S1). The ROIs (e.g. Fig. 2D, Fig. 3B) were exported as image stacks ('writeTiffStack' function, 'indianaBones').

2. 2. 4. Trabecular architecture quantification

We extracted traditional trabecular parameters, through the BoneJ plugin in FIJI, as well as topological indices, computed through 'indianaBones' in R (Veneziano et al. 2021). For the former, we imported the ROIs in FIJI and, through the respective BoneJ routines, we extracted degree of anisotropy (DA, no unit), trabecular thickness (Tb.Th, mm), connectivity (Conn., no unit, computed only to evaluate trabecular number, see below), Bone Volume (BV, mm^3) and Bone Surface (BS, mm^2). Conn. is assumed to be an approximation of trabecular number and in this study yielded values greater than 146 (Table S1), allowing us to follow the recommendation of studying only volumes with more than 50 trabeculae to reliably quantify trabecular architecture (Mielke et al., 2018). BV and BS values were used to obtain BV/TV and BS/TV. To do so, first we needed to compute the total volume represented by each ROI (TV, mm^3). Since the ROIs are not of regular shape (e.g. Fig. 3B), we exploited the 'indianaBones' function separating trabecular bone from intertrabecular voids and from compact bone (see above). After splitting these three components, one can add the trabecular bone volume to the total volume of intertrabecular voids, obtaining the whole inner volume, i.e. the entire joint excluding the compact shell. This represents TV. Hence, dividing BV and BS by TV, we obtained Bone volume fraction (BV/TV, no unit) and Bone surface density (BS/TV, mm^{-1}), respectively.

The topological indices were computed on skeletonized substacks ('Auto Skeleton' tool, Amira 6.0.0, Thermo Fisher Scientific, followed by exportation in ASCII format). We imported the skeletons in R ('readAmiraSkeleton' function, 'indianaBones') and using the respective 'indianaBones' functions (as detailed in Veneziano et al. 2021, Supplementary Material and the R code of this work), we extracted (see also Table 2): average and median of the node density ($NodDen_{Aver}$ and $NodDen_{Med}$, unit: nodes per mm^3),

average of the trabecular length ($TrabLen_{Aver}$, untiless), average and median of the trabecular tortuosity ($TrabTort_{Aver}$, $TrabTort_{Med}$, unitless) and fractal dimension (FD, unitless). For the computation of FD, that is obtained via the Box-counting algorithm (Annadhason, 2012), we used another R package, i.e. 'Rdimtools' (You and Shung, 2022) (see Supplementary Material).

2. 2. 5. Substrate preference

We aimed to test potential effects related to substrate preference, i.e. DOA, on distal fibular trabecular architecture. To each analyzed species we assigned one of three discrete states, based on previous descriptions and/or the reported amount of time spent on substrates (references in Table 1): 'arboreal' or 'terrestrial' were assigned to species living almost exclusively on trees or on the ground, respectively; 'semi-arboreal' was assigned to species spending a comparable amount of time on trees and ground (also defined 'scansorial' in other studies; e.g. Chen and Wilson, 2015).

2. 2. 6. Body mass

To estimate how distal fibular trabecular architecture is related to body mass, for each individual we measured the superoinferior diameter of the femoral head, recognized as a reliable body mass proxy in human and non-human primates (Ruff, 2003; Ruff et al., 2018). For fibulae collected in museums, we extracted this measure with calipers, from the femora of the same individuals available in the collection. When both femora were available, the right and left superoinferior diameters were measured, taking the average of the two values. For individuals whose fibulae were included by downloading µCT scans from MorphoSource (see above, Table S1), image stacks of the femur were available and downloaded too. We oriented the femora in standard position (following Ruff, 2002) in VG Studio, and measured the superoinferior diameter of the head, multiplying the µCT voxel size by the number of slices included between the most superior and the most inferior point of the head. To cope with outliers, e.g. human values largely lying outside the range of variation of all the other primate specimens, the body mass proxy values were natural log-transformed (hereafter, referred to as 'log-BMp') (Table S1, Fig. 1).

We are aware that the femora of the individuals from which the fibula is studied may be not available. The anteroposterior length of PAF measured at the 50% proximodistal level (PAF AP length in Table S1), i.e. one of the two sizes of the ellipse-rectangle which PAF resembles (e.g. the major size in Fig. 2C), when natural log-transformed shows a strong correlation with log-BMp (Pearson's correlation coefficient= 0.96, *p*-value <0.001). Thus, in distal fibula trabecular analyses in which only fibulae are available, e.g. when fossil fibulae are studied, this fibular metric can be used as an alternative body mass proxy.

2. 2. 7. Phylogenetic relationships

To determine the effect of phylogenetic relationships on primate distal fibular trabecular architecture (see below), we obtained a time-calibrated phylogeny of the studied species. A Maximum Clade Credibility DNA-only node-dated tree, including 4098 mammal species, devoid of polytomies and deriving from the posterior distribution of Upham et al., 2019, was modified in R ('drop.tip' function, 'ape' R package, Paradis et al., 2004) including only the studied species (Fig. 1).

2. 3. Statistical analysis

We performed all the statistical analyses in R. For each trabecular trait and log-BMp, we computed average species values. Noticeably, most species values are those of single specimens (see Potential Limitations, below, and Supplementary Material). The species for which we collected data from more than one fibula (sample size > 1, see Table 1) are *Ateles paniscus*, *Cercopithecus mitis*, *Colobus guereza* and *Homo sapiens* (for them, mean values, standard deviation and coefficient of variation for each trabecular trait are shown in Table S2). We estimated the relative effects of DOA, body mass and phylogenetic structure on the trabecular structure of the primate distal fibula in both a univariate and a multivariate way. To undertake the former, we ran several Phylogenetic Generalized Least Squares (PGLS) regressions ('gls' function, 'nlme' package, Pinheiro et al., 2020; including the use of 'corPagel' function, 'ape' R package) with morphological traits as dependent variables, DOA ('arboreal', 'semi-arboreal', 'terrestrial') as independent variable and log-BMp as covariate, besides phylogenetic ANOVAs (pANOVA)

('phylANOVA' function, 'phytools' package, Revell, 2012). We planned to run post-hoc Tukey tests ('glht' function, 'multcomp' package, Hothorn et al., 2008) after pANOVAs only in case of significant *p*-value (<0.05) from pANOVAs. For each PGLS, we log-transformed the respective morphological trait if the PGLS residuals showed a distribution clearly deviating from normality (traits summarized in Table 3). Importantly, we ensured that in each PGLS, DOA and body mass effects were not interacting by preliminarily running a PGLS + pANOVA, with log-BMp and DOA as dependent and independent variables, respectively. Since it excluded any correlation between body mass and DOA (*p*-value=0.17) we were sure that the p-values resulting from each PGLS informed on separate effects of DOA and body mass. When a parameter was significantly related to body mass (i.e. body mass *p*-value deriving from the respective PGLS being <0.05) to quantify DOA effects (with the ideal exclusion of allometric effects) we ran the pANOVA using size-corrected values for the parameter (with size-correction corresponding to taking the residuals of a linear regression of the parameter against log-BMp).

To determine the phylogenetic signal of each variable, we estimated the Pagel's λ ('phylosig' function, 'phytools' package), testing the null hypothesis of λ different from zero ('test'=TRUE). λ yields values ranging from 0 (i.e. no phylogenetic effects) to 1 (i.e. trait distribution is entirely explained by a Brownian motion model of morphological evolution and, hence, it exclusively depends on phylogenetic relationships among taxa). Moreover, we estimated how the log-BMp distribution is related to the phylogenetic structure through λ. It was needed because, in case of significant phylogenetic signal in log-BMp, an important implication would be that for variables related to both body mass and phylogenetic structure, it would not be possible to disentangle the effects of the two factors. For instance, the variable may be primarily affected by body mass and the phylogenetic structure results as a trabecular correlate only because of its interaction with body mass (or vice versa). In such cases, a size-correction may correct for a part of the effects of the phylogeny, too. In other words, if body mass and phylogeny are correlated, through size-correction it is possible to obtain values partially devoid of phylogenetic effects, and not only of size ones, that can be better studied for a relationship with DOA. Nevertheless, we have no way to determine which factor primarily affects a given trabecular feature. To test if and to what extent size-corrected values are also

574 corrected for phylogenetic effects, for variables showing a significant relationship with body mass, we
575 measured the phylogenetic signal both before (Table 3) and after size-correction (Table 4). To account for
576 problems deriving from multiple testing, all the PGLSs *p*-values were corrected through the Bonferroni
577 method ('p-adjust' function). We visualized how trabecular variables vary according to DOA through
578 boxplots ("ggplot" function, "ggplot2" R package; Wickham, 2016) (Fig. 4, Fig. S1), generating additional
579 boxplots with size-corrected values (as detailed above) when traits showed a significant relationship with
580 log-BMp (Table 3). To visualize how each trabecular variable is related to body mass we used bivariate
581 scatterplots (Fig. S2A, B). To visualize how traits are related to phylogeny, for each of them we mapped
582 average species values on the time-calibrated tree ('contMap" function, 'phytools' package), also using the
583 size-corrected values for traits showing significant relationship with body mass (Fig. S3).

584 By also running a multivariate analysis, we aligned to the approach suggested by Ryan and Shaw (2012)
585 when one aims to analyze functional adaptations of trabecular structure: i.e. accounting for suites of possibly
586 intercorrelated traits (as it often occurs for trabecular variables, e.g. Cotter et al., 2009; Mittra et al., 2008,
587 2005), instead of isolated variables, to better identify patterns related to locomotion (Ryan and Shaw, 2012).
588 The multivariate part of the analysis is based on two PCAs. PCA is often used when intercorrelated variables
589 are analyzed together with the aim of isolating the contribution of single variables (as cranial measurements,
590 e.g. Frost et al., 2003; Landi et al., 2021; Nishimura et al., 2019). We ran two different PCAs in order to
591 follow both an inferential quantitative and an exploratory approach:

592 1. A first PCA was run on a data matrix of the computed trabecular variables (i.e. variables in Table
593 3 excluding log-BMproxy) after scaling and centering ('scale' function). The extent to which DOA,
594 body mass and phylogeny are related to the whole trabecular architecture were quantified through
595 a phylogenetically informed multivariate Generalized Least Squares Regression. After regressing
596 PC1-PC4 (chosen since cumulatively explaining more than 90%, i.e. 93%, of the variance, Table
597 S3) against the discrete variable, i.e. DOA, and with log-BMp as covariate ('mvgls' function,
598 'mvMORPH' package, Clavel et al., 2015, model= 'lambda', REML=FALSE), we tested for

significance through a phylogenetic MANCOVA ('manova.gls' function, 'mvMORPH' package, test= 'Pillai', type= 'II'). As detailed above for univariate PGLSs, the absence of significant DOA-body mass correlation allowed us to compute *p*-values exclusively informing on the effects of DOA (separating them from those related to body mass) on trabecular structure. To assess the phylogenetic signal of PC1-PC4, we estimated λ through the 'transformPhylo.ML' function ('motmot' package, Puttick et al., 2019, model= 'lambda').

2. A second PCA was run to follow an exploratory, instead of a strictly inferential, statistical approach, i.e. to visualize patterns exploiting the decomposition of original variance into new variables, i.e. Principal Components, performed through PCA. We wanted to exploit this second PCA and the deriving morphospace to visualize potential effects related to DOA that may be not detected as significant by other statistical analyses (e.g. due to sample size) and that, ideally, do not include the potential body size effects on trabecular variables. Hence, the variables significantly related to body mass (Table 3) were included in this second PCA in their size-corrected version (see above). The resulting PC1-PC4 (cumulatively accounting for around 85% of the variance, Table S4) were used to build bivariate phylo-morphospaces (Fig. 5, Fig. S4). These plots allowed us to visualize how subsets of trabecular traits (size-corrected, if needed) relate each other, how they relate to DOA and how they relate to phylogenetic relationships. This is possible since the phylogeny is mapped on the plot and the phenotypes corresponding to specific taxa are shown by means of tips and nodes positions on the plot (i.e. closer points reflect phenotypes that are more similar each other). Specifically, actual data points (labeled in Fig. 5 and Fig. S4 and deriving from measures extracted in this work) determine the position of the tips of the phylogeny, while the position for the tree internal nodes (unlabeled in Fig. 5 and Fig. S4) is determined by ancestral phenotypes reconstructed from tip values and assuming a Brownian motion model of evolution (see 'phylomorphospace' R function, 'phytools' package).

3. Results

3. 1. Univariate analysis

Results of PGLSs, pANOVAs and Pagel's λ are summarized in Table 3. pANOVAs, including those on size-corrected variables, did not detect any significant relationship with DOA. Hence, we did not run any post-hoc Tukey tests. Almost no expected signal related to DOA for most of the trabecular parameters of the primate distal fibula is evident from the distribution of species trait values: data pooled by DOA do not reflect any pattern or, when their distribution apparently follows DOA, it involves large overlap (e.g. size-corrected $TrabLen_{Aver}$, and $TrabTort_{Aver}$). Also, when traits that appear to be partially related to DOA (e.g. Tb.Th, $log\text{-}NodDen_{Aver}$) are size-corrected, no pattern is evident anymore (Fig. S1). Two potential exceptions are represented by the patterns shown by BV/TV and size-corrected BS/TV. Indeed, although with some overlap and outliers (i.e. *H. sapiens* BV/TV value lying within the arboreal range and *P. troglodytes* size-corrected BS/TV value lying within the terrestrial range) and despite their non-significant relationship with locomotor habits (Table 3), in the two variables it seems to be involved a trend following DOA: terrestrial species values > semi-arboreal species values > arboreal species values (Fig. 4, Fig. S1, but see the strong phylogenetic signal of size-corrected BS/TV, Table 4 and below).

Overall, the trabecular structure of primate distal fibula appears to be substantially related to body mass, as one can evince from the fact that several trabecular traits are significantly related to log-BMp (i.e. six out of 10). The traits that show no relationship with size are DA, BV/TV and TrabTort (both $_{Aver}$ and $_{Med}$) (Table 3). The important effect of body mass on trabecular architecture is also clear from bivariate scatterplots of trabecular traits vs. log-BMp, from which it is also evident that the studied trabecular traits exhibit both direct, i.e. Tb.Th, $TrabLen_{Aver}$, FD, and inverse proportionality, i.e. BS/TV and NodDens (both $_{Aver}$ and $_{Med}$), with log-BMp. To compare our results to previously identified allometric patterns (see Discussion), for Tb.Th, we additionally ran a 'Tb.Th ~ logBMp' linear regression (using data on single specimens, hence not averaging for species) and we found that its covariation with body mass can be explained by the relationship 'Tb.Th= (0.07±0.01) * logBMp' (slope p-value<0.001, while the intercept estimate is not

significantly different from 0, intercept *p*-value=0.44). Consistent with PGLS results, DA, BV/TV, $TrabTort_{Aver}$ and $TrabTort_{Med}$ do not reveal any pattern related to body mass (Figs. S2A, B).

We found a strong phylogenetic signal in four out of 10 trabecular traits, i.e. Tb.Th, NodDen, both $_{Aver}$ and $_{Med,}$ and $TrabLen_{Aver}$, for which λ is very close to 1.0, i.e., 0.94-0.99, and the related *p*-values yield significance. For another trait, i.e., FD, λ is quite high but not extremely close to 1.0 (0.81) with a significant related *p*-value (Table 3). For these parameters, from the species values mapped on the time-tree it is evident that the strong relationship with phylogeny may be due to the fact that trabecular values often range in between two extremes represented by some/all platyrrhines, on the one hand, and catarrhines (especially hominids), on the other hand (Fig. S3). It should be noted that the traits not significantly affected by phylogeny are those that are not significantly related to body mass too, i.e., DA, BV/TV, $TrabTort_{Aver}$ and $TrabTort_{Med}$, with the only exception of BS/TV that, despite showing a significant relationship with body mass does not exhibit a significant phylogenetic signal (Table 3). It likely derives from an important outcome of this work: the body mass proxy is significantly related to phylogenetic relationships itself (λ = 0.99, *p*-value < 0.001). Hence, for the five traits that are correlated to both body-mass and phylogeny, i.e. Tb.Th, NodDen (both $_{Aver}$ and $_{Med}$), $TrabLen_{Aver}$ and FD, it is not possible to disentangle the body mass and phylogenetic effects. In support of this, for almost all the traits, size-correction results in a sharply weakened phylogenetic signal, i.e. phylogenetic effects that are not significant anymore for Tb.Th, NodDen (both $_{Aver}$ and $_{Med}$) and FD, with only $TrabLen_{Aver}$ retaining a significant phylogenetic signal but through a decreased λ, i.e. from 0.98 to 0.78 (Tables 3 and 4). Again, a particular case is represented by BS/TV, unique in showing raw values significantly related to body mass but without any phylogenetic signal (Table 3) and size-corrected values involving strong phylogenetic effects (Table 4).

3. 2. Multivariate analysis

The multivariate PGLS and pMANCOVA performed on PC1-PC4 extracted from the first PCA (including raw trabecular variables) suggests that, overall, the trabecular architecture of the primate distal fibula is not correlated to DOA (*p*-value = 0.5). Instead, PC1-PC4 result to be significantly related to body

673 mass (p-value < 0.001) and/or they involve a strong phylogenetic signal (λ=0.95: lower 95%CI = 0.73, upper
674 95%CI = 0.99), with the impossibility of determining which of the two factors exclusively/mostly relates to
675 primate distal fibula trabecular structure (see also above).

676 The exploratory multivariate analysis was based on a visual assessment on bivariate phylo-
677 morphospaces built with PC1-PC4 deriving from the second PCA, that included size-corrected values for
678 variables related to log-BMp. As detailed above, since log-BMp is correlated to phylogeny, size-correction
679 expectedly removed a part of the phylogenetic signal included in primate distal fibula trabecular structure
680 too (even if we expected that the PCs still involve minor phylogenetic effects, as suggested by the significant
681 phylogenetic signal of size-corrected $TrabLen_{Aver}$ and size-corrected BS/TV; Tables 3 and 4; see also below).
682 Accordingly, the observations on morphospaces built with PCs deriving from the second PCA, detailed as
683 follows, allowed us to focus on other effects than allometry and phylogeny.

684 On all the biplots built with PC1-PC4, arboreal species occupy a larger region, compared to the one
685 occupied by semi-arboreal and terrestrial taxa. PC1 (explaining 33.6% of the variance), yields a separation
686 between two species, i.e. *H. sapiens* and *C. jacchus*, showing lower PC1 scores, and the rest of the taxa,
687 showing higher PC1 scores. As suggested by vector orientations and lengths in the variable loading plots,
688 the trend of *H. sapiens* and *C. jacchus* to be set apart with lower PC1 from the other studied primates,
689 appears to be explained by higher NodDen (both $_{Aver}$ and $_{Med}$) and FD, and lower TrabTort (both $_{Aver}$ and
690 $_{Med}$). Other variables seem to contribute to PC1 scores (e.g. DA oriented at around 45° in the PC1-PC2 or
691 PC1-PC4 plots or Tb.Th oriented at around 45° in the PC1-PC4 plot, both suggesting similar contributions
692 to PC1 and other PCs) but the shorter related vector length also indicates a probable lower importance
693 compared to the other variables mentioned above (Fig. 5, Fig. S4). PC2, explaining 27.4% of the variance
694 and apparently driven by lower BS/TV, BV/TV, Tb.Th and $TrabLen_{Aver}$, yields a pattern that, although with
695 extensive overlap and with the outlying *H. sapiens* (see below), suggests a gradient going from terrestrial
696 species, (lower PC2 scores) to arboreal species (higher PC2 scores) with semi-arboreal species occupying
697 the lower range of the arboreal region and yielding slightly higher PC2 than terrestrial species (pattern

highlighted univariately in Fig. 5D, see also Fig. S4). Remarkably, it is also evident that PC2 separates platyrrhines (higher scores) from catarrhines and strepsirrhines (lower scores) and that, if we exclude *H. sapiens* and *C. jacchus*, the smaller taxa (e.g. *Mico* spp., *L. rosalia*) yield higher PC2 scores and the larger taxa (e.g. *Papio spp*., *P. troglodytes*) yield lower PC2 scores. PC3 and PC4, cumulatively explaining 24% of the variance, when plotted together show the relative isolation of *Otolemur crassicaudatus* from all the other taxa, toward the morphospace region corresponding to lower PC3 and PC4 scores and that appear to be explained by higher DA and $TrabLen_{Aver}$ (Fig. 5, Fig. S4). Interestingly, in the PC1-PC3 plot, *C. jacchus* tends to occupy the morphospace region corresponding to lower PC1 scores and higher PC3 scores, potentially driven by a low $TrabLen_{Aver}$ (while higher values of this parameter seem to contribute to set apart *O. crassicaudatus*, as mentioned above) and *H. sapiens* tends to occupy the region corresponding to lower PC1 and lower PC3 scores, potentially driven by higher DA and low TrabTort (both $_{Med}$ and $_{Aver}$). A remarkable result is represented by *H. sapiens* never clustering close to *P. hamadryas*, *P. cynocephalus* and *M. nemestrina*, the other terrestrial taxa, in all the phylo-morphospaces.

4. Discussion

In primate functional morphology, the fibula has long been neglected and, when addressed, it has been initially studied only in association with the tibia. The analysis of the tibia-fibula complex has highlighted a positive relationship between fibular relative diaphyseal robusticity and the frequency of laterally oriented loadings in the distal portion of the hindlimb, in turn suggested to be related to the DOA (e.g., Marchi, 2015b, 2007; Marchi and Borgognini-Tarli, 2004), hence providing a valuable tool to infer arboreal adaptations in extinct primates. However, the use of this proxy to reconstruct DOA of extinct primates is limited by the paucity of associated fossil tibiae and fibulae. Recent works, performed with different methodological approaches (e.g., diaphyseal CSG, functional indices and 3D GM, Marchi, 2015b; Marchi et al., 2022; Marchi and Shaw, 2011), have also shown that some traits of the fibula alone may relate to DOA. To identify further fibular characteristics potentially reflecting DOA and applicable for

palaeobiological inferences, in this work we addressed the distal epiphyseal trabecular architecture, an anatomical level never studied before in a primate comparative sample.

4. 1. Effects of different factors on primate distal fibula trabecular bone

4.1.1. Degree of arboreality (DOA)

The analyses performed in this study (Table 3, Figs. 4-5, Figs S1, S4) seem to indicate an overall absence of a relationship between the trabecular architecture of primate distal fibula and DOA. Indeed, no quantitative evidence arises from either univariate or multivariate PGLSs (even after size-correcting variables strongly related to body mass, in the case of univariate PGLSs). Moreover, a visual assessment of interspecific variation, in general does not yield any pattern related to DOA. Interestingly, some traits as BV/TV and BS/TV (the latter with size-corrected values) seem to follow a trend directly related to DOA (Fig. 4). However, we would not interpret these patterns as reflecting loadings related to DOA. Indeed, for the two parameters the trend is opposite to our expectations, since we expected higher BV/TV and BS/TV in arboreal primates, due to the hypothesized more frequent loadings on their distal fibula (see above), while, for both the traits terrestrial taxa show higher values. Instead, the patterns of BV/TV and size-corrected BS/TV are likely explained by phylogenetic effects. As for BS/TV, it is already clear from the strong and significant phylogenetic signal detected after size-correction (Table 4). As for BV/TV, although it does not show a significant *p*-value for λ (Table 3), the presence of a strong phylogenetic signal is clear from the trait values mapped on the phylogeny (Fig. 4A). Indeed, the higher BV/TV in terrestrial taxa is driven by higher values in baboons (*Papio* spp.,) and the southern pig-tailed macaque (*Macaca nemestrina*) which represent a clade in the phylogeny used in this work. The other terrestrial taxon, *H. sapiens*, instead shows a value comparable to the one of its sister taxon *P. troglodytes*, here categorized as semi-arboreal, a pattern supporting again the absence of an effect related to DOA on BV/TV. The BV/TV ancestral states (reconstructed to map BV/TV values on the phylogeny) would even suggest that a quite high BV/TV is plesiomorphic in cercopithecids (i.e. the group represented by *Chlorocebus* spp., *Cercopithecus mitis*.,

746 *Papio* spp., *M. nemestrina*, *Colobus guereza*) with an apomorphic BV/TV decrease in *Chlorocebus* spp.
747 However, caution is needed in proposing evolutionary patterns, since the species here sampled are far from
748 being a sufficient representation of cercopithecid diversity and efforts are still needed to clarify how
749 trabecular variables vary in ontogeny *vs.* phylogeny. Apart from this, the relatively low BV/TV in
750 *Chlorocebus* spp. is, together with other isolated non-phylogenetically related patterns (e.g. the very low
751 BV/TV in *Mico* spp., and *L. fuscicollis* within platyrrhines, Fig. 4A), probably the reason behind the absence
752 of significant phylogenetic signal for BV/TV.

753 From the multivariate visual assessment, a weak apparent pattern potentially related to DOA arose from
754 PC2 deriving from the second PCA (that was run with size-corrected variables, where needed). This PC is
755 inversely related to BV/TV, size-corrected BS/TV, size-corrected Tb.Th and, although with minor
756 contribution, size-corrected TrabLen, and yields a weak gradient going from terrestrial taxa (lower PC2
757 scores) to arboreal primates (higher PC2 scores) with semi-arboreal taxa showing an intermediate mean and
758 median (in the boxplots shown by triangles and vertical lines, respectively) (Fig. 5). As well as for BV/TV
759 and size-corrected BS/TV (discussed above and that are, not surprisingly, two of the four main driving
760 variables for PC2), we interpret the PC2 pattern as related to other factors, instead of DOA. It would be
761 suggested by the fact that three of the four variables mainly driving PC2, i.e. BV/TV, BS/TV (see discussion
762 above) and Tb.Th, yield a pattern that is opposite to what we expected in terms of biomechanical loadings.
763 Indeed, we hypothesized that arboreal species would show higher Tb.Th but since Tb.Th inversely correlates
764 to PC2 and terrestrial taxa show lower PC2 scores, it means that terrestrial primates are those that show
765 higher Tb.Th As for TrabLen, it would show a pattern consistent with the expectations, i.e. terrestrial taxa
766 exhibit longer trabeculae, i.e. higher TrabLen, due to the expected less frequent loadings. However, we do
767 not believe it is sufficient evidence in support of a DOA signal in the studied trabecular structure,
768 considering the lower contribution of TrabLen to PC2 (see the shorter vector length compared to the other
769 three variables driving PC2, Fig. 5A) and the fact that TrabLen was expected to negatively correlate with
770 NodDen. NodDen, instead mainly contributes to another PC (i.e. PC1, see discussion below). Apart from
771 these considerations, it is clear that PC2 mainly separates playthrrines (higher PC2 scores) from catarrhines

and strepsirrhines (lower PC2 scores). Furthermore, it is clear that there is a residual effect of body mass on this PC, i.e. PC2 separates larger taxa, as baboons and the chimpanzee, from smaller taxa, as *Mico* spp., *L. rosalia* (once the largest and the smallest taxa, *H. sapiens* and *C. jacchus* respectively, are excluded). It means that, despite the fact that the PCA from which PC2 derives was run on values corrected for body mass (and partially from phylogenetic effects, see above and Table 4), both the effects are instead still present and drive PC2, in turn representing 27.4% of the whole variability. Concerning the remaining effect of body mass, a possibility is that it depends on the procedure of size-correction that we used, i.e. taking the residuals of a variable-logBMp linear regression. Further dedicated investigation on this topic is needed to confirm this hypothesis or may put efforts into properly design samples to control for body mass (e.g. studying primate species with similar body sizes and different locomotor behaviors). The phylogenetic signal of PC2 can also be inferred from the fact that two of the four variables mainly driving PC2 are those that after size-correction showed a significant phylogenetic signal, i.e. BS/TV and $TrabLen_{Aver}$. We quantitatively confirmed that PC2 is driven by body mass and/or phylogeny, by running a PC2 vs. log-BMp regression (p-value=0.005) and computing the PC2 phylogenetic signal (λ=0.77, p-value=0.008). With both univariate (with BV/TV and size corrected BS/TV, Fig. 4) and multivariate (with PC2, Fig. 5) analyses, we found some apparent patterns related to DOA that were better ascribed to phylogeny and body mass. This reveals one potential limitation of this work. Although the distribution of DOA categories potentially allowed us to disentangle the effect of DOA from phylogenetic ones (e.g. in case of similar distinctive values shown by the terrestrial baboons, macaque and humans, or by the semi-arboreal *Cercopithecus* spp., *C. mitis* and chimpanzee), there is a tendency for taxa assigned to the same locomotor category to cluster in specific parts of the phylogeny (e.g. terrestrial baboons, arboreal platyrrhines). It limited our possibility to disentangle DOA effects from phylogenetic ones. Future works aiming to investigate the factors to which primate distal fibula trabecular structure relates and also testing the effect of DOA should overcome this limitation (besides others, discussed below) of this study.

According to our results, no obvious signal attributable to DOA is present in the trabecular bone of the distal fibula of primates. This finding is in contrast with previous evidence obtained on the relative

robusticity of the fibular diaphysis (e.g. Marchi, 2007, 2015a; Marchi and Borgognini-Tarli, 2004; Marchi and Shaw, 2011). The discrepant patterns between distal epiphyseal trabecular architecture and diaphyseal structure possibly suggest that diaphyseal and epiphyseal variables do not strongly co-vary (Shaw and Ryan, 2012; Saers et al., 2016). One possible explanation is linked to the different biomechanical environments to which these two anatomical regions are subjected, i.e., bending/torsion loadings are dominant in the diaphysis (Carter and Beaupré, 2007) while the epiphyses mainly adapt to axial loads (Barak et al., 2011; Biewener et al., 1996). In this framework it is plausible that bending/torsion predominate over tension/compression (i.e., the axial regime) in the biomechanical loadings acting on the primate fibula. Specifically, bending seems to be the main loading regime acting on the fibula. It is supported by SRF vector orientation in the hindlimb of capuchin monkeys during arboreal and terrestrial behaviors that, in turn, suggests the presence of substantial bending moments, with bending occurring around oblique axes of the hindlimb segments (Demes and Carlson, 2009). Specifically, since the SRF resultant is forced to pass through the foot when the limb contacts the substrate (Demes and Carlson, 2009), it is likely closer to the fibula distally than proximally, where the discrepancy angle between the SRF resultant and the limb segment increases (e.g. at the mid-shaft level, where CSG parameters are often quantified). A consequence of increased SRF resultant-limb segment discrepancy angles would be that the bending moments to which the fibular diaphysis is subject are probably larger than those to which the distal fibular epiphysis is subject. If it was true, it would be however challenging to place the evidence that external morphology of primate distal fibula relates to DOA (Marchi, 2015b; Marchi et al., 2022) in this scenario. Indeed, if the bending regime is assumed as dominant to justify the stronger signal due to arboreality detected in the diaphysis, the epiphyseal morphology, both external and internal, should consistently be poorly related to this factor. Hence, the fact that, instead, in the distal fibula external anatomy the effects of DOA are detectable, in contrast with internal architecture, is striking. We can hypothesize that, in the specific case of the ankle joint, loadings acting at this level influence the distal fibula external shape and the distal fibular internal structure to different extents. Moreover, since previous studies of trabecular bone in the other elements of the ankle joint mostly found significant relationships with locomotor habits (distal tibia; Barak et al., 2013a,

824 talus; Hébert et al., 2012; Su et al., 2013), we can assume that the transfer of loads reasonably occurring in
825 a functional unit as the ankle joint, results in the functional signal to be present in the internal structure of
826 other elements, but not in the distal fibula. In this direction, clinical studies have recently suggested
827 differential effects of loadings in human distal fibular vs. distal tibial trabecular architectures, with the
828 former proposed to be less sensitive (Ghasem-Zadeh et al., 2021; Stürznickel et al., 2021). If this condition
829 is widespread in primates, it may justify the apparently low functional locomotor signal borne by the
830 trabecular bone of the distal fibula. Further work is needed to better understand these discrepant trends
831 followed by the distal fibula internal and external anatomy, e.g., by comparing the evolutionary patterns in
832 the external shape and internal structure in the same sample of primate species. Related to this, one should
833 note that a relationship between DOA and the distal fibula external morphology has been detected in
834 hominids, i.e., hominins and great apes (Marchi, 2015b; Marchi et al., 2022). While the sample studied by
835 Marchi and colleagues is suitable to explore the range of arboreal habits from fully terrestrial to fully
836 arboreal, it is not taxonomically as wide as our sample, and does not include species that are terrestrial but
837 not bipedal, as in this work (e.g. baboons). These two aspects may have hidden large-scale phylogenetic
838 effects in analyses of distal fibula external morphology (despite phylogenetic relationships in hominids
839 being accounted for in Marchi et al., 2022) and a role potentially played by the distinctive hominin bipedal
840 locomotion (see discussion below on the influence of phylogeny and bipedalism). This emphasizes the
841 importance of studying how ecology is reflected by different anatomical levels on the same sample of
842 species (e.g. Alfieri et al., 2022, 2023).

843 While many of the studied trabecular properties yielded a strong relationship with body mass and/or
844 phylogenetic structure (but with the impossibility to disentangle these two effects; see discussion below),
845 trabecular anisotropy (i.e. DA), bone volume fraction (i.e. BV/TV) and tortuosity (i.e. TrabTort, both $_{Aver}$
846 and $_{Med}$) do not significantly correlate with any of the factors here addressed, i.e. DOA, body mass and
847 phylogeny (Table 3). It makes the interpretation of the overall patterns related to these traits on multivariate
848 phylo-morphospaces particularly interesting. As discussed above, BV/TV shows a pattern that only
849 apparently discriminates terrestrial from arboreal taxa, with semi-arboreal in between (and the same occurs

for the PC to which BV/TV primarily contributes, i.e. PC2). Indeed, although not yielding a significant phylogenetic signal (Table 3), this trait has a distribution that is mainly driven by phylogeny (Fig. 4).

TrabTort negatively correlates to PC1, that is also positively associated with NodDen and FD (apart from minor contributions deriving from other variables). PC1 sets apart *H. sapiens* and *C. jacchus* from the other species. Although PC1 reveals a pattern that is very likely not affected by allometric and phylogenetic effects (*H. sapiens* and *C. jacchus* are the largest and the smallest in the sample, respectively, and they are a hominid and a platyrrhine), the very different locomotor habits of *H. sapiens* and *C. jacchus* (not only in terms of DOA) make this axis of variation very unlikely to be associated with locomotor behavioral aspects too. Also, there is not consistency in the way through which the three variables mainly driving PC1 are expected to relate to loads (Table 2 and above). For instance, if NodDen varied as expected according to the experienced loads and strains, i.e. positively, NodDen and TrabTort should have been positively associated with each other, but they do not follow this pattern in affecting PC1; similarly, FD is expected to be negatively related to NodDen, but again it is not confirmed (Fig. 5). All of this suggests that the discrimination revealed by PC1 is challenging to explain in terms of locomotion, body mass and phylogeny and that probably the effect of other factors (e.g. genetic, developmental, hormonal) should be investigated.

Another portion of TrabTort variance is captured by PC3 and, interestingly, TrabTort together with DA contribute to set apart *H. sapiens* from all the other primates on the PC1-PC3 plot (Fig. 5). Specifically, *H. sapiens* is apparently set apart for relatively higher DA and relatively lower TrabTort. This pattern arising from our multivariate visual assessment opens up the possibility that at least the peculiar hominin bipedalism may relate to distal fibula trabecular structure. Indeed, the fact that *H. sapiens* is partially distinct from all the other primates because of its higher anisotropy value could have a functional explanation. As detailed above, DA is commonly associated with the extent to which movements in a joint follow repeated directions and a highly anisotropic trabecular structure is expected in highly stereotypically loaded joints. It led us to expect higher DA in terrestrial taxa (see above). It is possible, however, that the infrequent but not absent arboreal behaviors (not absent in any living non-human primates, as we specified defining DOA in this

work) of terrestrial but not bipedal primates (e.g. baboons) prevent their distal fibula trabecular bone to develop a particularly anisotropic structure. In this framework, higher anisotropy would be instead shown by *H. sapiens* which never experiences arboreal habits and obligatorily performs bipedalism, involving strong antero-posterior movements in the sagittal plane. From the distribution of DA values of the studied specimens, three of the five *H. sapiens* fibulae yielded the highest DA values in the entire sample, with a fourth *H. sapiens* fibula yielding the fifth highest DA value (Table S1). We used single specimens results distribution also to better interpret TrabTort outcomes, since this parameter yielded unclear trends in the PC1-PC2 plot (see above) but, similarly to DA, seems to set apart *H. sapiens* from all the other primates in the PC1-PC3 plot. Strikingly, the five *H. sapiens* fibulae yield the lowest $TrabTort_{Mean}$ of the entire sample (also after log-transforming the values in Table S1, since TrabTort was log-transformed for the univariate tests, see Table 3). It supports the presence of this additional distinctive feature in the human distal fibula. As for DA, a functional interpretation is possible for TrabTort, too. We expected TrabTort to directly relate to load frequency (Table 2) and we hypothesized that load frequency on the fibula would be proportional to the extent to which arboreal substrates are used. If, as suggested above, the infrequent but still present arboreal behaviors of baboons affect their distal fibula trabecular bone, *H. sapiens* would be distinctive since almost never experiencing, in its ankle, the frequent laterally directed SRFs of the arboreal environment (see above). It would explain the evidently less tortuous human trabecular structure in the distal fibula. Hence, raw results for DA and TrabTort fully support the hypothesis of a functionally higher DA and lower TrabTort in the distal fibula of *H. sapiens*. It may stimulate future dedicated works with properly built samples to test this pattern and exclude other factors (see for instance the fact that for $TrabTort_{Mean}$, the sixth lowest value is of the *H. sapiens*' sister taxon, *P. troglodytes*, Table S2, hence phylogenetic effects should also be tested). The raw DA value measured for *O. crassicaudatus* is not outstanding (Table S2), suggesting that the portion of DA variance contributing to set apart this species from the other primates in the PC3-PC4 plot (Fig. S4) is negligible. On the other hand, what mainly drives the morphospaces position of *O. crassicaudatus* (in PC1-PC3, PC2-PC3 and PC3-PC4 plots, Fig. 5, Fig. S4) is TrabLen, for which the species show the highest value, and the same is true for *C. jacchus*, yielding the lowest TrabLen value (Table S1

data after size-correction, to comply with results in Table 3). The fact that these two species are both arboreal and leapers (see discussion below) makes it challenging to relate such a pattern to locomotion. Since this trait is the only one that showed a significant phylogenetic signal both before and after size-correction (Table 3 and Table 4), the observed TrabLen pattern follows the phylogeny (e.g. a quite low TrabLen is shown by *C. jacchus* sister taxon too, i.e. *Mico* spp., and a pretty high TrabLen is shown by *O. crassicaudatus* sister taxon too, i.e. *P. diadema*; Fig. S3).

4.1.2. Body mass and phylogenetic relationships

Apart from minor trends potentially related to human bipedalism (see above), primate distal fibula trabecular architecture is overall strongly affected by body size and phylogenetic structure, as evinced from inferential univariate and multivariate analyses, and visualization of trait variability relative to body mass and phylogenetic relationship (Table 3, Table 4, Fig. 4, Fig. S2A, B, Fig. S3, Fig. S4). The particularly strong relationship of morphology with allometry and phylogeny, more than ecology, that we found here, mirrors the outcomes of previous works comparing primate anatomy across wide phylogenetic frameworks (e.g. studying mandibular shape, Plomp et al. 2024, Veneziano et al. 2019) (see also discussion above on large-scale phylogenetic effects). Before discussing the potential implications of body mass and phylogeny and their correlation with primate distal fibula trabecular structure, it is important to stress that in the sample that we studied, body mass and phylogenetic structure are highly correlated (Table 3), i.e. the distribution of body mass proxy is strongly related to phylogeny. A consequence of this outcome is that we did not separate the effects of these two factors. Hence, it is possible that only one of the two factors is primarily related to primate distal fibula trabecular structure, with the other factor that rather yielded significant correlation with morphology only because of significant correlation between size and phylogeny. With the data collected in this study, it is not possible to disentangle the effects of body mass and phylogenetic structure. As a supplementary analysis, we wanted to test if this issue is a limitation related to our sample or it may be a general problem in clade-wise comparative studies in primates. Using body mass estimates for 742 species of extinct and extant primates plus plesiadapiforms (Tillquist et al., 2016), we log-

transformed them and we matched body mass data to the mammal phylogeny of Upham et al., (2019), excluding all the taxa that are not represented by both phylogeny and the body mass dataset. We obtained a phylogenetically informed body mass dataset of 250 primate species. It allowed us to test how body mass is related to phylogeny on a wide taxonomic scale, computing the phylogenetic signal through Pagel's λ (see Methods). We obtained a $\lambda = 0.99$ with a p-value < 0.001, suggesting that the limitation of body mass - phylogenetic structure correlation is not depending on our studied sample but may be unavoidable for most of the comparative morphological studies in primates. We suggest researchers aiming to disentangle how different factors relate to primate anatomical evolution to account for this potential bias.

Concerning the effect of body mass on trabecular traits, numerous studies on different skeletal elements have proposed different trends in mammals and in primates (e.g. Bird et al., 2021; Christen et al., 2015; Cotter et al., 2009; Doube et al., 2011; Fajardo et al., 2013; Hernandez et al., 2009; Kivell, 2016; Kivell et al., 2018; Komza and Skinner, 2019; Ryan and Shaw, 2013; Scherf, 2008; Schilling et al., 2014; Swartz et al., 1998; Tsegai et al., 2017). For instance, it has been found that DA is often independent from body mass, that BV/TV scales with positive allometry (Barak et al., 2013b; Christen et al., 2015; Doube et al., 2011) and that Tb.Th frequently scales with negative allometry (Barak et al., 2013b; Doube et al., 2011; Ryan and Shaw, 2013; Swartz et al., 1998). For DA and Tb.Th, the distal fibula seems to align with other skeletal elements in primates. Indeed, we found that DA does not relate to body mass. As for the allometric pattern shown by Tb.Th, with a regression slope that is positive but lower than 1 (i.e. 0.07) , it apparently confirms that trabecular thickness scales with negative allometry in the distal fibula, too. On the other hand, our results for BV/TV, i.e. no significant relationship with body mass, apparently contrast what was found in some previous works. One should note that, however, exceptions to the proposed patterns of primate trabecular traits-body mass covariation have been found (e.g. Fajardo et al., 2013; Komza and Skinner, 2019; Ryan and Shaw, 2013; Tsegai et al., 2017), and that likely a bone and taxon-dependency exists (Bird et al., 2021; Cotter et al., 2009; Fajardo et al., 2013; Kivell, 2016; Ryan and Shaw, 2013). Hence, our outcomes add to the information on how trabecular traits relate to body size across the primate skeletal elements. Furthermore, we provide the first evidence for patterns of body size covariation concerning the

topological indices recently proposed by Veneziano et al. (2021). For both traditional trabecular parameters and topological indices, future analyses of allometric scaling patterns are needed.

As for the phylogenetic effect on primate trabecular structure, it is likewise challenging to outline general patterns (Kivell, 2016). Several works investigated how trabecular traits relate to the phylogenetic structure (Doube et al., 2011; Ryan and Shaw, 2012, 2013; Smaers and Vinicius, 2009; Tsegai et al., 2013) with some of them yielding a weak phylogenetic signal and others finding a complex scenario of anatomical variation (e.g. Doube et al., 2011, Ryan and Shaw, 2012, 2013). The pattern of differential evolutionary influence on different skeletal regions, i.e. mosaic evolution, is now recognized as a major factor to explain morphological diversity in primates (e.g. Bastir and Rosas, 2009), mammals (e.g. Barton and Harvey, 2000), and in other vertebrates (e.g. Navalón et al., 2022). With this work, we suggest that the distal fibula trabecular bone in primates may be strongly affected by the phylogenetic structure (but see discussion above on body mass-phylogeny correlation). Importantly, it was shown that the strength of the phylogenetic effect not only varies among anatomical regions but also among taxonomic groups (Kivell, 2016; Ryan and Shaw, 2013). Hence, although the results of this work led us to discourage the use of distal fibula trabecular structure to infer DOA in extinct primates due to the presence of phylogenetic signal, it is also possible that the effects of phylogeny may be less important if more restricted primate taxonomic contexts are studied (Marchi, 2007, 2015b; Marchi et al., 2022). Thus, it is still possible that if the fibula is compared among closely related primate species, as often occurs with the study of hominids in an anthropological context (e.g. see also Berles et al., 2024, studying closely related tamarins), a functional signal related to DOA can be detected because large scale phylogenetic effects would be minimized. It can also explain the discrepant patterns found for internal and external anatomy of the distal fibula in relation to DOA (see discussion above). Since we only included two hominids in this work, this very small sample prevents any assessment of trabecular structure diversity restricted to only hominids and, hence, we cannot here discuss on such short phylogenetic scale. However, the aforementioned potential relationships shown by DA and TrabTort with human bipedalism (representing the terrestrial extreme of the DOA range in hominids) should encourage future studies to address this aspect.

978 **4. 2. Potential limitations**

979 Some methodological and theoretical aspects potentially represent limitations of this work. First, we only
980 focused on the proximal articular facet (here termed PAF) of the fibulotalar articulation of the distal fibula,
981 not including the trabecular bone underlying the distal articular facet (DAF) of the same articulation (Fig.
982 2). Since the external morphology (e.g. surface area, morphometric indices) of DAF, similar to that of PAF,
983 proved to be related to different locomotor behaviors (Marchi, 2015b), one may expect a locomotor signal
984 in DAF internal bone, too. As mentioned in the Materials and Methods, one of the reasons behind our choice
985 to exclude DAF was the overly wide variability in external morphology of this articular facet. Based on
986 Marchi (2015b), we expected DAF to be approximately triangular in the studied sample but, probably due
987 to the taxonomical diversity considered here, we found it challenging to reliably recognize a homologous
988 region in all the specimens. Several works addressed bone inner structure by studying the regional variation
989 of trabecular traits within specific joints/epiphyses (both using multiple regularly shaped ROIs; e.g. Su et
990 al., 2013; Sylvester and Terhune, 2017, and mapping the variability within entire epiphyses, e.g. Georgiou
991 et al., 2019; Sukhdeo et al., 2020). Hence, it is possible that a regional variability in trabecular properties
992 exists across PAF and DAF and that, by excluding inner bone related to DAF, we hid some potentially
993 informative locomotor signal. Indeed, the same wide variability in DAF external morphology that prevented
994 us from extracting trabecular bone may reflect adaptations to different locomotor behaviors. However, it
995 should be noted that our approach of studying the entire trabecular bone volume underlying PAF already
996 represents an advance compared to the traditional approach based on the extraction of regularly-shaped
997 ROIs. The latter was tested at a preliminary stage of this work, but it proved challenging to be applied due
998 to the irregular 3D morphology of the distal fibula region corresponding to DAF (see Fig. 2D), e.g. humeral
999 head and femoral head are easily studied through spherical ROIs due to the approximately spherical 3D
1000 shape of the entire articulation itself, but this does not apply to the region we were interested in. While the
1001 issue of sampling complexly shaped joints through regularly shaped ROIs may be fixed by using multiple
1002 smaller volumes instead of a single larger one (e.g. Barak et al. 2013a; Su et al. 2013, Su and Carlson, 2017),
1003 in our particular case this approach would have been problematic due to another practical issue, that

additionally motivated our choice to exclude DAF and is partially related to the high morphological variability of DAF mentioned above. Indeed, due to the highly variable DAF shape, some species showed a DAF that is a dramatically wide and short 'triangle', i.e. with an extremely small proximodistal size. In such cases, the stack representing the trabecular bone underlying DAF is compounded by too few trabeculae (often fewer than the minimum recommended limit of 50, see Methods). If this issue prevented us from extracting a single informative stack for all trabecular bone underlying DAF, it is easy to imagine how this limitation would have been even more severe if multiple smaller volumes would have been used. Finally, it is remarkable that PAF, studied in this work, represents most of the trabecular bone of the fibulotalar articulation (as one can see from PAF and DAF size proportions in Fig. 2). A possible solution for future works is studying the trabecular bone underlying the entire fibulotalar articulation (PAF + DAF), developing another ad-hoc orientation protocol, and investigating variation in trabecular parameters in the whole region (e.g. using a heat-map approach, available in Veneziano et al., 2021).

Another potential limitation of this work may derive from the fact that testing the relationship between distal fibula trabecular bone and DOA may involve pooling in the same discrete state species that are quite different concerning other aspects of their locomotor behavior (e.g. forelimb vs. hindlimb reliance, presence of distinctive habits as leaping) that, in turn, reasonably involve different functional demands. Although these aspects were not the main focus of this work, one should consider the possibility that primate distal fibula trabecular bone does not vary according to DOA, as fibula CSG or distal fibula external morphology (see above), but instead it follows other locomotor factors. This issue is particularly exacerbated for taxa that in this work were categorized as 'arboreal', e.g. spider monkeys (*A. paniscus*) and sifakas (*P. diadema*), that are more specialized in their locomotor habits compared to more generalized arboreal quadrupeds as colobines (*C. guereza*) and howler monkeys (*A. seniculus*) (Fleagle, 2013b). To further evaluate potential locomotor effects undetected in this work, we ran a supplementary analysis accounting for the frequency of specific locomotor behaviors of the studied taxa, instead of their DOA. As detailed in Supplementary Note 1 and Fig. S5, we highlighted that, mirroring what we found for DOA, the primate distal fibula trabecular structure probably does not relate to other locomotor aspects.

Another issue partially related to locomotor categorization is the possibility that pooling *H. sapiens* - whose bipedalism involves a greater predominance of loads in the hindlimbs - with terrestrial baboons may skew the results. Also, pooling *P. troglodytes* - which shows dominant quadrupedal walking - with unspecialized taxa such as *Chlorocebus* spp. (Supplementary Note 1 and Fig. S5) may cause the same problem. To evaluate effects potentially deriving from this bias, we re-ran the PCA used to visualize interspecific patterns after excluding *H. sapiens* and then after excluding both *H. sapiens* and *P. troglodytes*. As shown by these additional PCAs (Figs. S6-S7) and as discussed in Supplementary Note 2, these exclusions do not change the main outcome of this work. Namely, the primate distal fibula trabecular bone does not appear to be associated with locomotor behaviors, neither DOA nor other locomotor aspects (see above and Supplementary Note 1), with the only possible exception represented by minor trends related to bipedalism in hominins (see discussion above).

Finally, while we studied interspecific patterns of distal fibula trabecular bone variation, our data are mostly based on single specimens for each species. Hence, in this work the effects related to intraspecific variability are not accounted for. Since for four of the studied taxa we sampled more than one fibula (Table 1), we were however able to assess potential biases deriving from intraspecific variability. To do so, we ran an additional PCA with the observations being the single specimens instead of the taxa (Fig. S8) and we measured the coefficient of variation (Table S2). As discussed in Supplementary Note 3, the intraspecific variability can be generally considered low to moderate.

5. Conclusions

In this study, we carried out the first three-dimensional quantitative interspecific analysis of distal fibula trabecular structure in primates, in order to test for a functional signal related to the degree of arboreality. We expected for such a signal to be present based on results from studies on other fibular traits (diaphyseal cross-sectional properties and distal epiphyseal external morphology). Contrasting previously highlighted trends, the internal trabecular bone in primate distal fibula does not correlate with the degree of arboreality. Although we identified some trends potentially related to alternative locomotor factors not strictly related

to DOA as defined in this work (i.e. human bipedalism), we found that body mass and phylogenetic relationships primarily and strongly affect the trabecular network in primate distal fibula. We provided evidence for the factors mainly associated with the previously unstudied primate distal fibula internal structure. We encourage future studies to address some critical aspects arisen from this work, e.g. the potential relationship between human bipedalism and specific trabecular traits of the distal fibula, i.e. degree of anisotropy and tortuosity, the strong correlation between primate body mass and phylogenetic structure in comparative analyses on a wide taxonomic scale.

Acknowledgements

We thank two anonymous reviewers and the Editor-in-Chief, Philip Cox, for their precious comments and suggestions. Moreover, we thank curators who allowed us to collect bone specimens: Paolo Agnelli (University of Florence, Florence Museal System, section La Specola) and Monica Zavattaro (University of Florence, Florence Museal System, section of Anthropology and Ethnology). We thank Ana Galvez, Léo Botton-Divet (Humboldt Universität zu Berlin, Berlin, Germany), Neil Duncan (American Museum of Natural History, AMNH, New York, USA), Sharon Grant (Field Museum of Natural History, FMNH, Chicago, USA), Janeen Jones (FMNH), Kate Webbink (FMNH), Adam Ferguson (FMNH) for uploading and/or allowing us access to µCT data on MorphoSource (see catalogue number and collections in Table S1). We also thank Aaron Clauset (University of Colorado Boulder, USA) and Lauren Glenny Shoemaker (University of Wyoming, USA) for allowing us to download and use data on primate body mass estimates (from Tillquist et al., 2016). A.V. is funded by the NextGenerationEU, Maria Zambrano fellowship (2021URV-MZ-16). F.A. is financed by the project grant TMPFP3_217022 from the Swiss National Science Foundation (https://www.snf.ch; SNSF Swiss Postdoctoral Fellowships, SPF).

Author contributions

F.A. and D.M. collected the sample. F.A. processed and analyzed µCT data, performed statistical analyses, and drafted the manuscript. D.P. and P.A.S. made possible the acquisition of new µCT data. A.V. and E.A. contributed to process and analyze of µCT data, to compute trabecular parameters and to perform

statistical analyses. All authors conceived the study, interpreted results and contributed to manuscript writing and editing.

Conflict of interest statement

The authors have no conflicts of interest to declare

Data availability statement

Raw data (Table S1), Supplementary Material (Additional Methods and Additional Results), time-tree (in nexus format) and the R code are downloadable from Figshare (https://figshare.com/s/5f267cb7aab364b2b019) (Alfieri et al. 2024). Data on isolated distal fibula trabecular architecture (both image stacks and skeletonized networks) and distal fibula µCT scans are made available upon reasonable request. The R package 'indianaBones' is available at https://github.com/AlessioVeneziano/IndianaBones and at https://zenodo.org/record/7615165.

References

Alfieri, F., Veneziano A., Panetta D., Salvadori P.A., Amson E., Marchi D. 2024. Data from: The relationship between primate distal fibula trabecular architecture and degree of arboreality, phylogeny and size. Figshare dataset. https://figshare.com/s/5f267cb7aab364b2b019

Alfieri, F., Botton-Divet, L., Wölfer, J., Nyakatura, J.A., Amson, E., 2023. A macroevolutionary common-garden experiment reveals differentially evolvable bone organization levels in slow arboreal mammals. Comms Bio 6(1), 995. https://doi.org/10.1038/s42003-023-05371-3

Alfieri, F., Botton-Divet, L., Nyakatura, J.A., Amson, E., 2022. Integrative approach uncovers new patterns of ecomorphological convergence in slow arboreal xenarthrans. J Mamm Evol. 29(2), 283-312 https://doi.org/10.1007/s10914-021-09590-5

Alfieri, F., Nyakatura, J.A., Amson, E., 2021. Evolution of bone cortical compactness in slow arboreal mammals. Evolution 75, 542–554. https://doi.org/10.1111/evo.14137

Ammann, P., Rizzoli, R., 2003. Bone strength and its determinants. Osteoporosis international 14, 13–18.

Amson, E., Bibi, F., 2021. Differing effects of size and lifestyle on bone structure in mammals. BMC Biol 19, 87. https://doi.org/10.1186/s12915-021-01016-1

Anapol, F., Turner, T.R., Mott, C.S., Jolly, C.J., 2005. Comparative postcranial body shape and locomotion in *Chlorocebus aethiops* and *Cercopithecus mitis*. Am. J. Phys. Anthropol. 127, 231–239.

Anemone, R.L., Covert, H.H., 2000. New skeletal remains of *Omomys* (Primates, Omomyidae): functional morphology of the hindlimb and locomotor behavior of a Middle Eocene primate. J. Hum. Evol. 38(5), 607–633.

Annadhason, A., 2012. Methods of fractal dimension computation. IJCSIS 2(1), 166–169.

1114 Auerbach, B.M, Ruff C.B. 2006. Limb bone bilateral asymmetry: variability and commonality among
1115 modern humans. J. Hum. Evol 50:203-218.
1116 Auerbach, B.M., Gooding, A.F., Shaw, C.N., Sylvester, A.D., 2017. The relative position of the human
1117 fibula to the tibia influences cross-sectional properties of the tibia. Am J Phys Anthropol 163,
1118 148–157. https://doi.org/10.1002/ajpa.23196
1119 Barak, M.M., Lieberman, D.E., Hublin, J.J., 2013b. Of mice, rats and men: trabecular bone architecture in
1120 mammals scales to body mass with negative allometry. J Struct Biol 183, 123-131.
1121 Barak, M.M., Lieberman, D.E., Hublin, J.-J., 2011. A Wolff in sheep's clothing: trabecular bone
1122 adaptation in response to changes in joint loading orientation. Bone 49, 1141–1151.
1123 https://doi.org/10.1016/j.bone.2011.08.020
1124 Barak, M. M., Lieberman, D.E., Raichlen, D., Pontzer, H., Warrener, A.G., Hublin, J.J., 2013a. Trabecular
1125 evidence for a human-like gait in *Australopithecus africanus*. PLoS ONE 8, e77687.
1126 Barnett, C.H., Napier, J.R., 1953. The rotatory mobility of the fibula in eutherian mammals. J Anat 87,
1127 11–21.
1128 Barnett, C.H., Napier, J.R., 1952. The axis of rotation at the ankle joint in man. Its influence upon the
1129 form of the talus and the mobility of the fibula. J Anat 86(1).
1130 Barrett, A.S., 2005. Foraging ecology of the vervet monkey (*Chlorocebus aethiops*) in mixed lowveld
1131 bushveld and sour lowveld bushveld of the Blydeberg Conservancy, Northern Province, South
1132 Africa. PhD dissertation. University of South Africa.
1133 Barton, R.A., Harvey, P.H., 2000. Mosaic evolution of brain structure in mammals. Nature 405, 1055–
1134 1058.
1135 Bassey, E.J., Ramsdale, S.J. 1994. Increase in femoral bone density in young women following high-
1136 impact exercise. Osteoporosis Int 4, 72–75.
1137 Bastir, M., Rosas, A., 2009. Mosaic evolution of the basicranium in *Homo* and its relation to modular
1138 development evolutionary biology. Evol. Biol. 36, 57–70.
1139 Berles, P., Heymann, E.W., Golcher, F., Nyakatura, J.A., 2022. Leaping and differential habitat use in
1140 sympatric tamarins in Amazonian Peru. J. Mammal. 103(1), 146–158.
1141 Berles, P., Wölfer, J., Alfieri, F., Botton-Divet, L., Guery, J.P., Nyakatura, J.A., 2024. Linking
1142 morphology, performance, and habitat utilisation: adaptation across biologically relevant "levels"
1143 in tamarins. BMC Ecol. Evol. In press.
1144 Biewener, A.A., Fazzalari, N.L., Konieczynski, D.D., Baudinette, R.V., 1996. Adaptive changes in
1145 trabecular architecture in relation to functional strain patterns and disuse. Bone 19, 1–8.
1146 https://doi.org/10.1016/8756-3282(96)00116-0
1147 Bird, E.E., Kivell, T.L., Skinner, M.M., 2021. Cortical and trabecular bone structure of the hominoid
1148 capitate. J Anat 239.2, 351–373.
1149 Burr, D.B., Piotrowski, G., Miller, G.J., 1981. Structural strength of the macaque femur. Am. J. Phys.
1150 Anthropol. 54, 305–319.
1151 Carleton, A., 1941. A comparative study of the inferior tibio-fibular joint. J Anat 76, 45–55.
1152 Carlson, K.J., 2005. Investigating the form-function interface in African apes: Relationships between
1153 principal moments of area and positional behaviors in femoral and humeral diaphyses. Am. J.
1154 Phys. Anthropol. 127, 312–334. https://doi.org/10.1002/ajpa.20124
1155 Carlson, K.J., Demes, B., Franz, T.M., 2005. Mediolateral forces associated with quadrupedal gaits of
1156 lemurids. J. Zool. Lond. 266, 261e273.
1157 Carlson, K.J., Lublinsky, S., Judex, S., 2008. Do different locomotor modes during growth modulate
1158 trabecular architecture in the murine hind limb? ICB 48, 385–393.
1159 https://doi.org/10.1093/icb/icn066
1160 Carlson, K.J., Marchi, D., 2014. Reconstructing Mobility: Environmental, Behavioral, and Morphological
1161 Determinants. Springer, New York.
1162 Carter, D.R., Beaupré, G.S., 2007. Skeletal Function and Form: Mechanobiology of Skeletal
1163 Development, Aging, and Regeneration. Cambridge: Cambridge University Press.
1164 Cendre, E., Mitton, D., Roux, J. P., Arlot, M. E., Duboeuf, F., Burt-Pichat, B., Rumelhart C., Peix G.,
1165 Meunier, P. J. 1999. High-resolution computed tomography for architectural characterization of

human lumbar cancellous bone: relationships with histomorphometry and biomechanics. Osteoporosis International, 10, 353-360.
Chang, G., Pakin, S.K., Schweitzer, M.E., Saha, P.K., Regatte, R.R., 2008. Adaptations in trabecular bone microarchitecture in Olympic athletes determined by 7T MRI. J Magn Reson Imaging. 27(5), 1089–95.
Chappard, D., Chennebault, A., Moreau, M., Legrand, E., Audran, M., Basle, M.F., 2001. Texture analysis of X-ray radiographs is a more reliable descriptor of bone loss than mineral content in a rat model of localized disuse induced by the *Clostridium botulinum* toxin. Bone 28(1), 72–79.
Chen, M., Wilson, G.P., 2015. A multivariate approach to infer locomotor modes in Mesozoic mammals. Paleobiology 41, 280–312. https://doi.org/10.1017/pab.2014.14
Chiu, C., Hamrick, M.W., 2002. Evolution and development of the primate limb skeleton. Evol. Anthropol. Issues News Rev. 11, 94–107. https://doi.org/10.1002/evan.2002
Christen, P., Ito, K., van Rietbergen, B., 2015. A potential mechanism for allometric trabecular bone scaling in terrestrial mammals. J Anat 226, 236–243.
Cichański, A., Nowicki, K., Mazurkiewicz, A., Topoliński, T., 2010. Investigation of statistical relationships between quantities describing bone architecture, its fractal dimensions and mechanical properties. Acta Bioeng Biomech, 12(4), 69–77.
Clavel, J., Escarguel, G., Merceron, G., 2015. mvmorph: an R package for fitting multivariate evolutionary models to morphometric data. Methods Ecol Evol 6, 1311–1319. https://doi.org/10.1111/2041-210X.12420
Cooper, K.L., 2019. Developmental and evolutionary allometry of the mammalian limb skeleton. ICB 59, 1356–1368. https://doi.org/10.1093/icb/icz082
Cotter, M.M., Simpson, S.W., Latimer, B.M., Hernandez, C.J., 2009. Trabecular microarchitecture of hominoid thoracic vertebrae. Anat Rec 292, 1098–1106.
Crompton, R.H., Günther, M., 2004. Humans and other bipeds: the evolution of bipedality. J Anat 204.5, 317.
Cunningham, C.A., Black, S.M., 2010. The neonatal ilium – metaphyseal drivers and vascular passengers. Anat Rec 293, 1297-1309.
Cunningham, C. A., Black, S.M., 2009a. Anticipating bipedalism: trabecular organization in the newborn ilium. J. Anat. 214, 817–829. https://doi.org/10.1111/j.1469-7580.2009.01073.x
Cunningham, C. A, Black, S.M., 2009b. Development of the fetal ilium – challenging concepts of bipedality. J Anat 214, 91–99. https://doi.org/10.1111/j.1469-7580.2008.01005.x
Currey, J.D., 2002. Bones: Structure and Mechanics. Princeton University Press.
Demes, B., Jungers, W.L., 1993. Long bone cross-sectional dimensions, locomotor adaptations and body size in prosimian primates. J Hum Evol 25, 57–74. https://doi.org/10.1006/jhev.1993.1038
Demes, B., Carlson K. J., Franz T.M. 2006. Cutting corners: the dynamics of turning behaviors in two primate species. J Exp Biol 209.5: 927-937.
Demes, B., Carlson, K. J. 2009. Locomotor variation and bending regimes of capuchin limb bones. Am J Phys Anthropol, 139(4), 558-571.
DeSilva, J.M., Devlin, M.J., 2012. A comparative study of the trabecular bony architecture of the talus in humans, non-human primates, and *Australopithecus*. J Hum Evol 63, 536–551. https://doi.org/10.1016/j.jhevol.2012.06.006
DeSilva, J.M., Morgan, M.E., Barry, J.C., Pilbeam, D., 2010. A hominoid distal tibia from the Miocene of Pakistan. J Hum Evol 58(2), 147-154.
Ding, Y., Song, Y., 2002. Function of fibula in stability of ankle joint. Zhongguo Xiu Fu Chong Jian Wai Ke Za Zhi 16, 245–247.
Doube, M., Kłosowski, M.M., Arganda-Carreras, I., Cordelières, F.P., Dougherty, R.P., Jackson, J.S., Schmid, B., Hutchinson, J.R., Shefelbine, S.J., 2010. BoneJ: Free and extensible bone image analysis in ImageJ. Bone 47, 1076–1079. https://doi.org/10.1016/j.bone.2010.08.023
Doube, M., Klosowski, M.M., Wiktorowicz-Conroy, A.M., Hutchinson, J.R., Shefelbine, S.J., 2011. Trabecular bone scales allometrically in mammals and birds. Proc. Biol. Sci. 278, 3067–3073. https://doi.org/10.1098/rspb.2011.0069

Eriksen, E.F., 2010. Cellular mechanisms of bone remodelling. Rev Endocr Metab Disord 11, 219–227.
Eriksen, E.F., 1986. Normal and pathological remodeling of human trabecular bone: three dimensional reconstruction of the remodeling sequence in normals and in metabolic bone disease. Endocr Rev 7, 379–408.
Fajardo, R.J., DeSilva, J.M., Manoharan, R.K., Schmitz, J.E., Maclatchy, L.M., Bouxsein, M.L., 2013. Lumbar vertebral body bone microstructural scaling in small to medium-sized strepsirhines. Anat Rec 296(2), 210–226.
Fajardo, R.J., Müller, R., 2001. Three-dimensional analysis of nonhuman primate trabecular architecture using micro-computed tomography: Primate Trabecular Bone and the 3-D μCT Method. Am. J. Phys. Anthropol. 115, 327–336. https://doi.org/10.1002/ajpa.1089
Falconer, K., 2004. Fractal geometry: Mathematical foundations and applications (2nd ed.). Chichester: Wiley.
Feder, J., 1988. Fractals. New York: Plenum.
Feltrin, G.P., Macchi, V., Saccavini, C., Tosi, E., Dus, C., Fassina, A., Parenti, A., De Caro, R., 2001. Fractal analysis of lumbar vertebral cancellous bone architecture. Clin Anat 14(6), 414–417.
Feltrin, G.P., Stramare, R., Miotto, D., Giacomini, D., Saccavini, C., 2004. Bone fractal analysis. Curr. Osteoporos. Rep. 2(2), 53-58.
Fleagle, J.G., 2013. Primate Adaptation and Evolution - 3rd Edition. Academic press. (doi:10.1016/C2009-0-01979-5).
Ford, S.M., Morgan, G.S., 1986. A new ceboid femur from the late Pleistocene of Jamaica. J. Vertebr. Paleontol. 6(3), 281–289.
Frost, H.M., 1987. Bone 'mass' and the 'mechanostat': a proposal. Anat Rec 219, 1–9.
Frost, S.R., Marcus, L.F., Bookstein, F.L., Reddy, D.P., Delson, E., 2003. Cranial allometry, phylogeography, and systematics of large-bodied papionins (primates: Cercopithecinae) inferred from geometric morphometric analysis of landmark data. Anat Rec 275(2), 1048–1072.
Funk, J.R., Rudd, R.W., Kerrigan, J.R., Crandall, J.R., 2004. The Effect of Tibial Curvature and Fibular Loading on the Tibia Index. Traffic Inj. Prev. 5, 164–172. https://doi.org/10.1080/15389580490436069
Fyhrie, D.P., Zauel, R., 2015. Directional tortuosity as a predictor of modulus damage for vertebral cancellous bone. J. Biomech. Eng. 137(1), 011007.
Garbino, G.S., Nascimento, F.O., 2014. *Mico humeralifer* (Primates: Callitrichidae). Mamm. Species 46(911), 40–47.
García-Vilana, S., Sánchez-Molina, D., Velázquez-Ameijide, J., Llumà, J., Arregui-Dalmases, C., 2023. Relation between mechanical and densimetric properties to fractal dimension in human rib cortical bone. Med. Eng. Phys. 104004.
Garrahan, N.J., Mellish, R.W.E., Vedi, S., Compston, J.E., 1987. Measurement of mean trabecular plate thickness by a new computerized method. Bone 8(4), 227–230.
Gebo, D.L., 2014. Primate Comparative Anatomy. JHU Press.
Gebo, D.L., 2011. Vertical clinging and leaping revisited: Vertical support use as the ancestral condition of strepsirrhine primates. Am. J. Phys. Anthropol. 146, 323–335. https://doi.org/10.1002/ajpa.21595
Gebo, D.L., 1989. Postcranial adaptation and evolution in lorisidae. Primates 30, 347–367. https://doi.org/10.1007/BF02381259
Gebo, D.L., Smith, R., Dagosto, M., Smith, T., 2015. Additional postcranial elements of *Teilhardina belgica*: The oldest European primate. Am. J. Phys. Anthropol. 156, 388–406. https://doi.org/10.1002/ajpa.22664
Georgiou, L., Kivell, T.L., Pahr, D.H., Buck, L.T., Skinner, M.M., 2019. Trabecular architecture of the great ape and human femoral head. J. Anat. 234, 679–693. https://doi.org/10.1111/joa.12957
Georgiou, L., Kivell, T.L., Pahr, D.H., Skinner, M.M., 2018. Trabecular bone patterning in the hominoid distal femur. PeerJ 6, e5156. https://doi.org/10.7717/peerj.5156

Ghasem-Zadeh, A., Galea, M.P., Nunn, A., Panisset, M., Wang, X.-F., Iuliano, S., Boyd, S.K., Forwood, M.R., Seeman, E., 2021. Heterogeneity in microstructural deterioration following spinal cord injury. Bone 142, 115778. https://doi.org/10.1016/j.bone.2020.115778
Godfrey, L.R., 1988. Adaptive diversification of Malagasy strepsirrhines. J Hum Evol 17. 1–2, 93–134.
Goh, J.C., Mech, A.M., Lee, E.H., Ang, E.J., Bayon, P., Pho, R.W., 1992. Biomechanical study on the load-bearing characteristics of the fibula and the effects of fibular resection. Clin. Orthop. Relat. Res. 223–228.
Gomberg, B.R., Saha, P.K., Song, H.K., Hwang, S.N., Wehrli, F.W., 2000. Topological analysis of trabecular bone MR images. IEEE TMI 19(3), 166-174.
Hagihara, Y., Nara, T., 2016. Morphological features of the fibula in Jomon hunter-gatherers from the shell mounds of the Pacific coastal area: morphological features of the fibula in the Jomon population. Am. J. Phys. Anthropol. 160, 708–718. https://doi.org/10.1002/ajpa.23000
Harmon, E.H., 2007. The shape of the hominoid proximal femur: a geometric morphometric analysis. J. Anat. 210, 170–185. https://doi.org/10.1111/j.1469-7580.2006.00688.x
Harrigan, T.P., Mann, R.W., 1984. Characterization of microstructural anisotropy in orthotropic materials using a second rank tensor. J Mater Sci 19, 761–767.
Heaton, J.L., Pickering, T.R., Carlson, K.J., Crompton, R.H., Jashashvili, T., Beaudet, A., Bruxelles, L., Kuman, K., Heile, A.J., Stratford, D., Clarke, R.J., 2019. The limb bones of the StW573 *Australopithecus* skeleton from Sterkfontein Memner 2: descriptions and proportions. J. Hum. Evol. 133, 167–197.
Hébert, D., Lebrun, R., Marivaux, L., 2012. Comparative three-dimensional structure of the trabecular bone in the talus of primates and its relationship to ankle joint loads generated during locomotion. Anat Rec 295, 2069–2088. https://doi.org/10.1002/ar.22608
Henderson, K., Pantinople, J., McCabe, K., Richards, H. L., Milne, N. 2017. Forelimb bone curvature in terrestrial and arboreal mammals. PeerJ, 5, e3229.
Hernandez, C.J., Loomis, D.A., Cotter, M.M., Schifle, A.L., Anderson, L.C., Elsmore, L., Kunos, C., Latimer, B., 2009. Biomechanical allometry in hominoid thoracic vertebrae. J Hum Evol 56, 462–470.
Hothorn, T., Bretz, F., Westfall, P., 2008. Simultaneous inference in general parametric models. Biom. J. 50(3), 346--363.
Huiskes, R., Ruimerman, R., van Lenthe, G.H., Janssen, J.D., 2000. Effects of mechanical forces on maintenance and adaptation of form in trabecular bone. Nature 405, 704–706.
Hunt, K.D., 1992. Positional behavior of *Pan troglodytes* in the Mahale mountains and Gombe stream national parks, Tanzania. Am. J. Phys. Anthropol 87.1, 83–105.
Jacobs, C.R., 2000. The mechanobiology of cancellous bone structural adaptation. J Rehab Research Devel 37, 209–216.
Judex, S., Carlson, K.J., 2009. Is bone's response to mechanical signals dominated by gravitational loading? Med Sci Sports Exerc 41, 2037–2043. https://doi.org/10.1249/MSS.0b013e3181a8c6e5
Jungers, W.L., Godfrey, L.R., Simons, E.L., Wunderlich, R.E., Richmond, B.G., Chatrath, P.S., 2002. Ecomorphology and Behavior of Giant Extinct Lemurs from Madagascar, in: In: Reconstructing Behavior in the Primate Fossil Record. Plavcan J.M., Kay R.F., Jungers W.L., van Schaik C.P. (doi: https://doi.org/10.1007/978-1-4615-1343-8_10), Kluwer Academic/Plenum Publishers, New York., pp. 371–411.
Karlsson, C., Obrant, K.J., Karlsson, M., 2001. Pregnancy and lactation confer reversible bone loss in humans. Osteoporos Int 828–834.
Kilbourne, B.M., Hutchinson, J.R., 2019. Morphological diversification of biomechanical traits: mustelid locomotor specializations and the macroevolution of long bone cross-sectional morphology. BMC Evol Biol 19, 37. https://doi.org/10.1186/s12862-019-1349-8
Kimura, T., 2003. Differentiation between fore- and hindlimb bones and locomotor behavior in primates. FPR 74, 17–32. https://doi.org/10.1159/000068391
Kimura, T., 2002. Primate limb bones and locomotor types in arboreal or terrestrial environments. Z. Morphol. Anthropol. 83, 201–219.

Kimura, T., 1995. Long bone characteristics of primates. Z. Morph. Anthrop. 80, 265–580.
Kivell, T.L., 2016. A review of trabecular bone functional adaptation: what have we learned from trabecular analyses in extant hominoids and what can we apply to fossils? J. Anat. 228, 569–594. https://doi.org/10.1111/joa.12446
Kivell, T.L., Davenport, R., Hublin, J.-J., Thackeray, J.F., Skinner, M.M., 2018. Trabecular architecture and joint loading of the proximal humerus in extant hominoids, *Ateles*, and *Australopithecus africanus*. Am J Phys Anthropol 167, 348–365. https://doi.org/10.1002/ajpa.23635
Kivell, T.L., Kibii, J.M., Churchill, S.E., Schmid, P., Berger, L.R. 2011. *Australopithecus sediba* hand demonstrates mosaic evolution of locomotor and manipulative abilities. Science 333, 1411–1417. https://doi.org/10.1126/science.1202625
Komza, K., Skinner, M.M., 2019. First metatarsal trabecular bone structure in extant hominoids and Swartkrans hominins. J Hum Evol 131, 1–21.
Lambers, F. M., Koch, K., Kuhn, G., Ruffoni, D., Weigt, C., Schulte, F. A., Müller, R. 2013. Trabecular bone adapts to long-term cyclic loading by increasing stiffness and normalization of dynamic morphometric rates. Bone, 55(2), 325-334.
Lambert, K.L., 1971. The weight-bearing function of the fibula. A strain gauge study. J Bone Joint Surg Am 53, 507–513.
Landi, F., Alfieri, F., Towle, I., Profico, A., Veneziano, A., 2021. Fluctuating asymmetry and stress in *Macaca fuscata*: does captivity affect morphology? Applied Sciences 11, 7879. https://doi.org/10.3390/app11177879
Libotte, M., Klein, P., Colpaert, H., Alameh, M., Blaimont, P., Halleux, P., 1982. Biomechanical study of the ankle joint. Rev Chir Orthop Reparatrice Appar Mot 68, 299–305.
Liu, X. S., Sajda, P., Saha, P. K., Wehrli, F. W., & Guo, X. E. 2006. Quantification of the roles of trabecular microarchitecture and trabecular type in determining the elastic modulus of human trabecular bone. Journal of Bone and Mineral Research, 21(10), 1608-1617
MacLatchy, L., Müller, R., 2002. A comparison of the femoral head and neck trabecular architecture of *Galago* and *Perodicticus* using micro-computed tomography (μCT). J Hum Evol 43, 89–105. https://doi.org/10.1006/jhev.2002.0559
MacLatchy, L.M., Bossert, W.H., 1996. An analysis of the articular surface distribution of the femoral head and acetabulum in anthropoids, with implications for hip function in Miocene hominoids. J Hum Evol 31, 425–453. https://doi.org/10.1006/jhev.1996.0070
Maga, M., Kappelman, J., Ryan, T.M., Ketcham, R.A., 2006. Preliminary observations on the calcaneal trabecular microarchitecture of extant large-bodied hominoids. Am. J. Phys. Anthropol. 129, 410–417. https://doi.org/10.1002/ajpa.20276
Maquer, G., Musy, S.N., Wandel, J., Gross, T., Zysset, P.K., 2015. Bone volume fraction and fabric anisotropy are better determinants of trabecular bone stiffness than other morphological variables. J. Bone Miner. Res. 30, 1000–1008. https://doi.org/10.1002/jbmr.2437
Marchi, D., 2015a. Variation in tibia and fibula diaphyseal strength and its relationship with arboreal and terrestrial locomotion: extending the investigation to non-hominoid primates. J. Anthropol. Sci 93, 153–156. https://doi.org/10.4436/jass.93005
Marchi, D., 2015b. Using the morphology of the hominoid distal fibula to interpret arboreality in *Australopithecus afarensis*. J Hum Evol 85, 136–148. https://doi.org/10.1016/j.jhevol.2015.06.002
Marchi, D., 2007. Relative strength of the tibia and fibula and locomotor behavior in hominoids. J Hum Evol 53, 647–655. https://doi.org/10.1016/j.jhevol.2007.05.007
Marchi, D., Borgognini-Tarli, M.S., 2004. Cross-sectional geometry of the limb bones of the Hominoidea by biplanar radiography and moulding techniques. J. Anthropol. Sci 82, 89–102.
Marchi, D., Harper, C.M., Chirchir, H., Ruff, C.B., 2019. Relative fibula strength and locomotor behavior in KNM-WT 15000 and OH 35. J. Hum. Evol. 131, 48–60.
Marchi, D., Rimoldi, A., García-Martínez, D., Bastir, M., 2022. Morphological correlates of distal fibular morphology with locomotion in great apes, humans, and *Australopithecus afarensis*. Am. J. Biol. Anthropol. 178(2), 286–300.

Marchi, D., Ruff, C.B., Capobianco, A., Rafferty, K.L., Habib, M.B., Patel, B.A., 2016. The locomotion of *Babakotia radofilai* inferred from epiphyseal and diaphyseal morphology of the humerus and femur. J. Morphol. 277, 1199–1218. https://doi.org/10.1002/jmor.20569

Marchi, D., Shaw, C.N., 2011. Variation in fibular robusticity reflects variation in mobility patterns. J Hum Evol 61, 609–616. https://doi.org/10.1016/j.jhevol.2011.08.005

Marchi, D., Sparacello, V., Shaw, C., 2011. Mobility and Lower Limb Robusticity of a Pastoralist Neolithic Population from North-Western Italy, in: Human Bioarchaeology of the Transition to Agriculture. John Wiley & Sons, Ltd, pp. 317–346. https://doi.org/10.1002/9780470670170.ch13

Marchi, D., Walker, C.S., Wei, P., Holliday, T.W., Churchill, S.E., Berger, L.R., DeSilva, J.M., 2017. The thigh and leg of *Homo naledi*. J. Hum. Evol 104, 174–204.

Meldrum, D.J., 1991. Kinematics of the Cercopithecine foot on arboreal and terrestrial substrates with implications for the interpretation of hominid terrestrial adaptations. Am. J. Phys. Anthropol. 84, 273–290.

Messent, E.A., Buckland-Wright, J.C., Blake, G.M., 2005a. Fractal analysis of trabecular bone in knee osteoarthritis (OA) is a more sensitive marker of disease status than bone mineral density (BMD). Calcif. Tissue Int. 76, 419–425.

Messent, E.A., Ward, R.J., Tonkin, C.J., Buckland-Wright, C., 2005b. Tibial cancellous bone changes in patients with knee osteoarthritis. A short-term longitudinal study using Fractal Signature Analysis. Osteoarthr. Cartil. 13(6), 463–470.

Mielke, M., Wölfer, J., Arnold, P., van Heteren, A.H., Amson, E., Nyakatura, J.A., 2018. Trabecular architecture in the sciuromorph femoral head: allometry and functional adaptation. Zool Lett 4, 10. https://doi.org/10.1186/s40851-018-0093-z

Mittra, E., Rubin, C., Gruber, B., Qin, Y.-X., 2008. Evaluation of trabecular mechanical and microstructural properties in human calcaneal bone of advanced age using mechanical testing, microCT, and DXA. J Biomech 41, 368-375.

Mittra, E., Rubin, C., Qin, Y.-X., 2005. Interrelationships of trabecular mechanical and microstructural properties in sheep trabecular bone. J Biomech 38, 1229–1237.

Moore, K.L., Dalley, A.F., 2006. Clinically Oriented Anatomy, 5th ed. Lippincott Williams & Wilkins, Baltimore.

Napier, J.R., Walker, A.C., 1967. Vertical clinging and leaping-a newly recognized category of locomotor behaviour of primates. Folia Primatol. 6, 204–219. https://doi.org/10.1159/000155079

Navalón, G., Bjarnason, A., Griffiths, E., Benson, R.B., 2022. Environmental signal in the evolutionary diversification of bird skeletons. Nature 611(7935), 306–311.

Ni, X., Gebo, D.L., Dagosto, M., Meng, J., Tafforeau, P., Flynn, J.J., Beard, K.C., 2013. The oldest known primate skeleton and early haplorhine evolution. Nature 498, 60–64. https://doi.org/10.1038/nature12200

Nishimura, T., Morimoto, N., Ito, T., 2019. Shape variation in the facial part of the cranium in macaques and African papionins using geometric morphometrics. Primates 60, 401–419.

Odgaard, A., 1997. Three-dimensional methods for quantification of cancellous bone architecture. Bone 20, 315–328.

O'Neill, M.C., Dobson, S.D., 2008. The degree and pattern of phylogenetic signal in primate long-bone structure. J Hum Evol 54, 309–322. https://doi.org/10.1016/j.jhevol.2007.08.008

O'Neill, M.C., Lee, L.F., Demes, B., Thompson, N.E., Larson, S.G., Stern Jr, J.T., Umberger, B.R., 2015. Three-dimensional kinematics of the pelvis and hind limbs in chimpanzee (*Pan troglodytes*) and human bipedal walking. J Hum Evol 86, 32–42.

Owen, R., 1866. Comparative Anatomy and Physiology of Vertebrates. II. London: Longmans, Green &: Co.

Paradis, E., Claude, J., Strimmer, K., 2004. APE: Analyses of Phylogenetics and Evolution in R language. Bioinformatics 20, 289–290. https://doi.org/10.1093/bioinformatics/btg412

Parkinson, I.H., Badiei, A., Stauber, M., Codrington, J., Müller, R., Fazzalari, N.L., 2012. Vertebral body bone strength: the contribution of individual trabecular element morphology. Osteoporos Int 23, 1957–1965.

Pau, G., Fuchs, F., Sklyar, O., Boutros, M., Huber, W., 2010. EBImage - an R package for image processing with applications to cellular phenotypes. Bioinformatics 26(7), 979–981. https://doi.org/10.1093/bioinformatics/btq046

Pinheiro, J., Bates, D., DebRoy, S., Sarkar, D., 2020. nlme: Linear and Nonlinear Mixed Effects Models. R package version 3.1-147. https://rdrr.io/cran/nlme/

Plomp, K. A., Owen, J., Dobney, K., Collard, M. 2024. Mandibular shape and diet in extant primates: a 3D geometric morphometric analysis. Anthropol Anz. https://doi.org/10.1127/anthranz/2024/1675

Polk, J.D., Demes, B., Jungers, W.L., Biknevicius, A.R., Heinrich, R.E., Runestad, J.A., 2000. A comparison of primate, carnivoran and rodent limb bone cross-sectional properties: are primates really unique? J Hum Evol 39, 297–325. https://doi.org/10.1006/jhev.2000.0420

Polly, P.D., 2007. Limbs in Mammalin Evolution, in: In: Fins into Limbs: Evolution, Development, and Transformation. Hall B.K. (ed), Chicago: University of Chicago Press., p. Chap. 15 (pp. 245-268).

Pontzer, H., Lieberman, D.E., Momin, E., Devlin, M.J., Polk, J.D., Hallgrímsson, B., Cooper, D.M.L., 2006. Trabecular bone in the bird knee responds with high sensitivity to changes in load orientation. J Exp Biol 209, 57–65. https://doi.org/10.1242/jeb.01971

Pornprasertsuk, S., Ludlow, J.B., Webber, R.L., Tyndall, D.A., Sanhueza, A.I., Yamauchi, M., 2001. Fractal dimension analysis of weight-bearing bones of rats during skeletal unloading. Bone 29(2), 180–184.

Pothuaud, L., Van Rietbergen, B., Mosekilde, L., Beuf, O., Levitz, P., Benhamou, C. L., & Majumdar, S. 2002. Combination of topological parameters and bone volume fraction better predicts the mechanical properties of trabecular bone. Journal of Biomechanics, 35(8), 1091-1099

Preuschoft, H., 1970. Functional Anatomy of the Lower Extremity, in: The Chimpanzee, Vol. 3. Bourne, G.H., Karger, Basel, pp. 221–294.

Puttick, M., Thomas, G., Freckleton, R., Clarke, M., Ingram, T., Orme, D., Paradis, E., 2019. motmot: Models of Trait Macroevolution on Trees. R package version 2.1.3 <https://CRAN.R-project.org/package=motmot>.

Rafferty, K.L., Walker, A., Ruff, C.B., Rose, M.D., Andrews, P.J., 1995. Postcranial estimates of body weight in *Proconsul*, with a note on a distal tibia of *P. major* from Napak, Uganda. Am. J. Phys. Anthropol. 97(4), 391–402.

Revell, L.J., 2012. phytools: an R package for phylogenetic comparative biology (and other things). Methods Ecol. Evol. 3, 217–223. https://doi.org/10.1111/j.2041-210X.2011.00169.x

Rittweger, J., Ireland, A., Lüscher, S., Nocciolino, L.M., Pilot, N., Pisani, L., Cointry, G.R., Ferretti, J.L., Capozza, R.F., 2018. Fibula: The forgotten bone-may it provide some insight on a wider scope for bone mechanostat control? Curr Osteoporos Rep 16, 775–778. https://doi.org/10.1007/s11914-018-0497-x

Robling, A.G., 2009. Is bone's response to mechanical signals dominated by muscle forces? Med Sci Sports Exerc 41, 2044–2049. https://doi.org/10.1249/MSS.0b013e3181a8c702

Rodman, P.S., 1979. Skeletal differentiation of *Macaca fascicularis* and *Macaca nemestrina* in relation to arboreal and terrestrial quadrupedalism. Am. J. Phys. Anthrop. 51, 51–62.

Rodríguez, L., Carretero, J.M., Carcía-González, R., Arsuaga, J.L., 2018. Cross-sectional properties of the lower limb long bones in the Middle Pleistocene Sima de los Huesos sample (Sierra de Atapuerca, Spain). J. Hum. Evol. 117, 1–12.

Roque, W.L., Alberich-Bayarri, A., 2015. Tortuosity Influence on the Trabecular Bone Elasticity and Mechanical Competence., in: Developments in Medical Image Processing and Computational Vision. R. N. Jorge, J. M. Tavares (Eds.), Cham: Springer, pp. 173–191.

Roque, W.L., Arcaro, K., Alberich-Bayarri, A., 2012. Mechanical competence of bone: a new parameter to grade trabecular bone fragility from tortuosity and elasticity. IEEE Trans. Biomed. Eng. 60(5), 1363–1370.

Rose, M.D., 1979. Positional Behavior of Natural Populations: Some Quantitative Results of a Field Study of *Colobus guereza* and *Cercopithecus aethiops*, in: Environment, Behavior, and Morphology. Morbeck ME, Preuschoft H, Gomberg N., New York: Gustav Fisher, pp. 75–94.

Rubin C, Turner AS, Bain S, et al. (2001) Anabolism: low mechanical signals strengthen long bones. Nature 412, 603–604.
Rubin C, Turner AS, Mallinckrodt C, et al. (2002) Mechanical strain, induced noninvasively in the high-frequency domain is anabolic to cancellous bone, but not cortical bone. Bone 30, 445–452.
Ruff, C., 1987. Sexual dimorphism in human lower limb bone structure: relationship to subsistence strategy and sexual division of labor. J. Hum. Evol. 16, 391–416. https://doi.org/10.1016/0047-2484(87)90069-8
Ruff, C., Holt, B., Trinkaus, E., 2006. Who's afraid of the big bad Wolff?: 'Wolff's law' and bone functional adaptation. Am. J. Phys. Anthropol. 129, 484–498. https://doi.org/10.1002/ajpa.20371
Ruff, C.B., 2003. Long bone articular and diaphyseal structure in Old World monkeys and apes. II: Estimation of body mass. Am. J. Phys. Anthropol. 120, 16–37. https://doi.org/10.1002/ajpa.10118
Ruff, C.B., 2002. Long bone articular and diaphyseal structure in old world monkeys and apes. I: locomotor effects. Am. J. Phys. Anthropol. 119, 305–342. https://doi.org/10.1002/ajpa.10117
Ruff, C.B., Burgess, M.L., Squyres, N., Junno, J.A., Trinkaus, E., 2018. Lower limb articular scaling and body mass estimation in Pliocene and Pleistocene hominins. J. Hum. Evol. 115, 85–111.
Ruff, C.B., Harper, C.M., Goldstein, D.M., Deegling, D.J., McGraw, W.C., 2019. Long bone structural proportions and locomotor behavior in Cercopithecidae. J Hum Evol 132, 47–60.
Ruff, C.B., Jones, H.H., 1981. Bilateral asymmetry in cortical bone of the humerus and tibia: Sex and age factors. Hum. Biol. 53, 69–86.
Ruff, C.B., Runestad, J.A., 1992. Primate limb bone structural adaptations. Annu. Rev. Anthropol. 21, 407–433. https://doi.org/10.1146/annurev.an.21.100192.002203
Runestad, J.A., 1997. Postcranial adaptations for climbing in Loridae (Primates). J. Zool. 242, 261–290. https://doi.org/10.1111/j.1469-7998.1997.tb05801.x
Ryan, T.M., Ketcham, R.A., 2002a. The three-dimensional structure of trabecular bone in the femoral head of strepsirrhine primates. J. Hum. Evol. 43, 1–26. https://doi.org/10.1006/jhev.2002.0552
Ryan, T.M., Ketcham, R.A., 2002b. Femoral head trabecular bone structure in two omomyid primates. J. Hum. Evol. 43, 241–263. https://doi.org/10.1006/jhev.2002.0575
Ryan, T.M., Shaw, C.N., 2015. Gracility of the modern *Homo sapiens* skeleton is the result of decreased biomechanical loading. Proc Natl Acad Sci USA 112, 372–377. https://doi.org/10.1073/pnas.1418646112
Ryan, T.M., Shaw, C.N., 2013. Trabecular bone microstructure scales allometrically in the primate humerus and femur. Proc. R. Soc. B 280, 20130172. https://doi.org/10.1098/rspb.2013.0172
Ryan, T.M., Shaw, C.N., 2012. Unique suites of trabecular bone features characterize locomotor behavior in human and non-human anthropoid primates. PLoS ONE 7, e41037. https://doi.org/10.1371/journal.pone.0041037
Saers, J.P.P., 2023. Skeletal indicators of developmental changes in arboreality and locomotor maturation in extant apes and their relevance to hominin paleobiology. Front. Ecol. Evol. 11, 1274762. https://doi.org/doi: 10.3389/fevo.2023.1274762
Saers, J.P.P., Cazorla-Bak, Y., Shaw, C.N., Stock, J.T., Ryan, T.M., 2016. Trabecular bone structural variation throughout the human lower limb. J. Hum. Evol 97, 97–108. https://doi.org/10.1016/j.jhevol.2016.05.012
Saers, J.P.P., Gordon, A.D., Ryan, T.M., Stock, J.T., 2022. Growth and development of trabecular structure in the calcaneus of Japanese macaques (*Macaca fuscata*) reflects locomotor behavior, life history, and neuromuscular development. J Anat 00, 1–15. https://doi.org/10.1111/joa.13641
Sanchez-Molina, D., Velazquez-Ameijide, J., Quintana, V., Arregui-Dalmases, C., Crandall, J. R., Subit, D., & Kerrigan, J. R. 2013. Fractal dimension and mechanical properties of human cortical bone. Med Eng Phys, 35(5), 576-582.
Schaffler, M.B., Burr, D.B., 1984. Primate cortical bone microstructure: Relationship to locomotion. Am. J. Phys. Anthrop. 65, 191–197. https://doi.org/10.1002/ajpa.1330650211
Schaffler, M.B., Burr, D.B., Jungers, W.L., Ruff, C.B., 1985. Structural and mechanical indicators of limb specialization in primates. Folia Primatol. 45, 61–75. https://doi.org/10.1159/000156218

Scherf, H., 2008. Locomotion-related Femoral Trabecular Architectures in Primates — High Resolution Computed Tomographies and Their Implications for Estimations of Locomotor Preferences of Fossil Primates, In: Anatomical Imaging: Towards a New Morphology. Endo, H., Frey, R. (Eds.), Springer Japan, Tokyo, pp. 39–59. https://doi.org/10.1007/978-4-431-76933-0_4

Scherf, H., Harvati, K., Hublin, J.-J., 2013. A comparison of proximal humeral cancellous bone of great apes and humans. J. Hum. Evol 65, 29–38. https://doi.org/10.1016/j.jhevol.2013.03.008

Schilling, A.M., Tofanelli, S., Hublin, J.J., Kivell, T.L., 2014. Trabecular bone structure in the primate wrist. J Morphol 275, 572–585.

Schmitt, D., 2003. Mediolateral reaction forces and forelimb anatomy in quadrupedal primates: implications for interpreting locomotor behaviour in fossil primates. J. Hum. Evol 44, 47e58.

Schneider, C.A., Rasband, W.S., Eliceiri, K.W., 2012. NIH Image to ImageJ: 25 years of image analysis. Nat. Methods 9, 671–675. https://doi.org/10.1038/nmeth.2089

Seiler, H., 1986. [Biomechanics of the upper ankle joint]. Orthopade 15, 415–422.

Shaw, C.N., Ryan, T.M. 2012. Does skeletal anatomy reflect adaptation to locomotor patterns? Cortical and trabecular architecture in human and nonhuman anthropoids. Am J Phys Anthropol. 147(2):187-200.

Simkin A, Leichter I, Swissa A, et al. (1989) The effect of swimming activity on bone architecture in growing rats. J Biomech 22, 845–851.

Skerry, T.M., Lanyon, L.E. 1995. Interruption of disuse by short duration walking exercise does not prevent bone loss in the sheep calcaneus. Bone 16, 269–274.

Smaers, J.B., Vinicius, L., 2009. Inferring macro-evolutionary patterns using an adaptive peak model of evolution. Evol Ecol Res 11, 991–1015.

Sode, M., Burghardt, A.J., Nissenson, R.A., Majumdar, S., 2008. Resolution dependence of the non-metric trabecular structure indices. Bone 42, 728–736. https://doi.org/10.1016/j.bone.2007.12.004

Souto, A., Bezerra, B.M., Schiel, N., Huber, L., 2007. Saltatory search in free-living *Callithrix jacchus*: environmental and age influences. Int. J. Primatol. 28, 881–893.

Sparacello, V.S., Marchi, D., Shaw, C.N., 2014. The Importance of Considering Fibular Robusticity when Inferring the Mobility Patterns of Past Populations., In: Reconstructing Mobility: Environmental, Behavioral, and Morphological Determinants. Carlson K.J, Marchi D. Springer, pp. 91–110.

Stauber, M., Rapillard, L., van Lenthe, G.H., Zysset, P., Müller, R., 2006. Importance of individual rods and plates in the assessment of bone quality and their contribution to bone stiffness. J Bone Min Res 21, 586–595.

Stürznickel, J., Schmidt, F.N., Schäfer, H.S., Beil, F.T., Frosch, K.H., Schlickewei, C., Amling, M., Barg, A., Rolvien, T., 2021. Bone microarchitecture of the distal fibula assessed by HR-pQCT. Bone 151, 116057. https://doi.org/10.1016/j.bone.2021.116057

Su, A., Carlson, K.J., 2017. Comparative analysis of trabecular bone structure and orientation in South African hominin tali. J. Hum. Evol. 106, 1–18. https://doi.org/10.1016/j.jhevol.2016.12.006

Su, A., Wallace, I.J., Nakatsukasa, M., 2013. Trabecular bone anisotropy and orientation in an Early Pleistocene hominin talus from East Turkana, Kenya. J. Hum. Evol. 64, 667–677. https://doi.org/10.1016/j.jhevol.2013.03.003

Su, A., Zeininger, A., 2022. The Primate Ankle and Hindfoot, In: The Evolution of the Primate Foot: Anatomy, Function, and Palaeontological Evidence. Zeininger A., Hatala, K. G., Wunderlich, R. E., Schmitt, D. (Eds.)., Springer., pp. 21–45.

Sukhdeo, S., Parsons, J., Niu, X.M., Ryan, T.M., 2020. Trabecular bone structure in the distal femur of humans, apes, and baboons. Anat Rec 303, 129–149. https://doi.org/10.1002/ar.24050

Swartz, S.M., 1989. The functional morphology of weight bearing: limb joint surface area allometry in anthropoid primates. J. Zool. 218, 441–460. https://doi.org/10.1111/j.1469-7998.1989.tb02556.x

Swartz, S.M., Parker, A., Huo, C., 1998. Theoretical and empirical scaling patterns and topological homology in bone trabeculae. J Exp Biol 201, 573–590. https://doi.org/10.1242/jeb.201.4.573

Sylvester, A.D., 2013. A geometric morphometric analysis of the medial tibial condyle of African hominids. Anat Rec 296, 1518–1525. https://doi.org/10.1002/ar.22762

Sylvester, A.D., Terhune, C.E., 2017. Trabecular mapping: Leveraging geometric morphometrics for analyses of trabecular structure. Am J Phys Anthropol 163, 553–569. https://doi.org/10.1002/ajpa.23231

Takebe, K., Nakagawa, A., Minami, H., Kanazawa, H., Hirohata, K., 1984. Role of the fibula in weight-bearing. Clin. Orthop. Relat. Res. 289–292.

Tardieu, C., 2010. Development of the human hind limb and its importance for the evolution of bipedalism. Evol. Anthropol. Issues News Rev. 19, 174–186. https://doi.org/10.1002/evan.20276

Tarquini, J., 2021. Femoral shape in procyonids (Carnivora, Procyonidae): morphofunctional implications, size and phylogenetic Signal. J Mammal Evol 28, 159–171. https://doi.org/10.1007/s10914-019-09491-8

Tegner, C., 2011. Behavioral patterns in a population of Samango monkeys (*Cercopithecus albogularis erythrarcus*). BSc thesis. Linköpings universitet, Sweden.

Tillquist, R.C., Shoemaker, L.G., Knight, K.B., Clauset, A., 2016. The evolution of primate body size: left-skewness, maximum size, and Cope's rule. Pre-print. https://doi.org/10.1101/092866

Tsegai, Z.J., Kivell, T.L., Gross, T., Nguyen, N.H., Pahr, D.H., Smaers, J.B., Skinner, M.M., 2013. Trabecular bone structure correlates with hand posture and use in hominoids. PLoS ONE 8, e78781. https://doi.org/10.1371/journal.pone.0078781

Tsegai, Z.J., Skinner, M.M., Gee, A.H., Pahr, D.H., Treece, G.M., Hublin, J.J., Kivell, T.L., 2017. Trabecular and cortical bone structure of the talus and distal tibia in *Pan* and *Homo*. Am J Phys Anthropol 163(4), 784–805.

Tsegai, Z.J., Skinner, M.M., Pahr, D.H., Hublin, J.-J., Kivell, T.L., 2018. Ontogeny and variability of trabecular bone in the chimpanzee humerus, femur and tibia. Am J Phys Anthropol 167, 713–736. https://doi.org/10.1002/ajpa.23696

Uchiyama, T., Tanizawa, T., Muramatsu, H., Endo, N., Takahashi, H.E., Hara, T., 1999. Three-dimensional microstructural analysis of human trabecular bone in relation to its mechanical properties. Bone 25(4), 487–491.

Upham, N.S., Esselstyn, J.A., Jetz, W., 2019. Inferring the mammal tree: species-level sets of phylogenies for questions in ecology, evolution, and conservation. PLoS Biol 17, e3000494. https://doi.org/10.1371/journal.pbio.3000494

Veneziano, A., Irish, J. D., Meloro, C., Stringer, C., & De Groote, I. 2019. The functional significance of dental and mandibular reduction in *Homo*: A catarrhine perspective. Am. J. Primatol., 81(3), e22953.

Veneziano, A., Cazenave, M., Alfieri, F., Panetta, D., Marchi, D., 2021. Novel strategies for the characterization of cancellous bone morphology: Virtual isolation and analysis. Am J Phys Anthropol 175(4), 920-930 https://doi.org/10.1002/ajpa.24272

Veracini, C., 2009. Habitat Use and Ranging Behavior of the Silvery Marmoset (*Mico argentatus*) at Caxiuanã National Forest (eastern Brazilian Amazonia)., In: The Smallest Anthropoids: The Marmoset/Callimico Radiation. Ford S. M., Porter L.M., Davis L.C, Springer (eds), pp. 221–240.

Walmsley, T., 1918. The reduction of the mammalian fibula. J Anat 52, 326–331.

Wang, H., Sherry Liu, X., Zhou, B., Wang, J., Ji, B., Huang, Y., Hwang, K-C & Edward Guo, X. 2013. Accuracy of individual trabecula segmentation based plate and rod finite element models in idealized trabecular bone microstructure. Journal of biomechanical engineering, 135(4), 044502.

White, T.D., Black, M.T., Folkens, P.A., 2011. Human Osteology, 3rd Edition. Academic Press. San Diego.

Wickham, H., 2016. ggplot2: Elegant Graphics for Data Analysis. Springer-Verlag New York.

Wund, M.A., 2012. Assessing the impacts of phenotypic plasticity on evolution. Integr Comp Biol 52(1), 5–15. https://doi.org/10.1093/icb/ics050.

Yeni, Y.N., Zinno, M.J., Yerramshetty, J.S., Zauel, R., Fyhrie, D.P., 2011. Variability of trabecular microstructure is age-, gender-, race- and anatomic sitedependent and affects stiffness and stress distribution properties of human vertebral cancellous bone. Bone 49, 886–894.

You, K., Shung, D., 2022. Rdimtools: An R package for dimension reduction and intrinsic dimension estimation. Software Impacts 14(1), 100414.

Youlatos, D., 2008. Locomotion and Positional Behavior of Spider Monkeys., In: Spider Monkeys. Behavior, Ecology and Evolution of the Genus *Ateles*. Campbell C.J. (ed), Cambridge Studies in Biological and Evolutionary Anthropology 55.

Youlatos, D., Gasc, J.P., 2011. Gait and Kinematics of Arboreal Quadrupedal Walking of Free-ranging Red Howlers (*Alouatta seniculus*) in French Guiana, In: Primate Locomotion. Linking Field and Laboratory Research. D'Aout K., Vereecke E.E. (eds), Springer. New York.

Figure captions

Fig. 1. Primate species studied in this work. The three factors potentially associated with their distal fibular trabecular architecture that were addressed in this work, are summarized: 1. phylogenetic relationships, shown through the time-calibrated tree; 2. locomotor habits, detailed with the color legend; 3. body mass, through the proxy used in this work, shown with bar plots. See Methods for details.

Fig. 2. The steps performed to orient all the fibulae in a standard position are exemplified on the distal fibula of *Cercopithecus mitis* UniFl-SPEC 3011. In both **A** (anterior view) and **B** (distal view) PAF, i.e. proximal part of the fibulotalar articulation of the distal fibula, is oriented to be parallel to the coronal plane (shown with a blue line in 2A and 2B). **C.** The bone is then oriented so that the two axes of PAF (visually recognized and highlighted in red, due to the quasi-regular shape of the articular facet) lie in the sagittal (shown in orange) and the transverse (shown in green) planes. DAF, i.e. distal part of the fibulotalar articulation of the distal fibula, is shown but was not studied in this work. **D.** The Region of Interest (ROI) ultimately analyzed is here shown in the context of the entire distal epiphysis. A sub-region of the distal fibula corresponding to the PAF cortical bone + trabecular bone was cropped (highlighted in aqua green, also shown in Fig. 3A) and from it a ROI representing only the PAF trabecular bone was extracted (highlighted in purple, also shown in Fig. 3B).

Fig. 3. Isolation of the whole articular trabecular architecture, exemplified on the distal fibula of *Cercopithecus mitis* UniFl-SPEC 3011. A. The oriented sub-stack corresponding to the isolated PAF. PAF is shown in red and its proximal and distal limits, used to isolate PAF, are highlighted. B. Exploiting the 'indianaBones' R package, the trabecular bone is isolated and used to compute BoneJ parameters. C. The trabecular network of B. is skeletonized in Amira. The skeleton is used to compute the topological indices of 'indianaBones'.

Fig. 4. A. Boxplots highlighting the univariate pattern of variation of BV/TV from the distal fibular trabecular architecture. Terrestrial taxa are shown in blue, semi-arboreal in green and arboreal in purple, and taxa yielding the maximum and minimum value for each category of the Degree of Arboreality are indicated. **B.** The BV/TV values for the studied species are mapped on the phylogeny used in this work, with ancestral states reconstructed. Here, the color legend instead indicates the variable values. **C.** Boxplots highlighting the univariate pattern of variation of size-corrected BS/TV from the distal fibular trabecular architecture. Terrestrial taxa are shown in blue, semi-arboreal in green and arboreal in red, and taxa yielding the maximum and minimum value for each category of the Degree of Arboreality are indicated. **D.** The size-corrected BS/TV values for the studied species are mapped on the phylogeny used in this work, with ancestral states reconstructed. Here, the color legend instead indicates the variable values.

Fig. 5. Multivariate patterns of variation in distal fibular trabecular architecture. **A, B** and **C.** Upper panels: phylomorphospaces built with PC1-PC2 (**A**), PC1-PC3 (**B**) and PC2-PC3 (**C**) resulting from a PCA on all the studied trabecular traits (using size-corrected values in case of variables significantly related to body mass, as detailed in Table 3). Abbreviations: *Cj* for *Callithrix jacchus*, *Hs* for *Homo sapiens*, *Pt* for *Pan troglodytes*, *Oc* for *Otolemur crassicaudatus*. Bottom panels: variable loading plots summarizing how single traits contribute to species distribution on the corresponding morphospaces in the upper panels. In **A**, **B** and **C**: Degree of arboreality categories are shown with colors: arboreal in purple, semi-arboreal in green, terrestrial in blue. Abbreviations for variables in the loading plots: DA (degree of anisotropy), BV/TV (bone volume fraction), BS/TV (bone surface density), Tb.Th (trabecular thickness), $NodDen_{Aver}$ (average node density), $NodDen_{Med}$ (median node density), $TrabLen_{Aver}$ (average trabecular length), $TrabTort_{Aver}$ (average trabecular tortouosity), $TrabTort_{Med}$ (median trabecular tortuosity), FD (fractal dimension). **D.** Boxplot highlighting the univariate pattern of variation of PC2 (used to build the bivariate scatterplots in **A** and **C**).

Terrestrial taxa are shown in blue, semi-arboreal in green and arboreal in red. The position of *Homo sapiens*, outlying other terrestrial taxa, is shown.

The relationship between primate distal fibula trabecular architecture and arboreality, phylogeny and size

Alfieri F.[1,2,3,4], Veneziano A.[5], Panetta D.[6], Salvadori P.A.[6], Amson E.[7], Marchi D.[8,9]

1. Institute of Ecology and Evolution, Universität Bern, Bern, Switzerland
2. Department of Earth Sciences, University of Cambridge, Cambridge, UK
3. Institut für Biologie, Humboldt Universität zu Berlin, Berlin, Germany
4. Museum Für Naturkunde, Leibniz-Institut Für Evolutions- Und Biodiversitätsforschung, Berlin, Germany
5. Departament d'Enginyeria Mecànica, Universitat Rovira i Virgili, Tarragona, Spain.
6. Institute of Clinical Physiology, IFC-CNR, Pisa, Italy,
7. Staatliches Museum für Naturkunde, Stuttgart, Germany.
8. Department of Biology, Università di Pisa, Pisa, Italy.
9. Centre for the Exploration of the Deep Human Journey, University of the Witwatersrand, Johannesburg, South Africa.

Corresponding author: Fabio Alfieri, email: fabio.alfieri@unibe.ch and fabio_alfieri@yahoo.it

ORCID:

Fabio Alfieri: 0000-0001-8241-7309

Alessio Veneziano: 0000-0002-2543-5188

Daniele Panetta: 0000-0002-4184-0175

Piero A. Salvadori: 0000-0001-6114-1059

Eli Amson: 0000-0003-1474-9613

Damiano Marchi: 0000-0002-6331-8783

Abstract

The fibula, despite being traditionally overlooked compared to the femur and the tibia, has recently received attention in primate functional morphology due to its correlation with the degree of arboreality. Highlighting further fibular features that are associated with arboreal habits would be key to ~~improve~~improving palaeobiological ~~inference on~~inferences in fossil specimens. Here we present the first investigation on the trabecular bone structure of the primate fibula, focusing on the distal epiphysis, across a vast array of species. We collected µCT data on the distal fibula for 21 species of primates, with representatives from most of the order, and we employed a recently developed approach implemented in the R package 'indianaBones' to isolate the entire trabecular bone underlying an epiphysis or articular facet. After extracting both traditional trabecular parameters and novel topological indices, we tested for the posited relationship between trabecular bone and degree of arboreality. To disentangle this effect from others related to body size and phylogenetic relationship, we included a body mass proxy as covariate and employed phylogenetic comparative methods. We ran univariate/multivariate and exploratory/inferential statistical analyses. The trabecular structure of the fibular distal epiphysis in primates does not appear to be associated with the degree of arboreality. Instead, it ~~results as~~is strongly affected by body mass and phylogenetic relationships. ~~Albeit~~Although we identified some minor trends related to human bipedalism, our findings overall discourage, at this stage, the study of distal fibula trabecular bone to infer arboreal behaviors in extinct primates. We further found that body size distribution is strongly related to phylogeny, an issue preventing us ~~to unravel~~from unravelling the influence of the two factors and that we believe can potentially affect future comparative analyses of primates. Overall, our results add to previous evidence of how trabecular traits show variable correlation with locomotor aspects, size and phylogenetic history across the primate skeleton, thus outlining a complex scenario in which a network of interconnected factors affects the morphological evolution of primates. This work may represent a starting point for future studies, e.g. focusing on the effect of human bipedalism on distal fibula trabecular bone, or aiming to better understand the effects of body size and phylogenetic history on primate morphological evolution.

Keywords: cancellous bone; ankle joint; substrate preference; body size; phylogenetic signal

1. Introduction

The study of mammal ~~limbs'~~limb long bones offers compelling evidence of the disparate factors related to anatomical diversity, such as ecology, body size and/or shared phylogenetic history (e.g. Alfieri et al., 2021, 2022, 2023; Cooper, 2019; Kilbourne and Hutchinson, 2019; Polly, 2007; Tarquini, 2021). Among mammalian clades, primate long bone functional morphology has been widely investigated (e.g. Chiu and Hamrick, 2002; Gebo, 1989, 2014; Ruff, 2003; Swartz, 1989) with special focus on adaptations to biomechanical loadings deriving from different locomotor specializations (e.g. Burr et al., 1981; Demes and Jungers, 1993; Kimura, 1995, 2003; Marchi et al., 2016; Ruff, 2002; Ruff et al., 2019; Ruff and Runestad, 1992; Runestad, 1997; Schaffler et al., 1985; Schaffler and Burr, 1984). In primates, hindlimb morphology is key to some of the most distinctive primate locomotor adaptations, such as vertical clinging and leaping in strepsirrhines (Gebo, 2011; Napier and Walker, 1967a) or bipedalism in hominins (O'Neill et al., 2015; Tardieu, 2010). Hence, the long bones of the primate hindlimbs represent an optimal context ~~to~~in which understand if anatomical traits are more related to the locomotor environment (Berles et al., 2024; Georgiou et al., 2018; Harmon, 2007; Marchi, 2007; Marchi et al., 2022; Ruff, 2002; Ryan and Ketcham, 2002a; Sylvester, 2013) or to other factors (e.g. allometric relationships, Ruff, 1987; Ryan and Shaw, 2013, or phylogenetic signal, O'Neill and Dobson, 2008; Ryan and Shaw, 2013). In primates, the femur and tibia have been by far the most studied hindlimb long bones, with the aim of identifying locomotor correlates through analyses involving different approaches and anatomical levels, as external joint proportions/shape (e.g. Godfrey, 1988; Harmon, 2007; Jungers et al., 2002; Marchi et al., 2016; Sylvester, 2013), diaphyseal cross-sectional geometry, (CSG; e.g. Carlson, 2005; Demes and Jungers, 1993; Kimura, 2002; Marchi et al., 2016; Polk et al., 2000; Ruff, 2002) and epiphyseal trabecular architecture (e.g. Barak et al., 2013a; Fajardo and Müller, 2001; Georgiou et al., 2019, 2018; MacLatchy and Müller, 2002; Scherf, 2008). This trend is possibly explained by the fact that the femur and tibia are the two main elements of the hindlimb and, thus, are expected to have a prominent role in sustaining the hindlimb mechanical loads. Moreover,

compared to other skeletal elements, the two bones are relatively abundant in the fossil record (e.g. Anemone and Covert, 2000; DeSilva et al., 2010; Ford and Morgan, 1986; MacLatchy and Bossert, 1996; Rafferty et al., 1995; Ryan and Ketcham, 2002b). These aspects are not independent, since the identification of anatomical features associated with specific locomotor behaviors in extant taxa can be leveraged, in turn, to infer locomotor habits in extinct primates for which fossil specimens are available.

1. 1. Primate fibula functional morphology

For the fibula, the other hindlimb long bone, a close relationship between fibular anatomy and the prehensile power of the foot has long been hypothesized (Owen, 1866), and some early analyses addressed the functional morphology of the fibula in mammals (Barnett and Napier, 1953; Carleton, 1941; Walmsley, 1918). Importantly, although these works have highlighted several fibular traits possibly related to locomotor behaviors, many of those features (e.g. degree of distal tibia-fibula fusion, fibular robusticity relative to the tibia) can be assessed only in association with the tibia (Barnett and Napier, 1953). This may explain why the fibula has long been overlooked in primate comparative anatomical studies (and even defined as 'the forgotten bone', Rittweger et al., 2018), being considered only the lateral strut of the ankle with almost no role in load bearing (White et al., 2011) or even vestigial (Moore and Dalley, 2006). Moreover, it explains why a renewed attention to the fibular functional morphology initially led to ~~address~~the study of this bone only in association with the tibia. Indeed, it has been highlighted that the relative (to the tibia) fibular diaphyseal robusticity ('relative robusticity' hereafter) relates to a specific aspect of locomotor behavior: substrate preference. Specifically, fibular relative robusticity is higher in primates with higher degree of arboreality (DOA) (Marchi, 2015a, 2007; Marchi and Borgognini-Tarli, 2004). As further detailed below, DOA is here and hereafter meant as a discrete grouping, e.g. splitting 'arboreal', 'semi-arboreal' and 'terrestrial' primates, defined according to the relative amount of time spent ~~on~~in trees (Table 1~~), and keeping~~). Importantly, it should be kept in mind that all non-human primates, however, show a minimum exploitation of arboreal substrates/superstrates. Hence, the effects of arboreality on fibular morphology have been assumed to be caused by frequent and repeated arboreal locomotion, not

by the simple capability of performing arboreal behaviors. The relationship between fibular relative robusticity and DOA is possibly explained by the fact that the distal portion of the hindlimb of arboreal species is subject to relatively more frequent laterally oriented loadings, compared to terrestrial ones (Carlson et al. 2005, see also below) and considering that the fibula is laterally located at this anatomical level. Moreover, a higher relative fibular diaphyseal robusticity has been found in humans performing activities involving frequent laterally oriented loadings in the distal segment of the hindlimb (Auerbach et al., 2017; Carlson and Marchi, 2014; Hagihara and Nara, 2016; Marchi et al., 2011; Marchi and Shaw, 2011; Sparacello et al., 2014). These results suggest that the fibula may not cover a negligible role in transmitting hindlimb loadings in primates, corroborating previous observations (e.g. Funk et al., 2004; Goh et al., 1992; Lambert, 1971; Takebe et al., 1984). However, the need to study the tibia-fibula system limits the design of comparative analyses (e.g. more demanding data collection) and the quantification of correlates for DOA on primate fossil specimens, due to the extreme rarity of complete associated tibiae and fibulae (Marchi et al., 2019). Thus, it appears advantageous to identify functional traits quantifiable on the primate fibula alone. In this regard, human individuals subject to frequent laterally oriented loadings in the distal portion of the hindlimb have been shown to exhibit a higher fibular diaphyseal absolute (i.e., regardless of tibial measures) robusticity (Marchi and Shaw, 2011), suggesting that a similar pattern may be present in arboreal primates. Moreover, the external morphology of the primate fibula has been recently linked to DOA through traditional morphometrics (Marchi, 2015b) and 3D geometric morphometrics (3D GM; Marchi et al., 2022). As of today, no interspecific comparisons across primate fibulae have been performed based on ~~diaphyseal~~epiphyseal internal bone structure, i.e. trabecular architecture. This gap in the literature is surprising if we consider the potential of the trabecular architecture of the ~~hindlimbs'~~hindlimb long bones to exhibit functional signals (e.g. Barak et al., 2013a; Fajardo and Müller, 2001; Georgiou et al., 2018; MacLatchy and Müller, 2002 and see below).

1. 2. Trabecular bone architecture

It has been suggested that internal bone, both cortical and trabecular, may record bone usage and behaviors performed during ~~the~~an individual's life and that it may respond to the functional constraints set by a species' ecology and environment more directly than external morphology (Kivell, 2016). Indeed, internal bone, despite its largely genetically determined morphology at birth, is responsive to mechanical loadings (Carter and Beaupré, 2007; Currey, 2002) acting through differential strains that in turn depend on bone actual usage (Ruff et al., 2006). Trabecular bone, being more porous and typically remodeling more frequently than cortical bone (Eriksen, 1986, 2010), ~~it~~ likely involves a larger amount of functionally responsive cells (also due to greater surface area) (Currey, 2002; Huiskes et al., 2000~~) and, ultimately, it is expectedly~~). Ultimately, trabecular bone is expected to be even more plastic than cortical bone in responding to differential loadings that reflect distinct locomotor habits (Currey, 2002; Jacobs, 2000; Kivell, 2016).

Several experimental works performed *in vivo*, e.g. applying controlled strains and measuring the trabecular bone response, highlighted that specific trabecular properties result from certain mechanical loads. For instance, the trabecular alignment tends to follow strain orientations, i.e. trabecular struts orient along the main loading vectors (e.g. Biewener et al., 1996; Pontzer et al., 2006). Although not yielding the specific direction (e.g. in degrees of arc) along which trabeculae orient, a commonly used parameter in this regard is the degree of anisotropy (DA~~), informing~~). This parameter informs on a more general but more straightforwardly interpreted property, i.e. the extent to which the trabeculae tend to align toward a uniform direction~~:~~. Indeed, the more homogeneous the orientation is in the studied region, the more the latter is anisotropic, the higher DA (as defined here) will be (Harrigan and Mann, 1984). DA is one of the most structurally informative trabecular properties, ~~it~~ measuring the fabric orientation, which is in turn closely associated with the mechanical main direction (Odgaard, 1997) (i.e. the direction, if any, along which biomechanical loadings are mainly applied), and ~~explaining the~~explains 10% of trabecular stiffness (Maquer et al., 2015). Accordingly, DA proved an informative parameter in primate interspecific analyses related to behavior, in that species with locomotor habits involving more directionally stereotyped loadings yielded more anisotropic trabecular structure, i.e. higher DA (e.g. leaping taxa discriminated from non-leaping ones in strepsirrhines, Ryan and Ketcham, 2002a). ~~Also, properties~~

Properties directly related to bone density are other suitable predictors of bone strength: i.e. regions characterized by increased strength show increased density and, hence, larger values for these traits. Although increased strength in a given anatomical region is often considered the direct consequence of increased magnitude of the load, this specific aspect of loading patterns (e.g. measured in terms of strain magnitude, in mm/mm) is only one of the factors contributing to trabecular remodeling. Indeed, besides load magnitudes, one should also consider how trabecular remodeling is affected by the duration (e.g. Barak et al. 2011; Lambers et al. 2013; Skerry and Lanyon, 1995) and frequency (e.g. Barak et al. 2011; Bassey and Ramsdale, 1994; Pontzer et al. 2006; Simkin et al. 1989) of loadings (Kivell, 2016). Importantly, concerning load frequency, Rubin et al. (2001; 2002) showed that even extremely low loadings when exerted with high frequency may cause a substantial (34.2%) increase in trabecular bone density (Rubin et al. 2001; 2002). This outcome suggests that, besides or even instead of the magnitude, other characteristics of the loading pattern acting on a specific joint, as the frequency, may be crucial in determining density related trabecular parameters. For this reason, here and throughout (see below and Table 2), we will refer to 'increased loadings' (keeping in mind that they may derive from increased loading magnitude and/or frequency and/or duration) as the factor to which some trabecular parameters may respond. Instances of density-related traits are bone volume fraction (BV/TV) (Barak et al., 2011; Chang et al., 2008; Mittra et al., 2005) and trabecular thickness (Tb.Th) (Barak et al., 2011; Mittra et al., 2005), with the former being particularly informative from a biomechanical point of view (besides DA, see above), accounting for the 88% of trabecular stiffness (Stauber et al., 2006). Both BV/TV. and Tb.Th, similarly to DA, proved suitable to discriminate locomotor categories in human and non-human primate samples (e.g. Ryan and Shaw, 2015; Sukhdeo et al., 2020).

The computation of parameters related to density (e.g. BV/TV and Tb.Th) and orientation (e.g. DA) is often combined with the characterization of additional features of the trabecular network, as the overall shape. A way to quantify the latter is through measures of trabecular bone surface, as the bone surface to total volume fraction (BS/TV, also termed 'bone surface density', Scherf et al., 2013). This parameter informs on the shape complexity of the intertrabecular spaces (in life filled with marrow that, in turn, directly

contacts the inner epiphysis bony parts through the surface of the trabeculae). Hence, a larger BS/TV corresponds to larger trabecular surface exposed to marrow in life and to more complex trabecular shape (Scherf et al., 2013). BS/TV has been proposed as correlated to ecological factors including locomotor adaptations, in recent interspecific evolutionary analyses of mammals~~, i.e.,~~. Specifically, low BS/TV is associated with low and/or infrequent loadings deriving from slow cautious arboreal lifestyle (Alfieri 2022) and hence we can assume that increased loadings would be associated with higher BS/TV.

The aforementioned properties and the related parameters were abundantly employed in the last decades, often computed on subsamples of trabecular bone virtually extracted from epiphyses of skeletal elements represented by µCT scans (e.g. Barak et al., 2013a; DeSilva and Devlin, 2012; Fajardo and Müller, 2001; Hébert et al., 2012; MacLatchy and Müller, 2002; Maga et al., 2006; Ryan and Ketcham, 2002a; Ryan and Shaw, 2015, 2012; Scherf, 2008; Scherf et al., 2013). Due to ~~the~~their well-established use, we can now consider this to be the traditional approach to trabecular structure quantification and we can refer to these traits as 'traditional parameters.' However, alternative approaches have been developed, as the one proposed by Veneziano et al. (2021), based on the study of trabecular bone from entire epiphyses/articulations, instead of subsamples, and, importantly, representing the studied trabecular regions as morphological skeletons. In other words, through a skeletonization procedure, the anatomical information is reduced to only nodes (deriving from the trabeculae connection regions) linked by branches (deriving from the trabeculae themselves). This minimized information provides researchers the advantage to focus only on topological properties of the studied inner epiphysis, i.e. only the spatial arrangement of trabecular struts (through the computation of 'topological indices', detailed below) (Veneziano et al. 2021), hence the skeletonized region is termed 'topological skeleton' hereafter.

Despite the recent work of Veneziano et al. (2021), the trabecular generalisation by means of a topological skeleton is not new and has been previously adopted, for example for the computation of trabecular thickness (Garrahan et al., 1987), and for some of the traditional parameters computed with the BoneJ plugin (Doube et al., 2010) of the FIJI software package (Schneider et al., 2012, see also below).

Wang et al. (2013) compared skeletonized and voxel-based finite element models and found that the former accurately preserves Young's modulus and yield strength of the latter (Wang et al. 2013). Furthermore, skeletonization-derived indices could provide additional information about material properties, besides those already available through bone volume fraction. For instance, Pothuaud et al. (2002) showed that combining topological indices with bone volume fraction leads to better predictions of trabecular material properties than using bone volume fraction alone (Pothuaud et al. 2002). This result suggests that skeletonization-derived indices could contribute to explain part of the material properties' variance not addressed by bone volume fraction. This idea is supported by Liu et al. (2006), who found that the trabecular network topology affects the cancellous mechanical properties regardless of bone volume fraction (Liu et al. 2006). These studies suggest that, because of their topological nature, skeletonization-derived indices could extend the mechanical significance of indices standardly adopted in the study of cancellous architecture.

The topological skeleton of the trabecular lattice allows ~~computing~~the computation of either geometric traits on single trabecular elements or indices devoid of geometric features other than the topology itself. Both these aspects are involved in the computation of the trabecular density, here intended as the number of trabecular elements per unit volume. Trabecular density can be interpreted as a generalisation of BV/TV, and this relationship is exemplified by a recent study: Tsegai et al., (2018) ~~(…)~~ did not directly measure ~~NodDen~~trabecular density but computed BV/TV over a grid enclosing the bone, and used an interpolation to obtain a virtually continuous map of BV/TV. When TV is expressed as a unit of volume (grid size) rather than the full volume, then BV/TV becomes a density. Skeletonization allows to extend this generalisation further to include only topological information in the computation of trabecular density via the computation of "node density" (NodDen hereafter), or the number of nodes of the topological skeleton per unit volume. Veneziano et al. (2021) have computed this density using a kernel-density estimation over a 3D grid: here, the grid size constitutes the volume over which the trabecular bone is counted (i.e., TV). In other words, it extends the computation of BV/TV over a virtually continuous resolution (dependent on the grid size). Considering that NodDen can be thought of as a generalisation of BV/TV, its mechanical significance could

be equivalent: i.e. increased loadings, as those deriving from specific bone uses, joint positions and loads borne during gait and stance, are expected to cause higher NodDen. NodDen results from the preliminary analysis of Veneziano et al. (2021) go in this direction, i.e. the femoral heads of *Gorilla*, *Pan* and *Homo* show higher NodDen compared to quadrupeds and brachiators, compatibly with a prevalent load-bearing use of the hip (Veneziano et al. 2021). Supporting this perspective, Cendre et al. (1999) used a similar index (i.e. node density over total volume) and found it to correlate positively with maximum compressive strength.

Another property whose calculation is simplified by skeletonization is the trabecular length (TrabLen hereafter), measured at each individual branch of the topological skeleton as the geodesic (or arc) length of the branch between the nodes it contacts. ~~Since longer~~Longer trabecular elements are expected within poorly dense structures and – apart from allometric patterns highlighted in mammals (Swartz, 1989) – the length *per se* is suggested to bear a relevance in terms of bone strength (Parkinson et al., 2012~~),~~). Hence, we can expect TrabLen to decrease with increased loadings, i.e. the latter cause shorter trabeculae, in association with a denser skeleton (i.e. higher NodDen). ~~Consistently with this expectation, the length of rod-like trabecular elements was found to correlate negatively with Young's modulus (Zhou et al., 2014), suggesting that short trabeculae provide stiffness and longer ones offer elasticity.~~ The role of TrabLen in the stiffness-elasticity spectrum is better quantified by trabecular tortuosity (TrabTort hereafter). This property is computed dividing the TrabLen (measured as arc length) by the euclidean end-to-end length of each trabecular element, i.e. here being the linear distance between two nodes delimiting one branch. TrabTort provides an intuitive way to describe variations from straight (low tortuosity) to curved/sinuous (high tortuosity) trabeculae. Measures of tortuosity were found to recapitulate bone mechanical properties (Fyhrie and Zauel, 2015), since tortuosity measures the trabecular flexibility under biomechanical load. Specifically, studying the mechanical competence of trabecular architecture, higher tortuosity was found in association with lower stiffness – i.e. higher elasticity (Roque et al., 2012; Roque and Alberich-Bayarri, 2015). Decreased stiffness in a more tortuous and flexible trabecular structure suggests an adaptation to increased

loads. Indeed, for a given stress exerted within a joint, a less stiff material is able to sustain higher strains derived from increased loadings.

Another index that can be computed from the topological skeleton is Fractal Dimension (FD hereafter), a measure of structural complexity based on the concept of statistical self-similarity, i.e. an ideal fractal structure is similar to itself at any degree of magnification (Feder, 1988; Pornprasertsuk et al., 2001). FD measures change in detail across changing scales (Falconer, 2004). The application of FD to trabecular bone has been common, e.g. in studies of fracture risk level and human bone pathology (Feltrin et al., 2004; Messent et al., 2005a, 2005b) thus suggesting a mechanical relevance. Specifically, evidence of the mechanical significance of FD may come from studies highlighting its correlation with bone mineral density, a proxy for bone strength (Ammann and Rizzoli, 2003), or density-related traits in general (in turn related to biomechanical strains, see above). While the correlation between density-related variables and FD seems well supported, it is not easy to establish if it is generally positive or negative, since both the former (Cichański et al., 2010; Feltrin et al., 2001; Uchiyama et al., 1999) and the latter (García-Vilana et al., 2023, Pornprasertsuk et al., 2001) arose. A positive relationship between density-related traits and FD would be theoretically supported by the fact that FD has been shown to be inversely related to Young's Modulus, that in turn positively co-varies with stiffness (Sanchez-Molina et al. 2013). Accordingly, FD would be expected to be inversely related to stiffness and, following what we suggested above for TrabTort, one should expect a direct relationship between FD and bone strength (i.e. the higher ~~is~~the FD, the lower ~~is~~ the stiffness, the more the trabeculae can withstand the loadings). However, this framework seems overly simplistic if one considers the many indirect and complex relationships among different variables, and, also, that the potential relationship between FD and Young's Modulus has been highlighted studying the cortical bone (Sanchez-Molina et al. 2013). In this work, we instead preferred to focus on direct evidence showing that bones experimentally subject to inactivity yield high FD combined with low density (Pornprasertsuk et al., 2001). Indeed, FD also proved useful in studies focusing on mammals to predict mechanically relevant properties or trabecular bone loss (e.g. Chappard et al., 2001). Following this interpretation, we expected higher FD in regions subject to decreased biomechanical loadings. For both the traditional trabecular parameters and the

topological indices, the traits that we treated (above) and computed (in this work) (summarized in Table 2) are only some of the available ones. For additional traits, see Kivell (2016), Veneziano et al. (2021) and references therein.

The potential relationships between the trabecular properties mentioned above and locomotor habits have long been considered as adaptations occurring only during lifetime due to the high ontogenetic plasticity of bone internal structure, i.e. a relationship traditionally known as 'Wolff's Law' or, more recently, 'bone functional adaptation' (Kivell, 2016; Ruff et al., 2006 and references). While this paradigm remains a key tenet in functional morphology, it is also noticeable that recent works studying ecologically-related trabecular bone diversity in wide phylogenetic contexts highlighted that disentangling ontogenetic adaptations from evolutionary acquisitions is challenging ~~(~~, e.g. the studies of Alfieri et al~~,~~. (2023~~;~~) and Amson and Bibi~~,~~ (2021~~;~~), with the former addressing how much internal structure tends to vary following ecological adaptations across generations and through evolutionary processes, a property termed evolvability, instead of adaptations occurring during ontogeny~~).~~. In other words, if distantly related taxa with similar locomotor ecology show the same trabecular properties, it is challenging to discriminate ontogenetic bone functional adaptation from repeated evolutionary acquisition of the same phenotype (i.e. convergent evolution), also considering that developmental patterns are subject to both evolutionary and environmental pressures (Wund, 2012). Trabecular analyses studying specimens at different ontogenetic stages from diverse taxonomic samples may contribute to clarify the extent to which some similarities are phylogenetically fixed. Thus far, trabecular studies with an ontogenetic dimension have only focused on few isolated taxa (e.g. Saers, 2023; Saers et al., 2022; Tsegai et al., 2018). This issue is strictly related to the phylogenetic signal, potentially involved in determining trabecular bone across primates and that, when studied, has yielded contrasting results, e.g. minor phylogenetic effects (Doube et al., 2011; Ryan and Shaw, 2012a), or complex anatomically and taxonomically variable phylogenetic influence (Ryan and Shaw, 2013). Thus, despite the potential of studying trabecular bone to highlight locomotion-related features (see above), one should also consider other influencing aspects, such as phylogeny. It indicates that, overall, the

locomotion of different species cannot be expected as the only factor affecting trabecular bone (as also suggested by experimental studies not yielding the expected trabecular response, e.g. Carlson et al., 2008).

Another major non-locomotor effect potentially at the base of trabecular bone diversity is size, with different allometric patterns found for different parameters (e.g. Barak et al., 2013b; Doube et al., 2011; Ryan and Shaw, 2013; Swartz et al., 1998). Further elements of complexity should be accounted for when interspecific trabecular bone analyses are undertaken (additional details in Kivell, 2016 and references), e.g. uncertainty on the prevalent types of loadings affecting trabecular bone (contractile forces from muscles *vs.* gravitational loads from substrate reaction forces, Judex and Carlson, 2009; Robling, 2009), presence of a loading threshold to trigger trabecular remodelling (Frost, 1987), influence on the trabecular response of genetic (Cunningham and Black, 2009a,b), hormonal (Karlsson et al., 2001; Yeni et al., 2011) and vascular factors (Cunningham and Black, 2010).

1. ~~2~~3. Distal fibula trabecular bone, DOA and functional hypotheses

As detailed above, some studies on primate fibular external morphology yielded a relationship with the DOA (Marchi, 2015b; Marchi et al., 2022). These works focused on the distal epiphysis. This region conceivably bears a functional signal because it articulates with the foot, which is one of the most informative skeletal regions in primates concerning locomotor adaptations (Su and Zeininger, 2022 and references therein), as substrate preference. The distal fibula, together with the distal tibia and the talus, makes up the ankle joint complex (Ding and Song, 2002; Libotte et al., 1982; Seiler, 1986). While for the tibia and talus interspecific trabecular analyses of primates were performed (for the talus, e.g. DeSilva and Devlin, 2012; Hébert et al., 2012; Su et al., 2013; Su and Carlson, 2017; for the distal tibia, e.g. Barak et al., 2013a; Saers et al., 2016; Tsegai et al., 2018) no such studies addressed the fibula. This scenario, together with evidence of a relationship between fibular morphology and locomotor activities, specifically DOA when dealing with non-human primates (e.g. Marchi, 2007; Marchi and Borgognini-Tarli, 2004; Marchi and Shaw, 2011), ~~encourage~~encouraged us to investigate the primate distal fibular trabecular architecture. Besides these aspects, further investigations of the distal fibula aiming to detect features related to substrate

preference, are particularly important because fossil preservation issues concern not only the associated tibiae and fibulae, as mentioned above, but also complete fibulae alone. Indeed, probably due to their extremely slender proportions, fibulae are often found as fragmentary specimens in fossil contexts (even compared to other elongate bones such as the femur and the tibia, the fibula evidently stands out in being particularly thin in primates, a condition that reasonably makes it more fragile and less able to be preserved without being broken along the diaphysis). Accordingly, distal fibular segments are present in the fossil record (e.g. Anemone and Covert, 2000; Gebo et al., 2015; Heaton et al., 2019; Marchi et al., 2017, 2022 and references therein, Ni et al., 2013; Rodríguez et al., 2018). Hence, we considered the distal epiphysis as the most suitable region to conduct this study, based on its expected functional role and presence in the fossil record. Identifying novel primate fibular traits diagnostic of specific locomotor habits and quantifiable on isolated distal epiphyses, can contribute crucially to palaeobiological inference. More specifically, identifying fibular features related to DOA may contribute to long-standing debates in palaeoanthropology, e.g. the extent to which *Australopithecus afarensis* was an arboreal species (Marchi et al. 2022 and references therein).

This being the first analysis of the internal structure of the distal fibula, we based our experimental hypotheses on previous results from functional morphological analyses of this bone, i.e. we tested DOA as the main locomotor factor influencing fibular anatomy (see above). Thus, we studied a set of primate species split in three discrete categories outlining a cline from arboreal to terrestrial taxa, with semi-arboreal ones in between (Table 1, Fig. 1). Apart from the aforementioned previous works on fibular functional morphology in primates, the approach of categorizing primates according to their DOA in these same three discrete categories has been used by Henderson et al. (2017). Moreover, DOA meant as the relative amount of time spent on trees (although not formalized in discrete categories) arose as a major factor able to explain morphological variation in the primate bone postcranial features studied in Carlson (2005).

Arboreal species are generally characterized by abducted and flexed limbs during quadrupedal locomotion, allowing them to control the center of gravity and to grasp supports of small diameters. The

presence of small diameter supports also involves the need for supinated (i.e. inverted, adducted and plantarflexed) foot postures. Moreover, the irregular, highly variable and discontinuous substrates represented by the arboreal environment cause a pronounced joint mobility and range of motion in arboreal species (Carlson, 2005). The arboreal configuration neatly contrasts with the adducted and extended limbs with a more everted foot posture of terrestrial taxa (Meldrum, 1991 and references therein). From these broad differences between arboreal and terrestrial primates, it ~~derives~~can be inferred that the ankle joint of an arboreal primate is likely extremely mobile, especially ~~medio-laterally~~in mediolateral (ML) direction, with associated higher mobility of the fibula and large dorsi-plantarflexion range of the foot (Barnett and Napier, 1952). As suggested by studies on both forelimbs and hindlimbs of lemurids, in arboreal environments primate limbs likely exert forces that are more frequently medially directed, while during terrestrial locomotion the side-to-side more frequent component is towards the lateral direction (Carlson et al., 2005). ~~Considering that substrate~~Substrate reaction forces (SRFs, in their vertical, fore-aft and side-to-side components) are opposite in direction compared to forces (in the respective component) primarily exerted by an animal's limb. Thus, we can expect that in the arboreal environment SRFs will be more frequently directed laterally, compared to what occurs on the ground, since arboreal primates mainly exert medially directed forces (see above). While this pattern was highlighted for lemurids, similar results arose for anthropoids too (although this is based on a study restricted to the forelimb; Schmitt, 2003). Hence, since the fibula is located on the lateral side of the ankle joint, we here hypothesize that the likely more frequent lateral SRFs in arboreal environments result in increased loadings on the distal fibula of arboreal primates compared to terrestrial taxa. Moreover, due to the highly variably directed loadings involved in the arboreal environment (e.g. Demes et al. 2001; Carlson, 2005) and the extremely mobile ankle joint of arboreal primates (see above), we expect that the range of directional variation of biomechanical loadings to which the distal fibula is subject, is larger for arboreal taxa compared to terrestrial species. For both the hypotheses related to increased/decreased loadings and more/less variable orientation, along the DOA range going from arboreal to terrestrial (see Table 1 and above), semi-arboreal taxa should be characterized by intermediate conditions.

It should be noted that our functional hypothesis, based on more frequent lateral SRFs in the ankle of arboreal compared to terrestrial primates (see above), refers to ML SRFs deriving from linear locomotion (Carlson et al. 2005). Besides them, ML SRFs caused by turning behaviors (i.e. deriving from changes of direction) are substantial in the primate ankle and the medial SRFs are higher than the lateral SRFs in terms of magnitude, both on the ground and on the trees (Demes et al., 2006). It is not surprising if one considers the evidently higher robustness of the tibia (medially located) compared to the fibula (laterally located), a condition that is widespread in primates and consistent with the fact that, in general and regardless of substrate, medial SRFs are higher than lateral SRFs. However, we base our hypothesis (detailed above) on a comparison of the SRFs on the lateral side of the ankle in arboreal *vs.* terrestrial environments (regardless of SRFs acting on the tibia) and, importantly, our hypothesis is based on ankle lateral loadings that are more frequent (and not with higher magnitude) for arboreal primates. If we consider that turning behaviors are expected to be more frequent during arboreal locomotion (as Demes et al. 2006 suggest), it is possible that in the resulting forces the ankle lateral SRFs in arboreal environment would be relatively more frequent (~~consistently~~consistent with the results of Carlson et al. ~~2005's results~~[2005] on linear locomotion), even if, just as the ankle lateral SRFs in terrestrial environment, they are characterized by relatively low magnitude. In other words, we expect that the low magnitude but frequent loadings experienced by the fibula of arboreal mammals can differentially affect trabecular remodeling compared to the low magnitude, but less frequent ~~ones~~loadings, experienced by the fibula of terrestrial species (see above and Rubin et al. 2001, 2002). Although Demes et al. (2006) did not detect any lateral SRFs in arboreal environment, their work ~~was~~did not ~~focusing~~focus on ~~SRFs~~SRF frequency (which is an aspect not tested, indeed) (Demes et al. 2006) and it may be possible that the absence of measured lateral SRFs during the arboreal behavior depends on the specific experimental setting and/or study system (the capuchin monkey *Cebus apella*). Apart from this, ~~while~~ Demes and Carlson (2009) showed that both on arboreal and terrestrial substrates the ~~SRFs~~SRF vectors are oriented medially to the segment of the distal portion of the hindlimb. However, if we consider the extremely abducted condition of arboreal ~~primates'~~primate limbs, the resultant SRFs in an arboreal environment tend to be relatively more laterally oriented than on the ground (Demes and Carlson, 2009). It

supports our hypothesis and the expected increased loadings on the fibula in an arboreal environment, not only in terms of frequency but also in terms of direction. Hence, although we recognize that the loading pattern in the primate ankle is probably more complex than how we modeled it, we will follow the hypotheses of previous functional morphological analyses of the primate fibula (e.g. Marchi, 2007; Marchi and Borgognini-Tarli, 2004; Marchi and Shaw, 2011).

In summary, considering the expected functional patterns for the trabecular parameters mentioned above and in Table 2, our hypotheses ~~involve~~predict that, due to the expected more frequent loadings on the lateral side of their ankle, arboreal primates should have a distal fibula trabecular structure ideally characterized by higher values for density-related traits (i.e. BV/TV, Tb.Th, NodDen), higher BS/TV, with trabeculae that are shorter (i.e. lower TrabLen), more curved and convoluted (higher TrabTort) and yielding lower FD. Furthermore, the largely multidirectional nature of loadings involved in the arboreal environment should result in lower DA for arboreal primates. For all these variables, the opposite configuration is expected for terrestrial primates, with semi-arboreal taxa showing intermediate values, e.g. significantly higher than those arboreal taxa but significantly lower than those of terrestrial taxa (depending on the expected pattern of co-variation with DOA, see above).

~~To test our hypotheses, we undertook the first three-dimensional quantitative analysis of fibular trabecular structure in a sample of primate species (Fig. 1, Table 1). To isolate the distal fibular inner structure, we extracted whole articular trabecular networks employing the segmentation approach of Veneziano et al. (2021). We extracted both traditional trabecular parameters and recently developed topological indices following Veneziano et al. (2021) (Table 2). Our primary aim was ascertaining the presence of a locomotor signal related to DOA in the trabecular architecture of the primate distal fibula according to the functional hypotheses detailed above. While we defined detailed expectations for each of the studied traits, we were also aware that, as proposed by Ryan and Shaw (2012), most trabecular properties are inter-related (as detailed above) and interpretations of functional relationships between single parameters and specific biomechanical aspects may be less straightforward, compared to e.g. diaphyseal properties~~

~~studied through CSG. It follows that, in some cases, identifying suites of functional traits discriminating locomotor categories may be preferred over univariate interspecific comparisons (Ryan and Shaw, 2012). For this reason, we analyzed trabecular variables both univariately and multivariately. Because this study is the first to directly address the trabecular bone of the primate fibula, we also aimed at disentangling the effects related to DOA from those of two other major factors that are related to skeletal morphology: i.e. body mass and phylogenetic relationships, by employing a body mass proxy and phylogenetic comparative methods, respectively.~~

2. Materials and Methods

2. 1. Sample

The analyzed sample is represented by µCT scans from 28 fibulae, representing 21 primate species and including representatives of Strepsirrhini, Platyrrhini and Catarrhini (Fig. 1, Table 1). These µCT data stem from new acquisitions (performed at the National Research Council, CNR, Pisa, Italy) on samples from University of Florence, Italy (Florence Museal System, section La Specola and section of Anthropology and Ethnology) or downloading from MorphoSource (https://www.morphosource.org/). Details on the analyzed fibulae and µCT scans (e.g. resolution, museum collection from which the specimens were sampled, catalogue numbers) are provided in Table S1. All non-human primate data derive from bones of wild-caught individuals, with the exception of *Leontocebus fuscicollis* FMNH 122268 and *Saguinus imperator* FMNH 121551. All fibulae come from adult non-pathological individuals, with adulthood determined by evaluating the degree of fusion of long bone epiphyses. Only one fibula, i.e. *Propithecus diadema* UniFl-SPEC 1505, may belong to a sub-adult individual since the femur, present in the same collection where the fibula was collected, shows incomplete fusion of the epiphysis. Right and left fibulae were pooled together, since bilateral asymmetry is regarded as a negligible factor in primate adult hindlimb analyses (Ruff and Jones, 1981, see also Auerbach and Ruff, 2006). After parameter extraction (see below), for each µCT scan we computed the relative resolution (i.e. Tb.Th divided by the voxel size, the former computed with the Bone

J plugin, see below), yielding an average value of 8.91. We found a relative resolution ranging from 5.4 to 13.22, hence above the minimum recommended limit (i.e. 5, Kivell et al., 2011; Sode et al., 2008), with the only exception of the µCT scan of *Otolemur crassicaudatus* AMNH 80801 (3.47) (Table S1). However, the latter was visually validated, evaluating resolution and contrast.

2. 2. Data collection

2. 2. 1. Anatomical region

We focused on the fibulotalar articulation of the distal fibula. In this region, it is possible to identify a proximal and a distal part, termed PAF (proximal articular facet) and DAF (distal articular facet), respectively (Marchi et al., 2022 and fig. 2 therein, Fig. 2). Both are involved in important functions, e.g. PAF/DAF surface ratio is possibly a fibula load-bearing indicator (Marchi, 2015b; Preuschoft, 1970). Across the studied primates, we expected to find PAF and DAF as quite regular-shaped (in medial view), i.e. PAF as approximately rectangular-elliptical and DAF as approximately triangular, based on previous observations on hominids (Marchi, 2015b). However, DAF, albeit being approximately triangular, showed large variation in size and proportions, preventing a repeatable extraction of anatomically homologous trabecular bone (see below). We hence only analyzed PAF.

2. 2. 2. Orientation and crop

The orientation in standard position and the subsequent crop of the distal fibula region corresponding to PAF were performed in VG Studio Max 3.3 (Volume Graphics, Heidelberg, Germany). First, we positioned PAF in the coronal plane (Fig. 2A, B). Then, we positioned the major and minor sizes of the quasi-elliptical/rectangular PAF in the sagittal and transverse plane (Fig. 2C). From oriented µCT stacks, we exported sub-stacks of images (16-bits in TIFF format) that in the following steps allowed us to isolate only the trabecular structure underlying PAF (see below) but at this stage are still including both cortical and trabecular bone (Fig. 2D, Fig. 3A). To do so, we cropped the volume between the proximal and the

distal limit of PAF. The sub-stacks were subsequently imported in FIJI, binarized and purified employing BoneJ (through the 'Optimise Threshold > Threshold Only' and 'Purify' routines) and then re-exported. The purifying step (https://bonej.org/purify) acts on binarized stacks, identifying and removing all the foreground particles (recognized as 'bone' by the binarizing algorithm) except for the largest one (i.e. the studied anatomical element, in this case). To be recognized as not belonging to the largest particle, a foreground voxel should not be connected (in 3D) at any point to the cortical or trabecular bone, i.e. it should be a particle that is isolated ('floating') in 3D (either within the intertrabecular voids or outside the bone). Due to the nature of trabecular bone, i.e. the material is always connected to other bone regions, such floating particles necessarily represent an artifact (i.e. isolated voxels outside the bone fraction that are erroneously recognized as bone) that, if not removed, may bias some trabecular parameters (e.g. they artificially increase BV/TV). Hence, by purifying we corrected for the potential presence of small isolated particles erroneously recognized as 'bone' that may derive from the binarizing algorithm and depending on the µCT scan grey values.

2. 2. 3. Trabecular bone isolation

We imported the oriented, binarized and purified sub-stacks in R (R Core Team, 2022) ('readTiffStack' function, 'indianaBones' package, Veneziano et al., 2021, https://zenodo.org/record/7615165). To isolate Regions of Interest representing the entire trabecular bone underlying PAF (Fig. 2D, Fig. 3B) (referred to as 'ROI' hereafter), we used the 'makeBrush' ('size'=11; 'EBImage' package, Pau et al., 2010) and the 'splitBone' functions ('indianaBones'). On each specimen, we iterated the isolation procedure calibrating the value of the 'iterFill' argument of 'splitBone', i.e. increasing it and decreasing it. We visually evaluated, for each iteration, the quality of trabecular isolation by comparing the result of the automatic procedure (hence, the ROIs, as shown in Fig. 3B) with the trabecular network visible in the stack representing both compact and trabecular bone (Fig. 3A). When we considered the isolation to be optimal, we used the corresponding 'iterFill' value of 'splitBone for that specimen (values used for all the specimens are listed

in Table S1). The ROIs (e.g. Fig. 2D, Fig. 3B) were exported as image stacks ('writeTiffStack' function, 'indianaBones').

2. 2. 4. Trabecular architecture quantification

We extracted traditional trabecular parameters, through the BoneJ plugin in FIJI, as well as topological indices, computed through 'indianaBones' in R (Veneziano et al. 2021). For the former, we imported the ROIs in FIJI and, through the respective BoneJ routines, we extracted degree of anisotropy (DA, no unit), trabecular thickness (Tb.Th, mm), connectivity (Conn., no unit, computed only to evaluate trabecular number, see below), Bone Volume (BV, mm^3) and Bone Surface (BS, mm^2). Conn. is assumed to be an approximation of trabecular number and in this study yielded values greater than 146 (Table S1), allowing us to follow ~~Mielke et al.'s~~the recommendation of studying only volumes with more than 50 trabeculae to reliably quantify trabecular architecture (Mielke et al., 2018). BV and BS values were used to obtain BV/TV and BS/TV. To do so, first we needed to compute the total volume represented by each ROI (TV, mm^3). Since the ROIs are not of regular shape (e.g. Fig. 3B), we exploited the 'indianaBones' function separating trabecular bone from intertrabecular voids and from compact bone (see above). After splitting these three components, one can add the trabecular bone volume to the total volume of intertrabecular voids, obtaining the whole inner volume, i.e. the entire joint excluding the compact shell. ~~It~~This represents TV. Hence, dividing BV and BS by TV, we obtained Bone volume fraction (BV/TV, no unit) and Bone surface density (BS/TV, mm^{-1}), respectively.

The topological indices were computed on skeletonized substacks ('Auto Skeleton' tool, Amira 6.0.0, Thermo Fisher Scientific, followed by exportation in ASCII format). We imported the skeletons in R ('readAmiraSkeleton' function, 'indianaBones') and using the respective 'indianaBones' functions (as detailed in Veneziano et al. 2021, Supplementary ~~material~~Material and the R code of this work), we extracted (see also Table 2): average and median of the node density ($NodDen_{Aver}$ and $NodDen_{Med}$, unit: nodes per mm^3), average of the trabecular length ($TrabLen_{Aver}$, untiless), average and median of the trabecular tortuosity ($TrabTort_{Aver}$, $TrabTort_{Med}$, unitless) and fractal dimension (FD, unitless). For the

computation of FD, that is obtained via the Box-counting algorithm (Annadhason, 2012), we ~~needed~~used another R package, i.e. 'Rdimtools' (You and Shung, 2022) (see Supplementary ~~material~~Material).

2. 2. 5. Substrate preference

We aimed to test potential effects related to substrate preference, i.e. DOA, on distal fibular trabecular architecture. To each analyzed species we assigned one of three discrete states, based on previous descriptions and/or the reported amount of time spent on substrates (references in Table 1): 'arboreal' or 'terrestrial' were assigned to species living almost exclusively on trees or on the ground, respectively; 'semi-arboreal' was assigned to species spending a comparable amount of time on trees and ground (also defined 'scansorial' in other studies; e.g. Chen and Wilson, 2015).

2. 2. 6. Body mass

To estimate how distal fibular trabecular architecture is related to body mass, for each individual we measured the superoinferior diameter of the femoral head, recognized as a reliable body mass proxy in human and non-human primates (Ruff, 2003; Ruff et al., 2018). For fibulae collected in museums, we extracted this measure with ~~a caliper~~calipers, from the femora of the same individuals available in the collection. When both femora were available, the right and left superoinferior diameters were measured, taking the average of the two values. For individuals whose fibulae were included by downloading µCT scans from MorphoSource (see above, Table S1), image stacks of the femur were available and downloaded too. We oriented the femora in standard position (following Ruff, 2002) in VG Studio, and measured the superoinferior diameter of the head, multiplying the µCT voxel size by the number of slices included between the most superior and the most inferior point of the head. To cope with outliers, e.g. human values largely lying outside the range of variation of all the other primate specimens, the body mass proxy values were natural log-transformed (hereafter, referred to as 'log-BMp') (Table S1, Fig. 1).

We are aware that the femora of the individuals from which the fibula is studied may be not available~~,~~ ~~as instead it occurred for this study.~~. The anteroposterior length of PAF measured at the 50% proximodistal level (PAF AP length in Table S1), i.e. one of the two sizes of the ellipse-rectangle which PAF resembles (e.g. the major size in Fig. 2C), when natural log-transformed shows a strong correlation with log-BMp (Pearson's correlation coefficient= 0.96, *p*-value <0.001). Thus, in distal fibula trabecular analyses in which only fibulae are available, e.g. when fossil fibulae are studied, this fibular metric can be used as an alternative body mass proxy.

2. 2. 7. Phylogenetic relationships

To determine the effect of phylogenetic relationships on primate distal fibular trabecular architecture (see below), we obtained a time-calibrated phylogeny of the studied species. A Maximum Clade Credibility DNA-only node-dated tree, including 4098 mammal species, devoid of polytomies and deriving from the posterior distribution of Upham et al., 2019, was modified in R ('drop.tip' function, 'ape' R package, Paradis et al., 2004) including only the studied species (Fig. 1).

2. 3. Statistical analysis

We performed all the statistical analyses in R. For each trabecular trait and log-BMp, we computed average species values. Noticeably, most species values are those of single specimens (see Potential Limitations, below~~).~~, and Supplementary Material). The species for which we collected data from more than one fibula (sample size > 1, see Table 1) are *Ateles paniscus*, *Cercopithecus mitis*, *Colobus guereza* and *Homo sapiens* (for them, mean values, standard deviation and coefficient of variation for each trabecular trait are shown in Table S2). We estimated the relative effects of DOA, body mass and phylogenetic structure on the trabecular structure of the primate distal fibula in both a univariate and a multivariate way. To undertake the former, we ran several Phylogenetic Generalized Least Squares (PGLS) regressions ('gls' function, 'nlme' package, Pinheiro et al., 2020; including the use of 'corPagel' function, 'ape' R package) with morphological traits as dependent variables, DOA ('arboreal', 'semi-arboreal', 'terrestrial') as

independent variable and log-BMp as covariate, besides phylogenetic ANOVAs (pANOVA) ('phylANOVA' function, 'phytools' package, Revell, 2012). We planned to run post-hoc Tukey tests ('glht' function, 'multcomp' package, Hothorn et al., 2008) after pANOVAs only in case of significant *p*-value (<0.05) from pANOVAs. For each PGLS, we log-transformed the respective morphological trait if the PGLS residuals showed a distribution clearly deviating from normality (traits summarized in Table 3). Importantly, we ensured that in each PGLS, DOA and body mass effects were not interacting by preliminarily running a PGLS + pANOVA, with log-BMp and DOA as dependent and independent variables, respectively. Since it excluded any correlation between body mass and DOA (*p*-value=0.17) we were sure that the p-values resulting from each PGLS informed on ~~separated~~separate effects of DOA and body mass. When a parameter was significantly related to body mass (i.e. body mass *p*-value deriving from the respective PGLS being <0.05) to quantify DOA effects (with the ideal exclusion of allometric effects) we ran the pANOVA using size-corrected values for the parameter (with size-correction corresponding to taking the residuals of a linear regression of the parameter against log-BMp).

To determine the phylogenetic signal of each variable, we estimated the Pagel's λ ('phylosig' function, 'phytools' package), testing the null hypothesis of λ different from zero ('test'=TRUE). λ yields values ranging from 0 (i.e. no phylogenetic effects) to 1 (i.e. trait distribution is entirely explained by a Brownian motion model of morphological evolution and, hence, it exclusively depends on phylogenetic relationships among taxa). Moreover, we estimated how the log-BMp distribution is related to the phylogenetic structure through λ. It was needed because, in case of significant phylogenetic signal in log-BMp, an important implication would be that for variables ~~resulting as~~ related to both body mass and phylogenetic structure, it ~~is~~would not be possible to disentangle the effects of the two factors~~, e.g.~~. For instance, the variable may be primarily affected by body mass and the phylogenetic structure results as a trabecular correlate only because of its interaction with body mass (or vice versa). In such cases, a size-correction may correct for a part of the effects of the phylogeny, too. ~~It is also suggested by previous works, where size-corrected values for trabecular parameters resulted in a minor phylogenetic signal (e.g. Ryan and Shaw, 2012) differently from non-size corrected value, instead showing significant phylogenetic effects (e.g. O'Neill and Dobson, 2008).~~

In other words, if body mass and phylogeny are correlated, through size-correction it is possible to obtain values partially devoid of phylogenetic effects, and not only of size ones, that can be better studied for a relationship with DOA. Nevertheless, we have no ~~ways~~way to ~~understand~~determine which ~~is~~ factor primarily affects a given trabecular feature. To test if and to ~~which~~what extent size-corrected values are also corrected for phylogenetic effects, for variables showing a significant relationship with body mass, we measured the phylogenetic signal both before (Table 3) and after size-correction (Table 4). To account for problems deriving from multiple testing, all the PGLSs *p*-values were corrected through the Bonferroni method ('p-adjust' function). We visualized how trabecular variables vary according to DOA through boxplots ("ggplot" function, "ggplot2" R package; Wickham, 2016) (Fig. 4, Fig. S1), generating additional boxplots with size-corrected values (as detailed above) when traits showed a significant relationship with log-BMp (Table 3). To visualize how each trabecular variable is related to body mass we used bivariate scatterplots (Fig. S2A, B). To visualize how traits are related to phylogeny, for each of them we mapped average species values on the time-calibrated tree ('contMap" function, 'phytools' package), also using the size-corrected values for traits showing significant relationship with body mass (Fig. S3).

By also running a multivariate analysis ~~too~~, we aligned to the approach suggested by Ryan and Shaw (2012) when one aims to analyze functional adaptations of trabecular structure: i.e. accounting for suites of possibly intercorrelated traits (as it often occurs for trabecular variables, e.g. Cotter et al., 2009; Mittra et al., 2008, 2005), instead of isolated variables, to better identify patterns related to locomotion (Ryan and Shaw, 2012). The multivariate part of the analysis is based on two PCAs. PCA is often used when intercorrelated variables are analyzed together with the aim of isolating the contribution of single variables (as cranial measurements, e.g. Frost et al., 2003; Landi et al., 2021; Nishimura et al., 2019). We ran two different PCAs in order to follow both an inferential quantitative and an exploratory approach:

1. A first PCA was run on a data matrix of the computed trabecular variables (i.e. variables in Table 3 excluding log-BMproxy) after scaling and centering ('scale' function). The extent to which DOA, body mass and phylogeny are related to the whole trabecular architecture were quantified through

a phylogenetically informed multivariate Generalized Least Squares Regression. After regressing PC1-PC4 (chosen since cumulatively explaining more than 90%, i.e. 93%, of the variance, Table S3) against the discrete variable, i.e. DOA, and with log-BMp as covariate ('mvgls' function, 'mvMORPH' package, Clavel et al., 2015, model= 'lambda', REML=FALSE), we tested for significance through a phylogenetic MANCOVA ('manova.gls' function, 'mvMORPH' package, test= 'Pillai', type= 'II'). As detailed above for univariate PGLSs, the absence of significant DOA-body mass correlation allowed us to compute *p*-values exclusively informing on the effects of DOA (separating them from those related to body mass) on trabecular structure. To assess the phylogenetic signal of PC1-PC4, we estimated λ through the 'transformPhylo.ML' function ('motmot' package, Puttick et al., 2019, model= 'lambda').

2. A second PCA was run to follow an exploratory, instead of a strictly inferential, statistical approach, i.e. to visualize patterns exploiting the decomposition of original variance into new variables, i.e. Principal Components, performed through PCA. We wanted to exploit this second PCA and the deriving morphospace to visualize potential effects related to DOA that may be not detected as significant by other statistical analyses (e.g. due to sample size) and that, ideally, do not include the potential body size effects on trabecular variables. Hence, the variables significantly related to body mass (Table 3) were included in this second PCA in their size-corrected version (see above). The resulting PC1-PC4 (cumulatively accounting for around 85% of the variance, Table S4) were used to build bivariate phylo-morphospaces (Fig. 5, Fig. S4). These plots allowed us to visualize how subsets of trabecular traits (size-corrected, if needed) relate each other, how they relate to DOA and how they relate to phylogenetic relationships~~,~~. This is possible since the ~~latter are~~phylogeny is mapped on the plot and the phenotypes corresponding ~~phenotypes~~ to specific taxa are shown by means of tips and nodes positions on the plot (i.e. closer points reflect phenotypes that are more similar each other). Specifically, actual data points (labeled in Fig. 5 and Fig. S4 and deriving from measures extracted in this work) determine the position of the tips of the phylogeny, while the position for the tree internal nodes (unlabeled in Fig. 5 and Fig. S4) is determined by

ancestral phenotypes reconstructed from tip values and assuming a Brownian motion model of evolution (see 'phylomorphospace' R function, 'phytools' package).

3. Results

3. 1. Univariate analysis

Results of PGLSs, pANOVAs and Pagel's λ are summarized in Table 3. pANOVAs, including those on size-corrected variables, did not detect any significant relationship with DOA. Hence, we did not run any post-hoc Tukey ~~test~~tests. Almost no expected signal related to DOA for most of the trabecular parameters of the primate distal fibula is evident from the distribution of species trait values: data pooled by DOA do not reflect any pattern or, when their distribution apparently follows DOA, it involves large overlap (e.g. size-corrected $TrabLen_{Aver}$, and $TrabTort_{Aver}$). Also, when traits that appear to be partially related to DOA (e.g. Tb.Th, log-$NodDen_{Aver}$) are size-corrected, no pattern is evident anymore (Fig. S1). Two potential exceptions are represented by the patterns shown by BV/TV and size-corrected BS/TV. Indeed, although with some overlap and outliers (i.e. *H. ~~sapiens~~'sapiens* BV/TV value lying within the arboreal range and *P. ~~troglodytes~~'troglodytes* size-corrected BS/TV value lying within the terrestrial range) and despite their non-significant relationship with locomotor habits (Table 3), in the two variables it seems to be involved a trend following DOA: terrestrial ~~species~~'species values > semi-arboreal ~~species~~'species values > arboreal ~~species~~'species values (Fig. 4, Fig. S1, but see the strong phylogenetic signal of size-corrected BS/TV, Table 4 and below).

Overall, the trabecular structure of primate distal fibula appears to be substantially related to body mass, as one can evince from the fact that several trabecular traits are significantly related to log-BMp (i.e. six out of 10). The traits that show no relationship with size are DA, BV/TV and TrabTort (both $_{Aver}$ and $_{Med}$) (Table 3). The important effect of body mass on trabecular architecture is also clear from bivariate scatterplots of trabecular traits vs. log-BMp, from which it is also evident that the studied trabecular traits exhibit both direct, i.e. Tb.Th, $TrabLen_{Aver}$, FD, and inverse proportionality, i.e. BS/TV and NodDens (both $_{Aver}$ and $_{Med}$),

with log-~~BMproxy. Consistently with PGLSs~~BMp. To compare our results to previously identified allometric patterns (see Discussion), for Tb.Th, we additionally ran a 'Tb.Th ~ logBMp' linear regression (using data on single specimens, hence not averaging for species) and we found that its covariation with body mass can be explained by the relationship 'Tb.Th= (0.07±0.01) * logBMp' (slope p-value<0.001, while the intercept estimate is not significantly different from 0, intercept p-value=0.44). Consistent with PGLS results, DA, BV/TV, $TrabTort_{Aver}$ and $TrabTort_{Med}$ do not reveal any pattern related to body mass (Figs. S2A, B).

We found a strong phylogenetic signal in four out of 10 trabecular traits, i.e. Tb.Th, NodDen, both $_{Aver}$ and $_{Med,}$ and $TrabLen_{Aver}$, for which λ is very close to 1.0, i.e., 0.94-0.99, and the related p-values yield significance. For another trait, i.e., FD, λ is quite high but not extremely close to 1.0 (0.81) with a significant related p-value (Table 3). For these parameters, from the species values mapped on the time-tree it is evident that the strong relationship with phylogeny may be due to the fact that trabecular values often range in between two extremes represented by some/all platyrrhines, on the one hand, and catarrhines (especially hominids), on the other hand (Fig. S3). It should be noted that the traits not significantly affected by phylogeny are those that are not significantly related to body mass too, i.e., DA, BV/TV, $TrabTort_{Aver}$ and $TrabTort_{Med}$, with the only exception of BS/TV that, despite showing a significant relationship with body mass does not exhibit a significant phylogenetic signal (Table 3). It likely derives from an important outcome of this work: the body mass proxy is significantly related to phylogenetic relationships itself (λ = 0.99, p-value < 0.001). Hence, for the five traits that are correlated to both body-mass and phylogeny, i.e. Tb.Th, NodDen (both $_{Aver}$ and $_{Med}$), $TrabLen_{Aver}$ and FD, it is not possible to disentangle the body mass and phylogenetic effects. In support of this, for almost all the traits, size-correction results in a sharply weakened phylogenetic signal, i.e. phylogenetic effects that are not significant anymore for Tb.Th, NodDen (both $_{Aver}$ and $_{Med}$) and FD, with only $TrabLen_{Aver}$ ~~that instead retains~~retaining a significant phylogenetic signal but through a decreased λ, i.e. from 0.98 to 0.78 (Tables 3 and 4). Again, a particular case is represented by BS/TV, unique in showing raw values significantly related to body mass but without any phylogenetic signal (Table 3) and size-corrected values involving strong phylogenetic effects (Table 4).

3. 2. Multivariate analysis

The multivariate PGLS and pMANCOVA performed on PC1-PC4 extracted from the first PCA (including raw trabecular variables) suggests that, overall, the trabecular architecture of the primate distal fibula is not correlated to DOA (p-value = 0.5). Instead, PC1-PC4 result to be significantly related to body mass (p-value < 0.001) and/or they involve a strong phylogenetic signal (λ=0.95: lower 95%CI = 0.73, upper 95%CI = 0.99), with the impossibility ~~to determine~~of determining which of the two factors exclusively/mostly relates to primate distal fibula trabecular structure (see also above).

The exploratory multivariate analysis was based on a visual assessment on bivariate phylomorphospaces built with PC1-PC4 deriving from the second PCA, that included size-corrected values for variables related to log-~~BMproxy~~BMp. As detailed above, since log-~~BMproxy~~BMp is correlated to phylogeny, size-correction expectedly removed a part of the phylogenetic signal included in primate distal fibula trabecular structure too (even if we expected that the PCs still involve minor phylogenetic effects, as suggested by the significant phylogenetic signal of size-corrected $TrabLen_{Aver}$ and size-corrected BS/TV; Tables 3 and 4; see also below). Accordingly, the observations on morphospaces built with PCs deriving from the second PCA, detailed as ~~following~~follows, allowed us to focus on other effects than allometry and phylogeny.

On all the biplots built with PC1-PC4, arboreal species occupy a ~~widely~~ larger region, compared to the one occupied by semi-arboreal and terrestrial taxa. ~~The PC~~ PC1 (explaining ~~most~~33.6% of the variance~~, i.e. PC1 (33.6%),~~), yields a separation between two species, i.e. *H. sapiens* and *C. jacchus*, showing lower PC1 scores, and the rest of the taxa, showing higher PC1 scores. As suggested by vector orientations and lengths in the variable loading plots, the trend of *H. sapiens* and *C. jacchus* to be set apart with lower PC1 from the other studied primates, appears to be explained by higher NodDen (both $_{Aver}$ and $_{Med}$) and FD, and lower TrabTort (both $_{Aver}$ and $_{Med}$). Other variables seem to contribute to PC1 scores (e.g. DA oriented at around 45° in the PC1-PC2 or PC1-PC4 plots or Tb.Th oriented at around 45° in the PC1-PC4 plot, both suggesting similar contributions to PC1 and other PCs) but the shorter related vector length also indicates a probable

lower importance compared to the other variables mentioned above (Fig. 5, Fig. S4). PC2, explaining 27.4% of the variance and apparently driven by lower BS/TV, BV/TV, Tb.Th and $TrabLen_{Aver}$, yields a pattern that, although with extensive overlap and with the outlying *H. sapiens* (see below), suggests a gradient going from terrestrial species, (lower PC2 scores) to arboreal species (higher PC2 scores) with semi-arboreal species occupying the lower range of the arboreal region and yielding slightly higher PC2 than terrestrial species (pattern highlighted univariately in Fig. 5D, see also Fig. S4). Remarkably, it is also evident that PC2 separates platyrrhines (higher scores) from catarrhines and strepsirrhines (lower scores) and that, if we exclude *H. sapiens* and *C. jacchus*, the smaller taxa (e.g. *Mico* spp., *L. rosalia*) yield higher PC2 scores and the larger taxa (e.g. *Papio spp*., *P. troglodytes*) yield lower PC2 scores. PC3 and PC4, cumulatively explaining 24% of the variance, when plotted together show the relative isolation of *Otolemur crassicaudatus* from all the other taxa, toward the morphospace region corresponding to lower PC3 and PC4 scores and that appear to be explained by higher DA and $TrabLen_{Aver}$ (Fig. 5, Fig. S4). Interestingly, in the PC1-PC3 plot, *C. jacchus* tends to occupy the morphospace region corresponding to lower PC1 scores and higher PC3 scores, potentially driven by a low $TrabLen_{Aver}$ (while higher values of this parameter seem to contribute to set apart *O. crassicaudatus*, as mentioned above) and *H. sapiens* tends to occupy the region corresponding to lower PC1 and lower PC3 scores, potentially driven by higher DA and low TrabTort (both $_{Med}$ and $_{Aver}$). A remarkable result is represented by *H. sapiens* never clustering close to *P. hamadryas*, *P. cynocephalus* and *M. nemestrina*, the other terrestrial taxa, in all the phylo-morphospaces.

4. Discussion

In primate functional morphology, the fibula has long been neglected and, when addressed, it has been initially studied only in association with the tibia. The analysis of the tibia-fibula complex has highlighted a positive relationship between fibular relative diaphyseal robusticity and the frequency of laterally oriented loadings in the distal portion of the hindlimb, in turn suggested to be related to the DOA (e.g., Marchi, 2015b, 2007; Marchi and Borgognini-Tarli, 2004), hence providing a valuable tool to infer arboreal adaptations in extinct primates. However, the use of this proxy to reconstruct DOA of extinct primates is

749 limited by the paucity of associated fossil tibiae and fibulae. Recent works, performed with different
750 methodological approaches (e.g., diaphyseal CSG, functional indices and 3D GM, Marchi, 2015b; Marchi
751 et al., 2022; Marchi and Shaw, 2011), have also shown that some traits of the fibula alone may relate to
752 DOA. To identify further fibular characteristics potentially reflecting DOA and applicable for
753 palaeobiological inferences, in this work we addressed the distal epiphyseal trabecular architecture, an
754 anatomical level never studied before in a primate comparative sample.

755 ~~Instead of the common approach based on extracting regularly-shaped ROIs (e.g. spherical, cubic)~~
756 ~~representing subsamples of trabecular bone, we here extracted ROIs representing the entire trabecular bone~~
757 ~~underlying a distal fibular articular facet, i.e. PAF. On these ROIs, we quantified the trabecular structure~~
758 ~~using both traditional parameters, i.e. DA, BV/TV, Tb.Th and BS/TV., and recently developed topological~~
759 ~~indices computed on morphological skeletons (Veneziano et al. 2021), NodDen, TrabLen, TrabTort and FD.~~
760 ~~For these parameters, a biomechanical significance is suggested by previous experimental and comparative~~
761 ~~evidence (see also Introduction). DA is expected to relate to the how the joint is loaded, in terms of load~~
762 ~~orientation, during movements, i.e. more stereotyped behaviors cause more directionally stereotyped~~
763 ~~loading which are, in turn, associated with higher DA (e.g. Biewener et al., 1996; Pontzer et al., 2006; Ryan~~
764 ~~and Ketcham, 2002a). BV/TV, Tb.Th and NodDen, density-related traits, are hypothesized to positively co-~~
765 ~~vary with the magnitude, duration and/or frequency of strains and loads acting on joints, (Barak et al., 2011;~~
766 ~~Chang et al., 2008; Mittra et al., 2005; Sukhdeo et al. 2020, Veneziano et al., 2021). BS/TV, TrabTort and~~
767 ~~FD, informing on shape and complexity properties of the ROI, reportedly relate to locomotor aspects. For~~
768 ~~instance, low BS/TV has been considered to be related to low intensity of loadings (Alfieri 2022). TrabTort~~
769 ~~is negatively correlated with trabecular stiffness (Roque et al., 2012; Roque and Alberich-Bayarri, 2015),~~
770 ~~hence low values of this parameter suggest high sustained loads. FD is reported to be inversely related to~~
771 ~~loading activities (Pornprasertsuk et al., 2001). We used this evidence to build our expectations, besides the~~
772 ~~experimental hypothesis based on previous results on primate fibula functional morphology suggesting that~~
773 ~~DOA primarily explains fibular anatomical diversity across primates. Since arboreal primates are~~
774 ~~characterized by high mobility of the ankle joint and the fibula (Barnett and Napier, 1952) and live in an~~

~~environment that involves a widely multidirectional nature of loadings (e.g. Demes et al. 2001; Carlson, 2005), we expected the DA of their distal fibula to be lower compared to terrestrial ones. Moreover, the lateral position of the fibula in the ankle joint besides the more frequent laterally directed SRFs expected to act on the ankle of arboreal species (Carlson et al., 2005; evidence used by Marchi, 2007 to build the experimental hypothesis studying fibula CSG) brought us to hypothesize increased loadings on the arboreal primate distal fibula. This, in turn, should result in the distal fibula trabecular structure of arboreal primates yielding higher density-related traits, higher BS/TV., lower TrabLen, higher TrabTort and lower FD. Terrestrial species were expected to show the opposite pattern, with semi-arboreal species yielding intermediate values. Apart from univariate comparisons between the three categories, we accounted for the complexity of trabecular properties (e.g. their correlation) hence analysing interspecific patterns multivariately and in terms of subsets of variables driving specific trends. Also, we quantified the effects of two other major factors expected to affect trabecular structure variability, i.e. body mass and phylogenetic relationships.~~

4. 1. Effects of different factors on primate distal fibula trabecular bone

4.1.1. Degree of arboreality (DOA)

The analyses performed in this study (Table 3, Figs. 4-5, Figs S1, S4) seem to indicate an overall absence of a relationship between the trabecular architecture of primate distal fibula and DOA. Indeed, no quantitative evidence ~~arose~~arises from ~~both~~either univariate ~~and~~or multivariate PGLSs (even after size-correcting variables strongly related to body mass, in the case of univariate PGLSs). Moreover, a visual assessment of interspecific variation, in general does not yield any pattern related to DOA. Interestingly, some traits as BV/TV and BS/TV (the latter with size-corrected values) seem to follow a trend directly related to DOA (Fig. 4). However, we would not interpret these patterns as reflecting loadings related to DOA. Indeed, for the two parameters the trend is opposite to our expectations, since we expected higher BV/TV and BS/TV in arboreal primates, due to the hypothesized more frequent loadings on their distal

fibula (see above), while, for both the traits terrestrial taxa show higher values. Instead, the patterns of BV/TV and size-corrected BS/TV are likely explained by phylogenetic effects. As for BS/TV, it is already clear from the strong and significant phylogenetic signal detected after size-correction (Table 4). As for BV/TV, although it does not show a significant *p*-value for λ (Table 3), ~~it~~the presence of a strong phylogenetic signal is clear from the trait values mapped on the phylogeny (Fig. 4A). Indeed, the higher BV/TV in terrestrial taxa is driven by higher values in baboons (*Papio* spp.,) and the southern pig-tailed macaque (*Macaca nemestrina*) which represent a clade in the phylogeny used in this work. The other terrestrial taxon, *H. sapiens*, instead shows a value comparable to the one of its sister taxon *P. troglodytes*, here categorized as semi-arboreal, a pattern supporting again the absence of an effect related to DOA on BV/TV. The BV/TV ancestral states (reconstructed to map BV/TV values on the phylogeny) would even suggest that a quite high BV/TV is plesiomorphic in cercopithecids (i.e. the group represented by *Chlorocebus* spp., *Cercopithecus mitis*., *Papio* spp., *M. nemestrina*, *Colobus guereza*) with an apomorphic BV/TV decrease in *Chlorocebus* spp. However, caution is needed in proposing evolutionary patterns, since the species here sampled are far from being a sufficient representation of cercopithecid diversity and efforts are still needed to clarify how trabecular variables vary in ontogeny *vs.* phylogeny. Apart from this, the relatively low BV/TV in *Chlorocebus* spp. is, together with other isolated non-phylogenetically related patterns (e.g. the very low BV/TV in *Mico* spp., and *L. fuscicollis* within platyrrhines, Fig. 4A), probably the reason behind the absence of significant phylogenetic signal for BV/TV.

From the multivariate visual assessment, a weak apparent pattern potentially related to DOA arose from PC2 deriving from the second PCA (that was run with size-corrected variables, where needed). This PC is inversely related to BV/TV, size-corrected BS/TV, size-corrected Tb.Th and, although with minor contribution, size-corrected TrabLen, and yields a weak gradient going from terrestrial taxa (lower PC2 scores) to arboreal primates (higher PC2 scores) with semi-arboreal taxa showing an intermediate mean and median (in the boxplots shown by triangles and vertical lines, respectively) (Fig. 5). As well as for BV/TV and size-corrected BS/TV (discussed above and that are, not surprisingly, two of the four main driving variables for PC2), we interpret the PC2 pattern as related to other factors, instead of DOA. It would be

suggested by the fact that three of the four variables mainly driving PC2, i.e. BV/TV, BS/TV (see discussion above) and Tb.Th, yield a pattern that is opposite to what we expected in terms of biomechanical loadings. Indeed, we hypothesized that arboreal species would show higher Tb.Th but since Tb.Th inversely correlates to PC2 and terrestrial taxa show lower PC2 scores, it means that terrestrial primates are those that show higher Tb.Th As for TrabLen, it would show a pattern consistent ~~to~~with the expectations, i.e. terrestrial taxa exhibit longer trabeculae, i.e. higher TrabLen, due to the expected less frequent loadings. However, we do not believe it is sufficient evidence in support of a DOA signal in the studied trabecular structure, considering the lower contribution of TrabLen to PC2 (see the shorter vector length compared to the other three variables driving PC2, Fig. 5A) and the fact that TrabLen was expected to negatively correlate with NodDen. NodDen, instead mainly contributes to another PC (i.e. PC1, see discussion below). Apart from these considerations, it is clear that PC2 mainly separates playthrrines (higher PC2 scores) from catarrhines and strepsirrhines (lower PC2 scores). Furthermore, it is clear that there is a residual effect of body mass on this PC, i.e. PC2 separates larger taxa, as baboons and the chimpanzee, from smaller taxa, as *Mico* spp., *L. rosalia* (once the largest and the smallest taxa, *H. sapiens* and *C. jacchus* respectively, are excluded). It means that, despite the fact that the PCA from which PC2 derives was run on values corrected for body mass (and partially from phylogenetic effects, see above and Table 4), both the effects are instead still present and drive PC2, in turn representing 27.4% of the whole variability. Concerning the remaining effect of body mass, a possibility is that it depends on the procedure of size-correction that we used, i.e. taking the residuals of a variable-logBMp linear regression. Further dedicated investigation on this topic is needed to confirm this hypothesis or may put efforts into properly design samples to control for body mass (e.g. studying primate species with similar body sizes and different locomotor behaviors). The phylogenetic signal of PC2 can also be ~~evinced by~~inferred from the fact that two of the four variables mainly driving PC2 are those that after size-correction showed a significant phylogenetic signal, i.e. BS/TV and $TrabLen_{Aver}$. We quantitatively confirmed that PC2 is driven by body mass and/or phylogeny, by running a PC2 vs. log-BMp regression (p-value=0.005) and computing the PC2 phylogenetic signal (λ=0.77, p-value=0.008). With both univariate (with BV/TV and size corrected BS/TV, Fig. 4) and multivariate (with PC2, Fig. 5) analyses,

we found some apparent patterns related to DOA that were ~~more likely to be~~better ascribed to phylogeny and body mass. This reveals one potential limitation of this work. Although the distribution of DOA categories potentially allowed us to disentangle the effect of DOA from phylogenetic ones (e.g. in case of similar distinctive values shown by the terrestrial baboons, macaque and humans, or by the semi-arboreal *Cercopithecus* spp., *C. mitis* and chimpanzee), there is a tendency for taxa assigned to the same locomotor category to cluster in specific parts of the phylogeny (e.g. terrestrial baboons, arboreal platyrrhines). It limited our possibility to disentangle DOA effects from phylogenetic ones. Future works aiming to investigate the factors to which primate distal fibula trabecular structure relates and also testing the effect of DOA should overcome this limitation (besides others, discussed below) of this study.

According to our results, no obvious signal attributable to DOA is present in the trabecular bone of the distal fibula of primates. This finding is in contrast with previous evidence obtained on the relative robusticity of the fibular diaphysis (e.g. Marchi, 2007, 2015a; Marchi and Borgognini-Tarli, 2004; Marchi and Shaw, 2011). The discrepant patterns between distal epiphyseal trabecular architecture and diaphyseal structure possibly suggest that diaphyseal and epiphyseal variables do not strongly co-vary (Shaw and Ryan, 2012; Saers et al., 2016). One possible explanation is linked to the different biomechanical environments to which these two anatomical regions are subjected, i.e., bending/torsion loadings are dominant in the diaphysis (Carter and Beaupré, 2007) while the epiphyses mainly adapt to axial loads (Barak et al., 2011; Biewener et al., 1996). In this framework it is plausible that bending/torsion predominate over tension/compression (i.e., the axial regime) in the biomechanical loadings acting on the primate fibula. Specifically, bending seems to be the main loading regime acting on the fibula. It is supported by ~~SRFs~~SRF vector orientation in the hindlimb of capuchin monkeys during arboreal and terrestrial behaviors that, in turn, suggests the presence of substantial bending moments, with bending occurring around oblique axes of the hindlimb segments (Demes and Carlson, 2009). Specifically, since the ~~SRFs~~SRF resultant is forced to pass through the foot when the limb contacts the substrate (Demes and Carlson, 2009), it is likely closer to the fibula distally than proximally, where the discrepancy angle between the SRF resultant and the limb segment increases (e.g. at the mid-shaft level, where CSG parameters are often quantified). A consequence

of increased SRF resultant-limb segment discrepancy angles would be that the bending moments to which the fibular diaphysis is subject are probably larger than those to which the distal fibular epiphysis is subject. ~~The hypothetical dominance of bending would be also consistent with the fact that, as mentioned above, the frequency of lateral loadings, regarding the mediolateral direction of loads, is expectedly the way through which arboreal habits act on fibular anatomy with axial loadings that, on the other hand, rather concern the proximo-distal direction of loads.~~ If it was true, it would be however challenging to place the evidence that external morphology of primate distal fibula relates to DOA (Marchi, 2015b; Marchi et al., 2022) in this scenario. Indeed, if the bending regime is assumed as dominant to justify the stronger signal due to arboreality detected in the diaphysis, the epiphyseal morphology, both external and internal, should consistently be poorly related to this factor. Hence, the fact that, instead, in the distal fibula external anatomy the effects of DOA are detectable, in contrast with internal architecture, is striking. We can hypothesize that, in the specific case of the ankle joint, loadings acting at this level influence the distal fibula external shape and the distal fibular internal structure to different extents. Moreover, since previous studies of trabecular bone in the other elements of the ankle joint mostly found significant relationships with locomotor habits (distal tibia; Barak et al., 2013a, talus; Hébert et al., 2012; Su et al., 2013), we can assume that the transfer of loads reasonably occurring in a functional unit as the ankle joint, results in the functional signal to be present in the internal structure of other elements, but not in the distal fibula. In this direction, clinical studies have recently suggested differential effects of loadings in human distal fibular vs. distal tibial trabecular architectures, with the former proposed to be less sensitive (Ghasem-Zadeh et al., 2021; Stürznickel et al., 2021). If this condition is widespread in primates, it may justify the apparently low functional locomotor signal borne by the trabecular bone of the distal fibula. Further work is needed to better understand these discrepant trends followed by the distal ~~fibula's~~fibula internal and external anatomy, e.g., by comparing the evolutionary patterns in the external shape and internal structure in the same sample of primate species. Related to this, one should note that a relationship between DOA and the distal ~~fibula's~~fibula external morphology has been detected in hominids, i.e., hominins and great apes (Marchi, 2015b; Marchi et al., 2022). While the sample studied by Marchi and colleagues is suitable to explore the range of arboreal habits

from fully terrestrial to fully arboreal, it is not taxonomically as wide as our sample, and does not include species that are terrestrial but not bipedal, as in this work (e.g. baboons). These two aspects may have hidden large-scale phylogenetic effects in analyses of distal ~~fibula's~~fibula external morphology (despite phylogenetic relationships in hominids ~~were~~being accounted for in Marchi et al., 2022) and a role potentially played by the distinctive hominin bipedal locomotion (see discussion below on the influence of phylogeny and bipedalism). This emphasizes the importance of studying how ecology is reflected by different anatomical levels on the same sample of species (e.g. Alfieri et al., 2022, 2023).

While many of the studied trabecular properties yielded a strong relationship with body mass and/or phylogenetic structure (but with the impossibility to disentangle these two effects; see discussion below), trabecular anisotropy (i.e. DA), bone volume fraction (i.e. BV/TV) and tortuosity (i.e. TrabTort, both $_{Aver}$ and $_{Med}$) do not significantly correlate with any of the factors here addressed, i.e. DOA, body mass and phylogeny (Table 3). It makes the interpretation of the overall patterns related to these traits on multivariate phylo-morphospaces particularly interesting. As discussed above, BV/TV shows a pattern that ~~is~~ only apparently ~~discriminating~~discriminates terrestrial from arboreal taxa, with semi-arboreal in between (and the same occurs for the PC to which BV/TV primarily contributes, i.e. PC2). Indeed, although not yielding a significant phylogenetic signal (Table 3), this trait has a distribution that is mainly driven by phylogeny (Fig. 4).

TrabTort negatively correlates to PC1, that is also positively associated with NodDen and FD (apart from minor contributions deriving from other variables). PC1 sets apart *H. sapiens* and *C. jacchus* from the other species. Although PC1 reveals a pattern that is very likely not affected by allometric and phylogenetic effects (*H. sapiens* and *C. jacchus* are the largest and the smallest in the sample, respectively, and they are a hominid and a platyrrhine), the very different locomotor habits of *H. sapiens* and *C. jacchus* (not only in terms of DOA) make this axis of variation very unlikely to be associated with locomotor behavioral aspects too. Also, there is not consistency in the way through which the three variables mainly driving PC1 are expected to relate to loads (Table 2 and above). For instance, if NodDen varied as expected according to the

experienced loads and strains, i.e. positively, NodDen and TrabTort should have been positively associated with each other, but they do not follow this pattern in affecting PC1; similarly, FD is expected to be negatively related to NodDen, but again it is not confirmed (Fig. 5). All of this suggests that the discrimination revealed by PC1 is challenging to explain in terms of locomotion, body mass and phylogeny and that probably the effect of other factors (e.g. genetic, developmental, hormonal) should be investigated.

Another portion of TrabTort variance is captured by PC3 and, interestingly, TrabTort together with DA contribute to set apart *H. sapiens* from all the other primates on the PC1-PC3 plot (Fig. 5). Specifically, *H. sapiens* is apparently set apart for relatively higher DA and relatively lower TrabTort. This pattern arising from our multivariate visual assessment opens up the possibility that at least the peculiar hominin bipedalism may relate to distal fibula trabecular structure. Indeed, the fact that *H. sapiens* is partially distinct from all the other primates because of its higher anisotropy value could have a functional explanation. As detailed above, DA is commonly associated with the extent to which movements in a joint follow repeated directions and a highly anisotropic trabecular structure is expected in highly stereotypically loaded joints. It led us to expect higher DA in terrestrial taxa. (see above). It is possible, however, that the infrequent but not absent arboreal behaviors (not absent in any living non-human primates, as we specified defining DOA in this work) of terrestrial but not bipedal primates (e.g. baboons) prevent their distal fibula trabecular bone to develop a particularly anisotropic structure. In this framework, higher anisotropy would be instead shown by *H. sapiens* thatwhich never experiences arboreal habits and obligatorily performs bipedalism, involving strong antero-posterior movements in the sagittal plane. From the distribution of DA values of the studied specimens, three of the five *H. sapiens*'*sapiens* fibulae yielded the highest DA values in the entire sample, with a fourth *H. sapiens*'*sapiens* fibula yielding the fifth highest DA value (Table S1). We used single specimens'specimens results distribution also to better interpret TrabTort outcomes, since this parameter yielded unclear trends in the PC1-PC2 plot (see above) but, similarly to DA, seem to contributeseems to set apart *H. sapiens* from all the other primates in the PC1-PC3 plot. Strikingly, the five *H. sapiens* fibulae yield the lowest $TrabTort_{Mean}$ of the entire sample (also after log-transforming the values in Table S1, since TrabTort was log-transformed for the univariate tests, see Table 3). It supports the presence of this additional

distinctive ~~features~~feature in the human distal fibula. As for DA, a functional interpretation is possible for TrabTort, too. We expected TrabTort to directly relate to load frequency (Table 2) and we hypothesized that load frequency on the fibula would be proportional to the extent to which arboreal substrates are used. If, as suggested above, the infrequent but still present arboreal behaviors of baboons affect their distal fibula trabecular bone, *H. sapiens* would be distinctive since almost never experiencing, in its ankle, the frequent laterally directed SRFs of the arboreal environment (see above). It would explain the evidently less tortuous human trabecular structure in the distal fibula. Hence, raw results for DA and TrabTort fully support the hypothesis of a functionally higher DA and lower TrabTort in the distal fibula of *H. sapiens*. It may stimulate future dedicated works with properly built samples to test this pattern and exclude other factors (see for instance the fact that for $TrabTort_{Mean}$, the sixth lowest value is of the *H. sapiens*' sister taxon, *P. troglodytes*, Table S2, hence phylogenetic effects should also be tested). The raw DA value measured for *O. crassicaudatus* is not outstanding (Table S2), suggesting that the portion of DA variance contributing to set apart this species from the other primates in the PC3-PC4 plot (Fig. S4) is negligible. On the other hand, what mainly drives the morphospaces position of *O. crassicaudatus* (in PC1-PC3, PC2-PC3 and PC3-PC4 plots, Fig. 5, Fig. S4) is TrabLen, for which the species show the highest value, and the same is true for *C. jacchus*, yielding the lowest TrabLen value (Table S1 data after size-correction, to comply with results in Table 3). The fact that these two species are both arboreal and ~~leaper~~leapers (see discussion below) makes it challenging to relate such a pattern to locomotion. Since this trait is the only one that showed a significant phylogenetic signal both before and after size-correction (Table 3 and Table 4), the observed TrabLen pattern follows the phylogeny (e.g. a quite low TrabLen is shown by *C. ~~jacchus~~'jacchus* sister taxon too, i.e. *Mico* spp., and a pretty high TrabLen is shown by *O. ~~crassicaudatus~~'crassicaudatus* sister taxon too, i.e. *P. diadema*; Fig. S3).

4.1.2. Body mass and phylogenetic relationships

Apart from minor trends potentially related to human bipedalism (see above), primate distal fibula trabecular architecture is overall strongly affected by body size and phylogenetic structure, as evinced from

inferential univariate and multivariate analyses, and visualization of trait variability relative to body mass and phylogenetic relationship (Table 3, Table 4, Fig. 4, Fig. S2A, B, Fig. S3, Fig. S4). The particularly strong relationship of morphology with allometry and phylogeny, more than ecology, that we found here, mirrors the outcomes of previous works comparing primate anatomy across wide phylogenetic frameworks (e.g. studying mandibular shape, ~~Plomb~~Plomp et al. 2024, Veneziano et al. 2019) (see also discussion above on large-scale phylogenetic effects). Before discussing the potential implications of body mass and phylogeny and their correlation with primate distal fibula trabecular structure, it is important to stress that in the sample that we studied, body mass and phylogenetic structure are highly correlated (Table 3), i.e. the distribution of body mass proxy is strongly related to phylogeny. A consequence of this outcome is that we did not separate the effects of these two factors. Hence, it is possible that only one of the two factors is primarily related to primate distal fibula trabecular structure, with the other factor that rather yielded significant correlation with morphology only because of significant correlation between size and phylogeny. With the data collected in this study, it is not possible to disentangle the effects of body mass and phylogenetic structure. As a supplementary analysis, we wanted to test if this issue is a limitation related to our sample or it may be a general problem in clade-wise comparative studies in primates. Using body mass estimates for 742 species of extinct and extant primates plus plesiadapiforms (Tillquist et al., 2016), we log-transformed them and we matched body mass data to the mammal phylogeny of Upham et al., (2019), excluding all the taxa that are not represented by both phylogeny and the body mass dataset. We obtained a phylogenetically informed body mass dataset of 250 primate species. It allowed us to test how body mass is related to phylogeny on a wide taxonomic scale, computing the phylogenetic signal through Pagel's λ (see Methods). We obtained a $\lambda = 0.99$ with a p-value < 0.001, suggesting that the limitation of body mass - phylogenetic structure correlation is not depending on our studied sample but may be unavoidable for most of the comparative morphological studies in primates. We suggest researchers aiming to disentangle how different factors relate to primate anatomical evolution to account for this potential bias.

Concerning the effect of body mass on trabecular traits, numerous studies on different skeletal elements have proposed different trends in mammals and in primates (e.g. Bird et al., 2021; Christen et al., 2015;

Cotter et al., 2009; Doube et al., 2011; Fajardo et al., 2013; Hernandez et al., 2009; Kivell, 2016; Kivell et al., 2018; Komza and Skinner, 2019; Ryan and Shaw, 2013; Scherf, 2008; Schilling et al., 2014; Swartz et al., 1998; Tsegai et al., 2017). For instance, it has been found that DA is often independent from body mass, that BV/TV scales with positive allometry (Barak et al., 2013b; Christen et al., 2015; Doube et al., 2011) and that Tb.Th frequently scales with negative allometry (Barak et al., 2013b; Doube et al., 2011; Ryan and Shaw, 2013; Swartz et al., 1998). For DA and Tb.Th, the distal fibula seems to align with other skeletal elements in primates. Indeed, we found that DA does not relate to body mass. As for the allometric pattern shown by Tb.Th, ~~we additionally ran~~ with a ~~'Tb.Th ~ logBMproxy' linear~~ regression ~~(using data on single specimens, hence not averaging for species) and we found that its covariation with body mass can be explained by the relationship 'Tb.Th= (0.07±0.01) * logBMproxy' (slope p-value<0.001, while the intercept estimate is not significantly different from 0, intercept p-value=0.44). With a~~ slope that is positive but lower than 1 (i.e. 0.07), it apparently confirms that trabecular thickness scales with negative allometry in the distal fibula, too. On the other hand, our results for BV/TV, i.e. no significant relationship with body mass, apparently contrast what was found in some previous works. One should note that, however, exceptions to the proposed patterns of primate trabecular traits-body mass covariation have been found (e.g. Fajardo et al., 2013; Komza and Skinner, 2019; Ryan and Shaw, 2013; Tsegai et al., 2017), and that likely a bone and taxon-dependency exists (Bird et al., 2021; Cotter et al., 2009; Fajardo et al., 2013; Kivell, 2016; Ryan and Shaw, 2013). Hence, our outcomes add to the information on how trabecular traits relate to body size across the primate skeletal elements. Furthermore, we provide the first evidence for patterns of body size covariation concerning the topological indices recently proposed by Veneziano et al. (2021). For both traditional trabecular parameters and topological indices, future analyses of allometric scaling patterns are needed.

As for the phylogenetic effect on primate trabecular structure, it is likewise challenging to outline general patterns (Kivell, 2016). Several works investigated how trabecular traits relate to the phylogenetic structure (Doube et al., 2011; Ryan and Shaw, 2012, 2013; Smaers and Vinicius, 2009; Tsegai et al., 2013) with some of them yielding a weak phylogenetic signal and others finding a complex scenario of anatomical

variation (e.g. Doube et al., 2011, Ryan and Shaw, 2012, 2013). The pattern of differential evolutionary influence on different skeletal regions, i.e. mosaic evolution, is now recognized as a major factor to explain morphological diversity in primates (e.g. Bastir and Rosas, 2009), mammals (e.g. Barton and Harvey, 2000), and in other vertebrates (e.g. Navalón et al., 2022). With this work, we suggest that the distal fibula trabecular bone in primates may be strongly affected by the phylogenetic structure (but see discussion above on body mass-phylogeny correlation). Importantly, it was shown that the strength of the phylogenetic effect not only varies among anatomical regions but also among taxonomic groups (Kivell, 2016; Ryan and Shaw, 2013). Hence, although the results of this work led us to discourage the use of distal fibula trabecular structure to infer DOA in extinct primates due to the presence of phylogenetic signal, it is also possible that the effects of phylogeny may be less important if more restricted primate taxonomic contexts are studied (Marchi, 2007, 2015b; Marchi et al., 2022). Thus, it is still possible that if the fibula is compared among closely related primate species, as often occurs with the study of hominids in an anthropological context (e.g. see also Berles et al., 2024, studying closely related tamarins), a functional signal related to DOA can be detected because large scale phylogenetic effects would be minimized. It can also explain the discrepant patterns found for internal and external anatomy of the distal fibula in relation to DOA (see discussion above). Since we only included two hominids in this work, this very small sample prevents any assessment of trabecular structure diversity restricted to only hominids and, hence, we cannot here discuss on such short phylogenetic scale. However, the aforementioned potential relationships shown by DA and TrabTort with human bipedalism (~~that within hominids represents~~representing the terrestrial extreme of the DOA range in hominids) should encourage future studies to address this aspect.

4. 2. Potential limitations

Some methodological and theoretical aspects potentially represent limitations of this work. First, we only focused on the proximal articular facet (here termed PAF) of the fibulotalar articulation of the distal fibula, not including the trabecular bone underlying the distal articular facet (DAF) of the same articulation (Fig. 2). Since the external morphology (e.g. surface area, morphometric indices) of DAF, ~~similarly~~similar to ~~the~~

~~one~~that of PAF, proved to be related to different locomotor behaviors (Marchi, 2015b), one may expect a locomotor signal in DAF internal bone, too. As mentioned in the Materials and Methods, one of the reasons behind our choice to exclude DAF was the overly wide variability in external morphology of this articular facet. Based on Marchi (2015b), we expected DAF to be approximately triangular in the studied sample but, probably due to the taxonomical diversity considered here, we found it challenging to reliably recognize a homologous region in all the specimens. Several works addressed bone inner structure by studying the regional variation of trabecular traits within specific joints/epiphyses (~~it has been done~~ both using multiple regularly shaped ROIs; e.g. Su et al., 2013; Sylvester and Terhune, 2017, and mapping the variability within entire epiphyses, e.g. Georgiou et al., 2019; Sukhdeo et al., 2020). Hence, it is possible that a regional variability in trabecular properties exists across PAF and DAF and that, by excluding inner bone related to DAF, we hid some potentially informative locomotor signal. Indeed, the same wide variability in DAF external morphology that prevented us ~~to extract~~from extracting trabecular bone may reflect adaptations to different locomotor behaviors. However, it should be noted that our approach of studying the entire trabecular bone volume underlying PAF already represents an advance compared to the traditional approach based on the extraction of regularly-shaped ROIs. The latter was tested at a preliminary stage of this work, but it proved challenging to be applied due to the ~~not regular~~irregular 3D morphology of the distal fibula region corresponding to DAF (see Fig. 2D), e.g. humeral head ~~or~~and femoral head are easily studied through spherical ROIs due to the approximately spherical 3D shape of the entire articulation itself, but ~~it~~this does not apply to the region we were interested in. While the issue of sampling complexly shaped joints through regularly shaped ROIs may be fixed by using multiple smaller volumes instead of a single larger one (e.g. Barak et al. 2013a; Su et al. 2013, Su and Carlson, 2017), in our particular case this approach would have been problematic due to another practical issue, that additionally motivated our choice to exclude DAF and ~~it~~ is partially related to the high morphological variability of DAF mentioned above. Indeed, due to the highly variable DAF shape, some species showed a DAF that is a dramatically wide and short ‘triangle’, i.e. with an extremely small proximodistal size. In such cases, the stack representing the trabecular bone underlying DAF is compounded by too few trabeculae (often ~~less~~fewer than the minimum recommended

limit of 50, see Methods). If this issue prevented us from extracting a single informative ~~(i.e. with more than ca. 50 trabeculae)~~ stack for all trabecular bone underlying DAF, it is easy to imagine how this limitation would have been even more severe if multiple smaller volumes would have been used. Finally, it is remarkable that PAF, studied in this work, represents most of the trabecular bone of the fibulotalar articulation (as one can see from PAF and DAF size proportions in Fig. 2). A possible solution for future works is studying the trabecular bone underlying the entire fibulotalar articulation (PAF + DAF), developing another ad-hoc orientation protocol, and investigating variation in trabecular parameters in the whole region (e.g. using a heat-map approach, available in Veneziano et al., 2021).

Another potential limitation of this work may derive from the fact that testing the relationship between distal fibula trabecular bone and DOA may involve pooling in the same discrete state species that are quite different concerning other aspects of their locomotor behavior (e.g. forelimb vs. hindlimb reliance, presence of distinctive habits as leaping) that, in turn, reasonably involve different functional demands. Although these aspects were not the main focus of this work, one should consider the possibility that primate distal fibula trabecular bone does not vary according to DOA, as fibula CSG or distal fibula external morphology (see above), but instead it follows other locomotor factors. This issue is particularly exacerbated for taxa that in this work were categorized as 'arboreal', e.g. spider monkeys (*A. paniscus*) and sifakas (*P. diadema*), that are more specialized in their locomotor habits compared to more generalized arboreal quadrupeds as colobines (*C. guereza*) and howler monkeys (*A. seniculus*) (Fleagle, 2013b). ~~To further evaluate potential locomotor effects undetected in this work, for a subset of the studied taxa (n=10, 7 of which were classified as 'arboreal' in this work) we collected quantitative data on locomotor behaviors from Granatosky (2018) (data for the remaining taxa of our sample are not present in Granatosky 2018). The collected data, provided as percentages in the original work, were transformed through an arcsine square root transformation (common procedure in the analysis of proportional ecological data, in order to minimize variance and normalize the distribution, Monclús-Gonzalo et al., 2023; Sokal and Rohlf, 1995). Then, data from multiple observations for the same species were averaged, obtaining a single value for each behavior for each taxon, and a PCA was run, building a PC1-PC3 (cumulatively explaining 64.2% of the total variance) 3D~~

~~scatterplot based on behavioral data, i.e. an 'ethospace' (Fig. S5). This plot confirmed that *A. paniscus* and *P. diadema* occupy extreme positions in the explored range of locomotor diversity, corresponding to regions related to predominant leaping (for *P. diadema*, region 1 in Fig. S5) and bimanual suspension/climbing (for *A. paniscus*, region 3 in Fig. S5). Other potential clusters may be represented by: species with predominant quadrupedal suspension/bounding (the taxon closer to this condition is *L. rosalia*, region 2 in Fig. S5), species with predominant quadrupedal walking as *P. troglodytes* (region 4 in Fig. S5) and two potential clusters of quite unspecialized species with arboreal habits (one of which shows less quadrupedal walking, including *L. fuscicollis* and *S. midas* and shown with region 5 in Fig. S5, compared to the other, including e.g. *A. seniculus* or *C. guereza*, and shown with region 6 in Fig. S5). A straightforward assessment of potential relationships between these differences and major trabecular features of primate distal fibula is checking if taxa with more derived and discrepant locomotor behaviors (e.g. leapers, bimanual suspensory) occupy distinct and peripheral regions of the morphospace, contrasting taxa with more similar behaviors instead expected to occupy the central regions of the scatterplot (following e.g. Ryan and Shaw, 2012). Exploring the morphological variability found in this work, it is clear that no patterns related to the frequency of specific locomotor behaviors arose. For instance, *P. diadema* and the other strepsirrhine leaper *O. crassicaudatus*, are close each other in some plots but also close to taxa with quite distinct locomotor behaviors (e.g. unspecialized *C. mitis* and *A. seniculus* or the prevalently terrestrial quadrupedal *P. hamadryas* in PC1-PC2 plot, Fig. 5), or they occupy different areas of the morphospaces (e.g. PC2-PC3 plot, Fig. 5). Also, *A. paniscus*, expected to occupy another peripheral position of the morphospace due to hindlimb lower activities deriving from its prevalent bimanual suspensory habits, is instead often occupying central regions of the plot, e.g. often close to *C. pygerythrus* (PC1-PC2, PC2-PC3 and PC1-PC3 plots, Fig. 5) that, in turn, is a relatively unspecialized taxon (since it largely mirrors its sister taxon *C. aethiops,* Fleagle, 2013) (Fig. S5).~~To further evaluate potential locomotor effects undetected in this work, we ran a supplementary analysis accounting for the frequency of specific locomotor behaviors of the studied taxa, instead of their DOA. As detailed in Supplementary Note 1 and Fig. S5, we highlighted that, mirroring what

we found for DOA, the primate distal fibula trabecular structure probably does not relate to other locomotor aspects.

Another issue partially related to locomotor categorization is the possibility that pooling *H. sapiens* - whose bipedalism involves a greater predominance of loads in the hindlimbs - with terrestrial baboons may skew the results. Also, pooling *P. troglodytes* - which shows dominant quadrupedal walking ~~(Fig. S5 and above)~~ - with unspecialized taxa such as *Chlorocebus* spp. (Supplementary Note 1 and Fig. S5) may cause the same problem. To evaluate effects potentially deriving from this bias, we re-ran the PCA used to visualize interspecific patterns after excluding *H. sapiens* ~~(Fig. S6)~~ and then after excluding both *H. sapiens* and *P. troglodytes* ~~(Fig. S7). The exclusion of *H. sapiens* causes the morphospace area occupied~~. As shown by ~~the remaining terrestrial taxa (*Papio* spp., + *M. nemestrina*) to be smaller. It, in turn causes terrestrial taxa to be discriminated from all the other primates with minor overlap (in PC1-PC2 and PC1-PC3 plots, Fig. S6). However, it should be noted that this condition may be related to phylogeny, since the exclusion of *H. sapiens* causes the terrestrial taxa to be represented by a clade in the phylogeny (Fig. 1) with the impossibility to disentangle locomotor and phylogenetic effects. In both PC1-PC2 and PC1-PC3 plots, terrestrial taxa tend to be discriminated from other primates for high BV/TV and BS/TV (and also high Tb.Th only in the PC1-PC2 plot) (Fig. S6). Since~~ these ~~patterns go against our expectations (Table 2 and above), the presence of a phylogenetic effect seems more likely. The same occurs to semi-arboreal taxa after the exclusion of *P. troglodytes* (besides *H. sapiens*, Fig. S7), since the remaining taxa in the category form the clade (*Chlorocebus* spp. + *C. mitis*) (Fig. 1). Although it is here impossible to disentangle locomotor from phylogenetic effects, it is interesting that a gradient from terrestrial taxa (higher PC1 and PC3 scores) to arboreal taxa (lower PC1 and PC3 scores) is yielded by this new PCA. However, it is again driven by high BV/TV and BS/TV in terrestrial taxa (hence, contrasting biomechanical expectations). Strikingly, terrestrial taxa are set apart also for their lower DA values, which clearly contrasts the biomechanical properties associated with this parameter (expected to be higher in terrestrial environments, where loadings are more directionally stereotyped, e.g. Alfieri et al., 2022; Amson et al., 2017) (Fig. S7). The exclusion of *H. sapiens* and *P. troglodytes* does not affect the overall apparent absence of relationships between the~~

frequency of different locomotor behaviors and distal fibula trabecular structure (see above). Indeed, a taxon with derived behavior such additional PCAs (Figs. S6-S7) and as *A. paniscus* (Fig. S5) occupies non-peripheral positions of the morphospace, often close to unspecialized taxa as *C. guereza* and/or *C. pygerythrus* (PC1-PC2, PC1-PC3, PC2-PC3 in both Fig. S6 and Fig. S7). Likewise, *P. diadema*, a specialized leaper (Fig. S5), frequently clusters close to unspecialized taxa (e.g. *C. aethiops* in PC1-PC2, PC1-PC3 plot, Fig. S6; and in PC2-PC3 plot, Fig. S7) or far from another leaper as *O. crassicaudatus* that, in turn, clusters close to unspecialized taxa (e.g. *C. aethiops* and *C. mitis* in PC1-PC2 plot, Fig. S7). We recognize that future works may address potential relationships between distal fibula trabecular structure and finer locomotor categorizations (as those arising from Fig. S5) building proper samples and running inferential statistical tests with larger sample sizes. Nevertheless, we interpret the trends discussed above as indicative of the fact thatin Supplementary Note 2, these exclusions do not change the main outcome of this work. Namely, the primate distal fibula trabecular bone maydoes not appear to be associated with locomotor behaviors, neither with DOA, as defined in this work, nor with other locomotor aspects as leaping or lower hindlimb reliance in suspensory species. The only potential (see above and Supplementary Note 1), with the only possible exception arising from this work is represented by the possible effectminor trends related to hominin bipedalism in hominins (see discussion above).

Finally, while we studied interspecific patterns of distal fibula trabecular bone variation, our data are mostly based on single specimens for each species. Hence, in this work the effects related to intraspecific variability are not accounted for. This is a common problem in phylogenetically informed analyses (see Garamszegi, 2014 for a discussion of potential solutions). Indeed, the introduction of phylogenetic data in comparative analyses (started with the work of Felsenstein, 1985) had several implications for zoological/anthropological comparative studies, including the fact that statistical observations are now represented by taxa, instead of specimens/individuals. It is a requirement of many statistical toolkits (e.g. those provided by the R packages mentioned in Materials and Methods) needed to apply phylogenetic comparative methods. Including multiple specimens for a single species (as we did for four taxa, Table 1), may represent a partial solution but, noticeably, even in this case before performing statistical analyses as

~~PGLS or phylogenetic ANOVA, data for all the specimens belonging to a single species should be averaged and minimized to a single value per trait per taxon. Keeping in mind this limitation, it should also be noticed that one of the main problems deriving from not taking intraspecific variability into account is the underestimation of potential overlap among species that, in turn, may inflate interspecific differences, e.g. causing significant *p*-values in phylogenetic ANOVAs, resulting in false-positives. Since we did not find confirmation for most of the expected differences related to locomotor aspects, we assume that accounting for intraspecific variability would have not changed the main result of this work, i.e. distal fibula trabecular structure does not relate to DOA. To observe the intraspecific variability for the four taxa for which we sampled more than one individual (*A. paniscus*, *C. mitis*, *C. guereza* and *H. sapiens*), we built a bivariate scatterplot with PC1-PC2 from a PCA having the observations represented by single specimens, instead of taxa (Fig. S8). Moreover, for these four taxa we summarized standard deviation (SD) and coefficient of variation (CV=SD/mean) for each trait (Table S2). On the morphospace, *C. mitis*, *C. guereza* and *A. paniscus* show a low to moderate intraspecific variability, since the specimens belonging to the same species show very similar PC2 scores while the variation along PC1 is wider. Specifically, the specimens belonging to *C. mitis* and *C. guereza* fall in the same quadrant, while the specimens belonging to *A. paniscus* fall in two different quadrants due to the PC1 scores variability. A low variability is shown by *H. sapiens*, since four out of five specimens lie in the same restricted region of the morphospace, with a single specimen instead likely representing an outlier (Fig. S8). The traits for the four species show an average CV of 0.119.~~Since for four of the studied taxa we sampled more than one fibula (Table 1), we were however able to assess potential biases deriving from intraspecific variability. To do so, we ran an additional PCA with the observations being the single specimens instead of the taxa (Fig. S8) and we measured the coefficient of variation (Table S2). As discussed in Supplementary Note 3, the intraspecific variability can be generally considered low to moderate.

5. Conclusions

In this study, we carried out the first three-dimensional quantitative interspecific analysis of distal fibula trabecular structure in primates, in order to test for a functional signal related to the degree of arboreality. We expected for such a signal to be present based on results from studies on other fibular traits (diaphyseal cross-sectional properties and distal epiphyseal external morphology). Contrasting previously highlighted trends, the internal trabecular bone in primate distal fibula does not correlate with the degree of arboreality. Although we identified some trends potentially related to alternative locomotor factors not strictly related to DOA as defined in this work (i.e. human bipedalism), we found that body mass and phylogenetic relationships primarily and strongly affect the trabecular network in primate distal fibula. We provided evidence for the factors mainly associated with the previously unstudied primate distal fibula internal structure. We encourage future studies to address some critical aspects arisen from this work, e.g. the potential relationship between human bipedalism and specific trabecular traits of the distal fibula, i.e. degree of anisotropy and tortuosity, the strong correlation between primate body mass and phylogenetic structure in comparative analyses on a wide ~~taxonomical~~taxonomic scale.

Acknowledgements

We thank two anonymous reviewers and the Editor-in-Chief, Philip Cox, for their precious comments and suggestions. Moreover, we thank curators who allowed us to collect bone specimens: Paolo Agnelli (University of Florence, Florence Museal System, section La Specola) and Monica Zavattaro (University of Florence, Florence Museal System, section of Anthropology and Ethnology). We thank Ana Galvez, Léo Botton-Divet (Humboldt Universität zu Berlin, Berlin, Germany), Neil Duncan (American Museum of Natural History, AMNH, New York, USA), Sharon Grant (Field Museum of Natural History, FMNH, Chicago, USA), Janeen Jones (FMNH), Kate Webbink (FMNH), Adam Ferguson (FMNH) for uploading and/or allowing us access to µCT data on MorphoSource (see catalogue number and collections in Table S1). We also thank Aaron Clauset (University of Colorado Boulder, USA) and Lauren Glenny Shoemaker (University of Wyoming, USA) for allowing us to download and use data on primate body mass estimates (from Tillquist et al., 2016). A.V. is funded by the NextGenerationEU, Maria Zambrano fellowship

(2021URV-MZ-16). F.A. is financed by the project grant TMPFP3_217022 from the Swiss National Science Foundation (https://www.snf.ch; SNSF Swiss Postdoctoral Fellowships, SPF).

Author contributions

F.A. and D.M. collected the sample. F.A. processed and analyzed µCT data, performed statistical analyses, and drafted the manuscript. D.P. and P.A.S. made possible the acquisition of new µCT data. A.V. and E.A. contributed to process and analyze of µCT data, to compute trabecular parameters and to perform statistical analyses. All authors conceived the study, interpreted results and contributed to manuscript writing and editing.

Conflict of interest statement

The authors have no conflicts of interest to declare

Data availability statement

Raw data (Table S1), Supplementary Material (Additional Methods and Additional Results), time-tree (in nexus format) and the R code are downloadable from Figshare (https://figshare.com/s/5f267cb7aab364b2b019) (Alfieri et al. 2024). Data on isolated distal fibula trabecular architecture (both image stacks and skeletonized networks) and distal fibula µCT scans are made available upon reasonable request. The R package 'indianaBones' is available at https://github.com/AlessioVeneziano/IndianaBones and at https://zenodo.org/record/7615165.

References

Alfieri, F., Veneziano A., Panetta D., Salvadori P.A., Amson E., Marchi D. 2024. Data from: The relationship between primate distal fibula trabecular architecture and degree of arboreality, phylogeny and size. Figshare dataset. https://figshare.com/s/5f267cb7aab364b2b019

Alfieri, F., Botton-Divet, L., Wölfer, J., Nyakatura, J.A., Amson, E., 2023. A macroevolutionary common-garden experiment reveals differentially evolvable bone organization levels in slow arboreal mammals. Comms Bio 6(1), 995. https://doi.org/10.1038/s42003-023-05371-3

Alfieri, F., Botton-Divet, L., Nyakatura, J.A., Amson, E., 2022. Integrative approach uncovers new patterns of ecomorphological convergence in slow arboreal xenarthrans. J Mamm Evol. 29(2), 283-312 https://doi.org/10.1007/s10914-021-09590-5

Alfieri, F., Nyakatura, J.A., Amson, E., 2021. Evolution of bone cortical compactness in slow arboreal mammals. Evolution 75, 542–554. https://doi.org/10.1111/evo.14137

Ammann, P., Rizzoli, R., 2003. Bone strength and its determinants. Osteoporosis international 14, 13–18.

Amson, E., ~~Arnold, P., van Heteren, A.H., Canoville, A., Nyakatura, J.A., 2017. Trabecular architecture in the forelimb epiphyses of extant xenarthrans (Mammalia). Front Zool 14, 52. https://doi.org/10.1186/s12983-017-0241-x~~

~~Amson, E.,~~ Bibi, F., 2021. Differing effects of size and lifestyle on bone structure in mammals. BMC Biol 19, 87. https://doi.org/10.1186/s12915-021-01016-1

Anapol, F., Turner, T.R., Mott, C.S., Jolly, C.J., 2005. Comparative postcranial body shape and locomotion in *Chlorocebus aethiops* and *Cercopithecus mitis*. Am. J. Phys. Anthropol. 127, 231–239.

Anemone, R.L., Covert, H.H., 2000. New skeletal remains of *Omomys* (Primates, Omomyidae): functional morphology of the hindlimb and locomotor behavior of a Middle Eocene primate. J. Hum. Evol. 38(5), 607–633.

Annadhason, A., 2012. Methods of fractal dimension computation. IJCSIS 2(1), 166–169.

Auerbach, B.M, Ruff C.B. 2006. Limb bone bilateral asymmetry: variability and commonality among modern humans. J. Hum. Evol 50:203-218.

Auerbach, B.M., Gooding, A.F., Shaw, C.N., Sylvester, A.D., 2017. The relative position of the human fibula to the tibia influences cross-sectional properties of the tibia. Am J Phys Anthropol 163, 148–157. https://doi.org/10.1002/ajpa.23196

Barak, M.M., Lieberman, D.E., Hublin, J.J., 2013b. Of mice, rats and men: trabecular bone architecture in mammals scales to body mass with negative allometry. J Struct Biol 183, 123-131.

Barak, M.M., Lieberman, D.E., Hublin, J.-J., 2011. A Wolff in sheep's clothing: trabecular bone adaptation in response to changes in joint loading orientation. Bone 49, 1141–1151. https://doi.org/10.1016/j.bone.2011.08.020

Barak, M. M., Lieberman, D.E., Raichlen, D., Pontzer, H., Warrener, A.G., Hublin, J.J., 2013a. Trabecular evidence for a human-like gait in *Australopithecus africanus*. PLoS ONE 8, e77687.

Barnett, C.H., Napier, J.R., 1953. The rotatory mobility of the fibula in eutherian mammals. J Anat 87, 11–21.

Barnett, C.H., Napier, J.R., 1952. The axis of rotation at the ankle joint in man. Its influence upon the form of the talus and the mobility of the fibula. J Anat 86(1).

Barrett, A.S., 2005. Foraging ecology of the vervet monkey (*Chlorocebus aethiops*) in mixed lowveld bushveld and sour lowveld bushveld of the Blydeberg Conservancy, Northern Province, South Africa. PhD dissertation. University of South Africa.

Barton, R.A., Harvey, P.H., 2000. Mosaic evolution of brain structure in mammals. Nature 405, 1055–1058.

Bassey, E.J., Ramsdale, S.J. 1994. Increase in femoral bone density in young women following high-impact exercise. Osteoporosis Int 4, 72–75.

Bastir, M., Rosas, A., 2009. Mosaic evolution of the basicranium in *Homo* and its relation to modular development evolutionary biology. Evol. Biol. 36, 57–70.

Berles, P., Heymann, E.W., Golcher, F., Nyakatura, J.A., 2022. Leaping and differential habitat use in sympatric tamarins in Amazonian Peru. J. Mammal. 103(1), 146–158.

Berles, P., Wölfer, J., Alfieri, F., Botton-Divet, L., Guery, J.P., Nyakatura, J.A., 2024. Linking morphology, performance, and habitat utilisation: adaptation across biologically relevant "levels" in tamarins. BMC Ecol. Evol. In press.

Biewener, A.A., Fazzalari, N.L., Konieczynski, D.D., Baudinette, R.V., 1996. Adaptive changes in trabecular architecture in relation to functional strain patterns and disuse. Bone 19, 1–8. https://doi.org/10.1016/8756-3282(96)00116-0

Bird, E.E., Kivell, T.L., Skinner, M.M., 2021. Cortical and trabecular bone structure of the hominoid capitate. J Anat 239.2, 351–373.
Burr, D.B., Piotrowski, G., Miller, G.J., 1981. Structural strength of the macaque femur. Am. J. Phys. Anthropol. 54, 305–319.
Carleton, A., 1941. A comparative study of the inferior tibio-fibular joint. J Anat 76, 45–55.
Carlson, K.J., 2005. Investigating the form-function interface in African apes: Relationships between principal moments of area and positional behaviors in femoral and humeral diaphyses. Am. J. Phys. Anthropol. 127, 312–334. https://doi.org/10.1002/ajpa.20124
Carlson, K.J., Demes, B., Franz, T.M., 2005. Mediolateral forces associated with quadrupedal gaits of lemurids. J. Zool. Lond. 266, 261e273.
Carlson, K.J., Lublinsky, S., Judex, S., 2008. Do different locomotor modes during growth modulate trabecular architecture in the murine hind limb? ICB 48, 385–393. https://doi.org/10.1093/icb/icn066
Carlson, K.J., Marchi, D., 2014. Reconstructing Mobility: Environmental, Behavioral, and Morphological Determinants. Springer, New York.
Carter, D.R., Beaupré, G.S., 2007. Skeletal Function and Form: Mechanobiology of Skeletal Development, Aging, and Regeneration. Cambridge: Cambridge University Press.
Cendre, E., Mitton, D., Roux, J. P., Arlot, M. E., Duboeuf, F., Burt-Pichat, B., Rumelhart C., Peix G., Meunier, P. J. 1999. High-resolution computed tomography for architectural characterization of human lumbar cancellous bone: relationships with histomorphometry and biomechanics. Osteoporosis International, 10, 353-360.
Chang, G., Pakin, S.K., Schweitzer, M.E., Saha, P.K., Regatte, R.R., 2008. Adaptations in trabecular bone microarchitecture in Olympic athletes determined by 7T MRI. J Magn Reson Imaging. 27(5), 1089–95.
Chappard, D., Chennebault, A., Moreau, M., Legrand, E., Audran, M., Basle, M.F., 2001. Texture analysis of X-ray radiographs is a more reliable descriptor of bone loss than mineral content in a rat model of localized disuse induced by the *Clostridium botulinum* toxin. Bone 28(1), 72–79.
Chen, M., Wilson, G.P., 2015. A multivariate approach to infer locomotor modes in Mesozoic mammals. Paleobiology 41, 280–312. https://doi.org/10.1017/pab.2014.14
Chiu, C., Hamrick, M.W., 2002. Evolution and development of the primate limb skeleton. Evol. Anthropol. Issues News Rev. 11, 94–107. https://doi.org/10.1002/evan.2002
Christen, P., Ito, K., van Rietbergen, B., 2015. A potential mechanism for allometric trabecular bone scaling in terrestrial mammals. J Anat 226, 236–243.
Cichański, A., Nowicki, K., Mazurkiewicz, A., Topoliński, T., 2010. Investigation of statistical relationships between quantities describing bone architecture, its fractal dimensions and mechanical properties. Acta Bioeng Biomech, 12(4), 69–77.
Clavel, J., Escarguel, G., Merceron, G., 2015. mvmorph: an R package for fitting multivariate evolutionary models to morphometric data. Methods Ecol Evol 6, 1311–1319. https://doi.org/10.1111/2041-210X.12420
Cooper, K.L., 2019. Developmental and evolutionary allometry of the mammalian limb skeleton. ICB 59, 1356–1368. https://doi.org/10.1093/icb/icz082
Cotter, M.M., Simpson, S.W., Latimer, B.M., Hernandez, C.J., 2009. Trabecular microarchitecture of hominoid thoracic vertebrae. Anat Rec 292, 1098–1106.
Crompton, R.H., Günther, M., 2004. Humans and other bipeds: the evolution of bipedality. J Anat 204.5, 317.
Cunningham, C.A., Black, S.M., 2010. The neonatal ilium – metaphyseal drivers and vascular passengers. Anat Rec 293, 1297-1309.
Cunningham, C. A., Black, S.M., 2009a. Anticipating bipedalism: trabecular organization in the newborn ilium. J. Anat. 214, 817–829. https://doi.org/10.1111/j.1469-7580.2009.01073.x
Cunningham, C. A, Black, S.M., 2009b. Development of the fetal ilium – challenging concepts of bipedality. J Anat 214, 91–99. https://doi.org/10.1111/j.1469-7580.2008.01005.x
Currey, J.D., 2002. Bones: Structure and Mechanics. Princeton University Press.

Demes, B., Jungers, W.L., 1993. Long bone cross-sectional dimensions, locomotor adaptations and body size in prosimian primates. J Hum Evol 25, 57–74. https://doi.org/10.1006/jhev.1993.1038
Demes, B., Carlson K. J., Franz T.M. 2006. Cutting corners: the dynamics of turning behaviors in two primate species. J Exp Biol 209.5: 927-937.
Demes, B., Carlson, K. J. 2009. Locomotor variation and bending regimes of capuchin limb bones. Am J Phys Anthropol, 139(4), 558-571.
DeSilva, J.M., Devlin, M.J., 2012. A comparative study of the trabecular bony architecture of the talus in humans, non-human primates, and *Australopithecus*. J Hum Evol 63, 536–551. https://doi.org/10.1016/j.jhevol.2012.06.006
DeSilva, J.M., Morgan, M.E., Barry, J.C., Pilbeam, D., 2010. A hominoid distal tibia from the Miocene of Pakistan. J Hum Evol 58(2), 147-154.
Ding, Y., Song, Y., 2002. Function of fibula in stability of ankle joint. Zhongguo Xiu Fu Chong Jian Wai Ke Za Zhi 16, 245–247.
Doube, M., Kłosowski, M.M., Arganda-Carreras, I., Cordelières, F.P., Dougherty, R.P., Jackson, J.S., Schmid, B., Hutchinson, J.R., Shefelbine, S.J., 2010. BoneJ: Free and extensible bone image analysis in ImageJ. Bone 47, 1076–1079. https://doi.org/10.1016/j.bone.2010.08.023
Doube, M., Klosowski, M.M., Wiktorowicz-Conroy, A.M., Hutchinson, J.R., Shefelbine, S.J., 2011. Trabecular bone scales allometrically in mammals and birds. Proc. Biol. Sci. 278, 3067–3073. https://doi.org/10.1098/rspb.2011.0069
Eriksen, E.F., 2010. Cellular mechanisms of bone remodelling. Rev Endocr Metab Disord 11, 219–227.
Eriksen, E.F., 1986. Normal and pathological remodeling of human trabecular bone: three dimensional reconstruction of the remodeling sequence in normals and in metabolic bone disease. Endocr Rev 7, 379–408.
Fajardo, R.J., DeSilva, J.M., Manoharan, R.K., Schmitz, J.E., Maclatchy, L.M., Bouxsein, M.L., 2013. Lumbar vertebral body bone microstructural scaling in small to medium-sized strepsirhines. Anat Rec 296(2), 210–226.
Fajardo, R.J., Müller, R., 2001. Three-dimensional analysis of nonhuman primate trabecular architecture using micro-computed tomography: Primate Trabecular Bone and the 3-D μCT Method. Am. J. Phys. Anthropol. 115, 327–336. https://doi.org/10.1002/ajpa.1089
Falconer, K., 2004. Fractal geometry: Mathematical foundations and applications (2nd ed.). Chichester: Wiley.
Feder, J., 1988. Fractals. New York: Plenum.
~~Felsenstein, J., 1985. Phylogenies and the comparative method. Am. Nat. 125(1), 1–15. https://doi.org/https ://doi.org/10.1086/284325~~
Feltrin, G.P., Macchi, V., Saccavini, C., Tosi, E., Dus, C., Fassina, A., Parenti, A., De Caro, R., 2001. Fractal analysis of lumbar vertebral cancellous bone architecture. Clin Anat 14(6), 414–417.
Feltrin, G.P., Stramare, R., Miotto, D., Giacomini, D., Saccavini, C., 2004. Bone fractal analysis. Curr. Osteoporos. Rep. 2(2), 53-58.
Fleagle, J.G., 2013. Primate Adaptation and Evolution - 3rd Edition. Academic press. (doi:10.1016/C2009-0-01979-5).
Ford, S.M., Morgan, G.S., 1986. A new ceboid femur from the late Pleistocene of Jamaica. J. Vertebr. Paleontol. 6(3), 281–289.
Frost, H.M., 1987. Bone 'mass' and the 'mechanostat': a proposal. Anat Rec 219, 1–9.
Frost, S.R., Marcus, L.F., Bookstein, F.L., Reddy, D.P., Delson, E., 2003. Cranial allometry, phylogeography, and systematics of large-bodied papionins (primates: Cercopithecinae) inferred from geometric morphometric analysis of landmark data. Anat Rec 275(2), 1048–1072.
Funk, J.R., Rudd, R.W., Kerrigan, J.R., Crandall, J.R., 2004. The Effect of Tibial Curvature and Fibular Loading on the Tibia Index. Traffic Inj. Prev. 5, 164–172. https://doi.org/10.1080/15389580490436069
Fyhrie, D.P., Zauel, R., 2015. Directional tortuosity as a predictor of modulus damage for vertebral cancellous bone. J. Biomech. Eng. 137(1), 011007.

~~Garamszegi, L.Z., 2014. Uncertainties Due to Within-Species Variation in Comparative Studies: Measurement Errors and Statistical Weights, in: Modern Phylogenetic Comparative Methods and Their Application in Evolutionary Biology: Concepts and Practice. Garamszegi L.Z. (ed), Springer, pp. 157–199.~~

Garbino, G.S., Nascimento, F.O., 2014. *Mico humeralifer* (Primates: Callitrichidae). Mamm. Species 46(911), 40–47.

García-Vilana, S., Sánchez-Molina, D., Velázquez-Ameijide, J., Llumà, J., Arregui-Dalmases, C., 2023. Relation between mechanical and densimetric properties to fractal dimension in human rib cortical bone. Med. Eng. Phys. 104004.

Garrahan, N.J., Mellish, R.W.E., Vedi, S., Compston, J.E., 1987. Measurement of mean trabecular plate thickness by a new computerized method. Bone 8(4), 227–230.

Gebo, D.L., 2014. Primate Comparative Anatomy. JHU Press.

Gebo, D.L., 2011. Vertical clinging and leaping revisited: Vertical support use as the ancestral condition of strepsirrhine primates. Am. J. Phys. Anthropol. 146, 323–335. https://doi.org/10.1002/ajpa.21595

Gebo, D.L., 1989. Postcranial adaptation and evolution in lorisidae. Primates 30, 347–367. https://doi.org/10.1007/BF02381259

Gebo, D.L., Smith, R., Dagosto, M., Smith, T., 2015. Additional postcranial elements of *Teilhardina belgica*: The oldest European primate. Am. J. Phys. Anthropol. 156, 388–406. https://doi.org/10.1002/ajpa.22664

Georgiou, L., Kivell, T.L., Pahr, D.H., Buck, L.T., Skinner, M.M., 2019. Trabecular architecture of the great ape and human femoral head. J. Anat. 234, 679–693. https://doi.org/10.1111/joa.12957

Georgiou, L., Kivell, T.L., Pahr, D.H., Skinner, M.M., 2018. Trabecular bone patterning in the hominoid distal femur. PeerJ 6, e5156. https://doi.org/10.7717/peerj.5156

Ghasem-Zadeh, A., Galea, M.P., Nunn, A., Panisset, M., Wang, X.-F., Iuliano, S., Boyd, S.K., Forwood, M.R., Seeman, E., 2021. Heterogeneity in microstructural deterioration following spinal cord injury. Bone 142, 115778. https://doi.org/10.1016/j.bone.2020.115778

Godfrey, L.R., 1988. Adaptive diversification of Malagasy strepsirrhines. J Hum Evol 17. 1–2, 93–134.

Goh, J.C., Mech, A.M., Lee, E.H., Ang, E.J., Bayon, P., Pho, R.W., 1992. Biomechanical study on the load-bearing characteristics of the fibula and the effects of fibular resection. Clin. Orthop. Relat. Res. 223–228.

Gomberg, B.R., Saha, P.K., Song, H.K., Hwang, S.N., Wehrli, F.W., 2000. Topological analysis of trabecular bone MR images. IEEE TMI 19(3), 166-174.

~~Granatosky, M.C., 2018. A review of locomotor diversity in mammals with analyses exploring the influence of substrate use, body mass and intermembral index in primates. J. Zool 306, 207–216. https://doi.org/10.1111/jzo.12608~~

Hagihara, Y., Nara, T., 2016. Morphological features of the fibula in Jomon hunter-gatherers from the shell mounds of the Pacific coastal area: morphological features of the fibula in the Jomon population. Am. J. Phys. Anthropol. 160, 708–718. https://doi.org/10.1002/ajpa.23000

Harmon, E.H., 2007. The shape of the hominoid proximal femur: a geometric morphometric analysis. J. Anat. 210, 170–185. https://doi.org/10.1111/j.1469-7580.2006.00688.x

Harrigan, T.P., Mann, R.W., 1984. Characterization of microstructural anisotropy in orthotropic materials using a second rank tensor. J Mater Sci 19, 761–767.

Heaton, J.L., Pickering, T.R., Carlson, K.J., Crompton, R.H., Jashashvili, T., Beaudet, A., Bruxelles, L., Kuman, K., Heile, A.J., Stratford, D., Clarke, R.J., 2019. The limb bones of the StW573 *Australopithecus* skeleton from Sterkfontein Memner 2: descriptions and proportions. J. Hum. Evol. 133, 167–197.

Hébert, D., Lebrun, R., Marivaux, L., 2012. Comparative three-dimensional structure of the trabecular bone in the talus of primates and its relationship to ankle joint loads generated during locomotion. Anat Rec 295, 2069–2088. https://doi.org/10.1002/ar.22608

Henderson, K., Pantinople, J., McCabe, K., Richards, H. L., Milne, N. 2017. Forelimb bone curvature in terrestrial and arboreal mammals. PeerJ, 5, e3229.

Hernandez, C.J., Loomis, D.A., Cotter, M.M., Schifle, A.L., Anderson, L.C., Elsmore, L., Kunos, C., Latimer, B., 2009. Biomechanical allometry in hominoid thoracic vertebrae. J Hum Evol 56, 462–470.

Hothorn, T., Bretz, F., Westfall, P., 2008. Simultaneous inference in general parametric models. Biom. J. 50(3), 346--363.

Huiskes, R., Ruimerman, R., van Lenthe, G.H., Janssen, J.D., 2000. Effects of mechanical forces on maintenance and adaptation of form in trabecular bone. Nature 405, 704–706.

Hunt, K.D., 1992. Positional behavior of *Pan troglodytes* in the Mahale mountains and Gombe stream national parks, Tanzania. Am. J. Phys. Anthropol 87.1, 83–105.

Jacobs, C.R., 2000. The mechanobiology of cancellous bone structural adaptation. J Rehab Research Devel 37, 209–216.

Judex, S., Carlson, K.J., 2009. Is bone's response to mechanical signals dominated by gravitational loading? Med Sci Sports Exerc 41, 2037–2043. https://doi.org/10.1249/MSS.0b013e3181a8c6e5

Jungers, W.L., Godfrey, L.R., Simons, E.L., Wunderlich, R.E., Richmond, B.G., Chatrath, P.S., 2002. Ecomorphology and Behavior of Giant Extinct Lemurs from Madagascar, in: In: Reconstructing Behavior in the Primate Fossil Record. Plavcan J.M., Kay R.F., Jungers W.L., van Schaik C.P. (doi: https://doi.org/10.1007/978-1-4615-1343-8_10), Kluwer Academic/Plenum Publishers, New York., pp. 371–411.

Karlsson, C., Obrant, K.J., Karlsson, M., 2001. Pregnancy and lactation confer reversible bone loss in humans. Osteoporos Int 828–834.

Kilbourne, B.M., Hutchinson, J.R., 2019. Morphological diversification of biomechanical traits: mustelid locomotor specializations and the macroevolution of long bone cross-sectional morphology. BMC Evol Biol 19, 37. https://doi.org/10.1186/s12862-019-1349-8

Kimura, T., 2003. Differentiation between fore- and hindlimb bones and locomotor behavior in primates. FPR 74, 17–32. https://doi.org/10.1159/000068391

Kimura, T., 2002. Primate limb bones and locomotor types in arboreal or terrestrial environments. Z. Morphol. Anthropol. 83, 201–219.

Kimura, T., 1995. Long bone characteristics of primates. Z. Morph. Anthrop. 80, 265–580.

Kivell, T.L., 2016. A review of trabecular bone functional adaptation: what have we learned from trabecular analyses in extant hominoids and what can we apply to fossils? J. Anat. 228, 569–594. https://doi.org/10.1111/joa.12446

Kivell, T.L., Davenport, R., Hublin, J.-J., Thackeray, J.F., Skinner, M.M., 2018. Trabecular architecture and joint loading of the proximal humerus in extant hominoids, *Ateles*, and *Australopithecus africanus*. Am J Phys Anthropol 167, 348–365. https://doi.org/10.1002/ajpa.23635

Kivell, T.L., Kibii, J.M., Churchill, S.E., Schmid, P., Berger, L.R. 2011. *Australopithecus sediba* hand demonstrates mosaic evolution of locomotor and manipulative abilities. Science 333, 1411–1417. https://doi.org/10.1126/science.1202625

Komza, K., Skinner, M.M., 2019. First metatarsal trabecular bone structure in extant hominoids and Swartkrans hominins. J Hum Evol 131, 1–21.

Lambers, F. M., Koch, K., Kuhn, G., Ruffoni, D., Weigt, C., Schulte, F. A., Müller, R. 2013. Trabecular bone adapts to long-term cyclic loading by increasing stiffness and normalization of dynamic morphometric rates. Bone, 55(2), 325-334.

Lambert, K.L., 1971. The weight-bearing function of the fibula. A strain gauge study. J Bone Joint Surg Am 53, 507–513.

Landi, F., Alfieri, F., Towle, I., Profico, A., Veneziano, A., 2021. Fluctuating asymmetry and stress in *Macaca fuscata*: does captivity affect morphology? Applied Sciences 11, 7879. https://doi.org/10.3390/app11177879

Libotte, M., Klein, P., Colpaert, H., Alameh, M., Blaimont, P., Halleux, P., 1982. Biomechanical study of the ankle joint. Rev Chir Orthop Reparatrice Appar Mot 68, 299–305.

Liu, X. S., Sajda, P., Saha, P. K., Wehrli, F. W., & Guo, X. E. 2006. Quantification of the roles of trabecular microarchitecture and trabecular type in determining the elastic modulus of human trabecular bone. Journal of Bone and Mineral Research, 21(10), 1608-1617

MacLatchy, L., Müller, R., 2002. A comparison of the femoral head and neck trabecular architecture of *Galago* and *Perodicticus* using micro-computed tomography (μCT). J Hum Evol 43, 89–105. https://doi.org/10.1006/jhev.2002.0559

MacLatchy, L.M., Bossert, W.H., 1996. An analysis of the articular surface distribution of the femoral head and acetabulum in anthropoids, with implications for hip function in Miocene hominoids. J Hum Evol 31, 425–453. https://doi.org/10.1006/jhev.1996.0070

Maga, M., Kappelman, J., Ryan, T.M., Ketcham, R.A., 2006. Preliminary observations on the calcaneal trabecular microarchitecture of extant large-bodied hominoids. Am. J. Phys. Anthropol. 129, 410–417. https://doi.org/10.1002/ajpa.20276

Maquer, G., Musy, S.N., Wandel, J., Gross, T., Zysset, P.K., 2015. Bone volume fraction and fabric anisotropy are better determinants of trabecular bone stiffness than other morphological variables. J. Bone Miner. Res. 30, 1000–1008. https://doi.org/10.1002/jbmr.2437

Marchi, D., 2015a. Variation in tibia and fibula diaphyseal strength and its relationship with arboreal and terrestrial locomotion: extending the investigation to non-hominoid primates. J. Anthropol. Sci 93, 153–156. https://doi.org/10.4436/jass.93005

Marchi, D., 2015b. Using the morphology of the hominoid distal fibula to interpret arboreality in *Australopithecus afarensis*. J Hum Evol 85, 136–148. https://doi.org/10.1016/j.jhevol.2015.06.002

Marchi, D., 2007. Relative strength of the tibia and fibula and locomotor behavior in hominoids. J Hum Evol 53, 647–655. https://doi.org/10.1016/j.jhevol.2007.05.007

Marchi, D., Borgognini-Tarli, M.S., 2004. Cross-sectional geometry of the limb bones of the Hominoidea by biplanar radiography and moulding techniques. J. Anthropol. Sci 82, 89–102.

Marchi, D., Harper, C.M., Chirchir, H., Ruff, C.B., 2019. Relative fibula strength and locomotor behavior in KNM-WT 15000 and OH 35. J. Hum. Evol. 131, 48–60.

Marchi, D., Rimoldi, A., García-Martínez, D., Bastir, M., 2022. Morphological correlates of distal fibular morphology with locomotion in great apes, humans, and *Australopithecus afarensis*. Am. J. Biol. Anthropol. 178(2), 286–300.

Marchi, D., Ruff, C.B., Capobianco, A., Rafferty, K.L., Habib, M.B., Patel, B.A., 2016. The locomotion of *Babakotia radofilai* inferred from epiphyseal and diaphyseal morphology of the humerus and femur. J. Morphol. 277, 1199–1218. https://doi.org/10.1002/jmor.20569

Marchi, D., Shaw, C.N., 2011. Variation in fibular robusticity reflects variation in mobility patterns. J Hum Evol 61, 609–616. https://doi.org/10.1016/j.jhevol.2011.08.005

Marchi, D., Sparacello, V., Shaw, C., 2011. Mobility and Lower Limb Robusticity of a Pastoralist Neolithic Population from North-Western Italy, in: Human Bioarchaeology of the Transition to Agriculture. John Wiley & Sons, Ltd, pp. 317–346. https://doi.org/10.1002/9780470670170.ch13

Marchi, D., Walker, C.S., Wei, P., Holliday, T.W., Churchill, S.E., Berger, L.R., DeSilva, J.M., 2017. The thigh and leg of *Homo naledi*. J. Hum. Evol 104, 174–204.

Meldrum, D.J., 1991. Kinematics of the Cercopithecine foot on arboreal and terrestrial substrates with implications for the interpretation of hominid terrestrial adaptations. Am. J. Phys. Anthropol. 84, 273–290.

Messent, E.A., Buckland-Wright, J.C., Blake, G.M., 2005a. Fractal analysis of trabecular bone in knee osteoarthritis (OA) is a more sensitive marker of disease status than bone mineral density (BMD). Calcif. Tissue Int. 76, 419–425.

Messent, E.A., Ward, R.J., Tonkin, C.J., Buckland-Wright, C., 2005b. Tibial cancellous bone changes in patients with knee osteoarthritis. A short-term longitudinal study using Fractal Signature Analysis. Osteoarthr. Cartil. 13(6), 463–470.

Mielke, M., Wölfer, J., Arnold, P., van Heteren, A.H., Amson, E., Nyakatura, J.A., 2018. Trabecular architecture in the sciuromorph femoral head: allometry and functional adaptation. Zool Lett 4, 10. https://doi.org/10.1186/s40851-018-0093-z

Mittra, E., Rubin, C., Gruber, B., Qin, Y.-X., 2008. Evaluation of trabecular mechanical and microstructural properties in human calcaneal bone of advanced age using mechanical testing, microCT, and DXA. J Biomech 41, 368-375.

Mittra, E., Rubin, C., Qin, Y.-X., 2005. Interrelationships of trabecular mechanical and microstructural properties in sheep trabecular bone. J Biomech 38, 1229–1237.
~~Moncl\u00fas-Gonzalo, O., Alba, D.M., Duhamel, A., Fabre, A.C., Marigó, J., 2023. Early euprimates already had a diverse locomotor repertoire: Evidence from ankle bone morphology. J Hum Evol 181, 103395.~~
Moore, K.L., Dalley, A.F., 2006. Clinically Oriented Anatomy, 5th ed. Lippincott Williams & Wilkins, Baltimore.
Napier, J.R., Walker, A.C., 1967. Vertical clinging and leaping-a newly recognized category of locomotor behaviour of primates. Folia Primatol. 6, 204–219. https://doi.org/10.1159/000155079
Navalón, G., Bjarnason, A., Griffiths, E., Benson, R.B., 2022. Environmental signal in the evolutionary diversification of bird skeletons. Nature 611(7935), 306–311.
Ni, X., Gebo, D.L., Dagosto, M., Meng, J., Tafforeau, P., Flynn, J.J., Beard, K.C., 2013. The oldest known primate skeleton and early haplorhine evolution. Nature 498, 60–64. https://doi.org/10.1038/nature12200
Nishimura, T., Morimoto, N., Ito, T., 2019. Shape variation in the facial part of the cranium in macaques and African papionins using geometric morphometrics. Primates 60, 401–419.
Odgaard, A., 1997. Three-dimensional methods for quantification of cancellous bone architecture. Bone 20, 315–328.
O'Neill, M.C., Dobson, S.D., 2008. The degree and pattern of phylogenetic signal in primate long-bone structure. J Hum Evol 54, 309–322. https://doi.org/10.1016/j.jhevol.2007.08.008
O'Neill, M.C., Lee, L.F., Demes, B., Thompson, N.E., Larson, S.G., Stern Jr, J.T., Umberger, B.R., 2015. Three-dimensional kinematics of the pelvis and hind limbs in chimpanzee (*Pan troglodytes*) and human bipedal walking. J Hum Evol 86, 32–42.
Owen, R., 1866. Comparative Anatomy and Physiology of Vertebrates. II. London: Longmans, Green &: Co.
Paradis, E., Claude, J., Strimmer, K., 2004. APE: Analyses of Phylogenetics and Evolution in R language. Bioinformatics 20, 289–290. https://doi.org/10.1093/bioinformatics/btg412
Parkinson, I.H., Badiei, A., Stauber, M., Codrington, J., Müller, R., Fazzalari, N.L., 2012. Vertebral body bone strength: the contribution of individual trabecular element morphology. Osteoporos Int 23, 1957–1965.
Pau, G., Fuchs, F., Sklyar, O., Boutros, M., Huber, W., 2010. EBImage - an R package for image processing with applications to cellular phenotypes. Bioinformatics 26(7), 979–981. https://doi.org/10.1093/bioinformatics/btq046
Pinheiro, J., Bates, D., DebRoy, S., Sarkar, D., 2020. nlme: Linear and Nonlinear Mixed Effects Models. R package version 3.1-147. https://rdrr.io/cran/nlme/
Plomp, K. A., Owen, J., Dobney, K., Collard, M. 2024. Mandibular shape and diet in extant primates: a 3D geometric morphometric analysis. Anthropol Anz. https://doi.org/10.1127/anthranz/2024/1675
Polk, J.D., Demes, B., Jungers, W.L., Biknevicius, A.R., Heinrich, R.E., Runestad, J.A., 2000. A comparison of primate, carnivoran and rodent limb bone cross-sectional properties: are primates really unique? J Hum Evol 39, 297–325. https://doi.org/10.1006/jhev.2000.0420
Polly, P.D., 2007. Limbs in Mammalin Evolution, in: In: Fins into Limbs: Evolution, Development, and Transformation. Hall B.K. (ed), Chicago: University of Chicago Press., p. Chap. 15 (pp. 245-268).
Pontzer, H., Lieberman, D.E., Momin, E., Devlin, M.J., Polk, J.D., Hallgrímsson, B., Cooper, D.M.L., 2006. Trabecular bone in the bird knee responds with high sensitivity to changes in load orientation. J Exp Biol 209, 57–65. https://doi.org/10.1242/jeb.01971
Pornprasertsuk, S., Ludlow, J.B., Webber, R.L., Tyndall, D.A., Sanhueza, A.I., Yamauchi, M., 2001. Fractal dimension analysis of weight-bearing bones of rats during skeletal unloading. Bone 29(2), 180–184.
Pothuaud, L., Van Rietbergen, B., Mosekilde, L., Beuf, O., Levitz, P., Benhamou, C. L., & Majumdar, S. 2002. Combination of topological parameters and bone volume fraction better predicts the mechanical properties of trabecular bone. Journal of Biomechanics, 35(8), 1091-1099

Preuschoft, H., 1970. Functional Anatomy of the Lower Extremity, in: The Chimpanzee, Vol. 3. Bourne, G.H., Karger, Basel, pp. 221–294.
Puttick, M., Thomas, G., Freckleton, R., Clarke, M., Ingram, T., Orme, D., Paradis, E., 2019. motmot: Models of Trait Macroevolution on Trees. R package version 2.1.3 <https://CRAN.R-project.org/package=motmot>.
Rafferty, K.L., Walker, A., Ruff, C.B., Rose, M.D., Andrews, P.J., 1995. Postcranial estimates of body weight in *Proconsul*, with a note on a distal tibia of *P. major* from Napak, Uganda. Am. J. Phys. Anthropol. 97(4), 391–402.
Revell, L.J., 2012. phytools: an R package for phylogenetic comparative biology (and other things). Methods Ecol. Evol. 3, 217–223. https://doi.org/10.1111/j.2041-210X.2011.00169.x
Rittweger, J., Ireland, A., Lüscher, S., Nocciolino, L.M., Pilot, N., Pisani, L., Cointry, G.R., Ferretti, J.L., Capozza, R.F., 2018. Fibula: The forgotten bone-may it provide some insight on a wider scope for bone mechanostat control? Curr Osteoporos Rep 16, 775–778. https://doi.org/10.1007/s11914-018-0497-x
Robling, A.G., 2009. Is bone's response to mechanical signals dominated by muscle forces? Med Sci Sports Exerc 41, 2044–2049. https://doi.org/10.1249/MSS.0b013e3181a8c702
Rodman, P.S., 1979. Skeletal differentiation of *Macaca fascicularis* and *Macaca nemestrina* in relation to arboreal and terrestrial quadrupedalism. Am. J. Phys. Anthrop. 51, 51–62.
Rodríguez, L., Carretero, J.M., Carcía-González, R., Arsuaga, J.L., 2018. Cross-sectional properties of the lower limb long bones in the Middle Pleistocene Sima de los Huesos sample (Sierra de Atapuerca, Spain). J. Hum. Evol. 117, 1–12.
Roque, W.L., Alberich-Bayarri, A., 2015. Tortuosity Influence on the Trabecular Bone Elasticity and Mechanical Competence., in: Developments in Medical Image Processing and Computational Vision. R. N. Jorge, J. M. Tavares (Eds.), Cham: Springer, pp. 173–191.
Roque, W.L., Arcaro, K., Alberich-Bayarri, A., 2012. Mechanical competence of bone: a new parameter to grade trabecular bone fragility from tortuosity and elasticity. IEEE Trans. Biomed. Eng. 60(5), 1363–1370.
Rose, M.D., 1979. Positional Behavior of Natural Populations: Some Quantitative Results of a Field Study of *Colobus guereza* and *Cercopithecus aethiops*, in: Environment, Behavior, and Morphology. Morbeck ME, Preuschoft H, Gomberg N., New York: Gustav Fisher, pp. 75–94.
Rubin C, Turner AS, Bain S, et al. (2001) Anabolism: low mechanical signals strengthen long bones. Nature 412, 603–604.
Rubin C, Turner AS, Mallinckrodt C, et al. (2002) Mechanical strain, induced noninvasively in the high-frequency domain is anabolic to cancellous bone, but not cortical bone. Bone 30, 445–452.
Ruff, C., 1987. Sexual dimorphism in human lower limb bone structure: relationship to subsistence strategy and sexual division of labor. J. Hum. Evol. 16, 391–416. https://doi.org/10.1016/0047-2484(87)90069-8
Ruff, C., Holt, B., Trinkaus, E., 2006. Who's afraid of the big bad Wolff?: 'Wolff's law' and bone functional adaptation. Am. J. Phys. Anthropol. 129, 484–498. https://doi.org/10.1002/ajpa.20371
Ruff, C.B., 2003. Long bone articular and diaphyseal structure in Old World monkeys and apes. II: Estimation of body mass. Am. J. Phys. Anthropol. 120, 16–37. https://doi.org/10.1002/ajpa.10118
Ruff, C.B., 2002. Long bone articular and diaphyseal structure in old world monkeys and apes. I: locomotor effects. Am. J. Phys. Anthropol. 119, 305–342. https://doi.org/10.1002/ajpa.10117
Ruff, C.B., Burgess, M.L., Squyres, N., Junno, J.A., Trinkaus, E., 2018. Lower limb articular scaling and body mass estimation in Pliocene and Pleistocene hominins. J. Hum. Evol. 115, 85–111.
Ruff, C.B., Harper, C.M., Goldstein, D.M., Deegling, D.J., McGraw, W.C., 2019. Long bone structural proportions and locomotor behavior in Cercopithecidae. J Hum Evol 132, 47–60.
Ruff, C.B., Jones, H.H., 1981. Bilateral asymmetry in cortical bone of the humerus and tibia: Sex and age factors. Hum. Biol. 53, 69–86.
Ruff, C.B., Runestad, J.A., 1992. Primate limb bone structural adaptations. Annu. Rev. Anthropol. 21, 407–433. https://doi.org/10.1146/annurev.an.21.100192.002203

Runestad, J.A., 1997. Postcranial adaptations for climbing in Loridae (Primates). J. Zool. 242, 261–290. https://doi.org/10.1111/j.1469-7998.1997.tb05801.x
Ryan, T.M., Ketcham, R.A., 2002a. The three-dimensional structure of trabecular bone in the femoral head of strepsirrhine primates. J. Hum. Evol. 43, 1–26. https://doi.org/10.1006/jhev.2002.0552
Ryan, T.M., Ketcham, R.A., 2002b. Femoral head trabecular bone structure in two omomyid primates. J. Hum. Evol. 43, 241–263. https://doi.org/10.1006/jhev.2002.0575
Ryan, T.M., Shaw, C.N., 2015. Gracility of the modern *Homo sapiens* skeleton is the result of decreased biomechanical loading. Proc Natl Acad Sci USA 112, 372–377. https://doi.org/10.1073/pnas.1418646112
Ryan, T.M., Shaw, C.N., 2013. Trabecular bone microstructure scales allometrically in the primate humerus and femur. Proc. R. Soc. B 280, 20130172. https://doi.org/10.1098/rspb.2013.0172
Ryan, T.M., Shaw, C.N., 2012. Unique suites of trabecular bone features characterize locomotor behavior in human and non-human anthropoid primates. PLoS ONE 7, e41037. https://doi.org/10.1371/journal.pone.0041037
Saers, J.P.P., 2023. Skeletal indicators of developmental changes in arboreality and locomotor maturation in extant apes and their relevance to hominin paleobiology. Front. Ecol. Evol. 11, 1274762. https://doi.org/doi: 10.3389/fevo.2023.1274762
Saers, J.P.P., Cazorla-Bak, Y., Shaw, C.N., Stock, J.T., Ryan, T.M., 2016. Trabecular bone structural variation throughout the human lower limb. J. Hum. Evol 97, 97–108. https://doi.org/10.1016/j.jhevol.2016.05.012
Saers, J.P.P., Gordon, A.D., Ryan, T.M., Stock, J.T., 2022. Growth and development of trabecular structure in the calcaneus of Japanese macaques (*Macaca fuscata*) reflects locomotor behavior, life history, and neuromuscular development. J Anat 00, 1–15. https://doi.org/10.1111/joa.13641
Sanchez-Molina, D., Velazquez-Ameijide, J., Quintana, V., Arregui-Dalmases, C., Crandall, J. R., Subit, D., & Kerrigan, J. R. 2013. Fractal dimension and mechanical properties of human cortical bone. Med Eng Phys, 35(5), 576-582.
Schaffler, M.B., Burr, D.B., 1984. Primate cortical bone microstructure: Relationship to locomotion. Am. J. Phys. Anthrop. 65, 191–197. https://doi.org/10.1002/ajpa.1330650211
Schaffler, M.B., Burr, D.B., Jungers, W.L., Ruff, C.B., 1985. Structural and mechanical indicators of limb specialization in primates. Folia Primatol. 45, 61–75. https://doi.org/10.1159/000156218
Scherf, H., 2008. Locomotion-related Femoral Trabecular Architectures in Primates — High Resolution Computed Tomographies and Their Implications for Estimations of Locomotor Preferences of Fossil Primates, In: Anatomical Imaging: Towards a New Morphology. Endo, H., Frey, R. (Eds.), Springer Japan, Tokyo, pp. 39–59. https://doi.org/10.1007/978-4-431-76933-0_4
Scherf, H., Harvati, K., Hublin, J.-J., 2013. A comparison of proximal humeral cancellous bone of great apes and humans. J. Hum. Evol 65, 29–38. https://doi.org/10.1016/j.jhevol.2013.03.008
Schilling, A.M., Tofanelli, S., Hublin, J.J., Kivell, T.L., 2014. Trabecular bone structure in the primate wrist. J Morphol 275, 572–585.
Schmitt, D., 2003. Mediolateral reaction forces and forelimb anatomy in quadrupedal primates: implications for interpreting locomotor behaviour in fossil primates. J. Hum. Evol 44, 47e58.
Schneider, C.A., Rasband, W.S., Eliceiri, K.W., 2012. NIH Image to ImageJ: 25 years of image analysis. Nat. Methods 9, 671–675. https://doi.org/10.1038/nmeth.2089
Seiler, H., 1986. [Biomechanics of the upper ankle joint]. Orthopade 15, 415–422.
Shaw, C.N., Ryan, T.M. 2012. Does skeletal anatomy reflect adaptation to locomotor patterns? Cortical and trabecular architecture in human and nonhuman anthropoids. Am J Phys Anthropol. 147(2):187-200.
Simkin A, Leichter I, Swissa A, et al. (1989) The effect of swimming activity on bone architecture in growing rats. J Biomech 22, 845–851.
Skerry, T.M., Lanyon, L.E. 1995. Interruption of disuse by short duration walking exercise does not prevent bone loss in the sheep calcaneus. Bone 16, 269–274.
Smaers, J.B., Vinicius, L., 2009. Inferring macro-evolutionary patterns using an adaptive peak model of evolution. Evol Ecol Res 11, 991–1015.

Sode, M., Burghardt, A.J., Nissenson, R.A., Majumdar, S., 2008. Resolution dependence of the non-metric trabecular structure indices. Bone 42, 728–736. https://doi.org/10.1016/j.bone.2007.12.004

~~Sokal, R., Rohlf, F., 1995. Biometry: The Principles and Practice of Statistics in Biological Research 3rd ed., Freeman, New York. ed.~~

Souto, A., Bezerra, B.M., Schiel, N., Huber, L., 2007. Saltatory search in free-living *Callithrix jacchus*: environmental and age influences. Int. J. Primatol. 28, 881–893.

Sparacello, V.S., Marchi, D., Shaw, C.N., 2014. The Importance of Considering Fibular Robusticity when Inferring the Mobility Patterns of Past Populations., In: Reconstructing Mobility: Environmental, Behavioral, and Morphological Determinants. Carlson K.J, Marchi D. Springer, pp. 91–110.

Stauber, M., Rapillard, L., van Lenthe, G.H., Zysset, P., Müller, R., 2006. Importance of individual rods and plates in the assessment of bone quality and their contribution to bone stiffness. J Bone Min Res 21, 586–595.

Stürznickel, J., Schmidt, F.N., Schäfer, H.S., Beil, F.T., Frosch, K.H., Schlickewei, C., Amling, M., Barg, A., Rolvien, T., 2021. Bone microarchitecture of the distal fibula assessed by HR-pQCT. Bone 151, 116057. https://doi.org/10.1016/j.bone.2021.116057

Su, A., Carlson, K.J., 2017. Comparative analysis of trabecular bone structure and orientation in South African hominin tali. J. Hum. Evol. 106, 1–18. https://doi.org/10.1016/j.jhevol.2016.12.006

Su, A., Wallace, I.J., Nakatsukasa, M., 2013. Trabecular bone anisotropy and orientation in an Early Pleistocene hominin talus from East Turkana, Kenya. J. Hum. Evol. 64, 667–677. https://doi.org/10.1016/j.jhevol.2013.03.003

Su, A., Zeininger, A., 2022. The Primate Ankle and Hindfoot, In: The Evolution of the Primate Foot: Anatomy, Function, and Palaeontological Evidence. Zeininger A., Hatala, K. G., Wunderlich, R. E., Schmitt, D. (Eds.)., Springer., pp. 21–45.

Sukhdeo, S., Parsons, J., Niu, X.M., Ryan, T.M., 2020. Trabecular bone structure in the distal femur of humans, apes, and baboons. Anat Rec 303, 129–149. https://doi.org/10.1002/ar.24050

Swartz, S.M., 1989. The functional morphology of weight bearing: limb joint surface area allometry in anthropoid primates. J. Zool. 218, 441–460. https://doi.org/10.1111/j.1469-7998.1989.tb02556.x

Swartz, S.M., Parker, A., Huo, C., 1998. Theoretical and empirical scaling patterns and topological homology in bone trabeculae. J Exp Biol 201, 573–590. https://doi.org/10.1242/jeb.201.4.573

Sylvester, A.D., 2013. A geometric morphometric analysis of the medial tibial condyle of African hominids. Anat Rec 296, 1518–1525. https://doi.org/10.1002/ar.22762

Sylvester, A.D., Terhune, C.E., 2017. Trabecular mapping: Leveraging geometric morphometrics for analyses of trabecular structure. Am J Phys Anthropol 163, 553–569. https://doi.org/10.1002/ajpa.23231

Takebe, K., Nakagawa, A., Minami, H., Kanazawa, H., Hirohata, K., 1984. Role of the fibula in weight-bearing. Clin. Orthop. Relat. Res. 289–292.

Tardieu, C., 2010. Development of the human hind limb and its importance for the evolution of bipedalism. Evol. Anthropol. Issues News Rev. 19, 174–186. https://doi.org/10.1002/evan.20276

Tarquini, J., 2021. Femoral shape in procyonids (Carnivora, Procyonidae): morphofunctional implications, size and phylogenetic Signal. J Mammal Evol 28, 159–171. https://doi.org/10.1007/s10914-019-09491-8

Tegner, C., 2011. Behavioral patterns in a population of Samango monkeys (*Cercopithecus albogularis erythrarcus*). BSc thesis. Linköpings universitet, Sweden.

Tillquist, R.C., Shoemaker, L.G., Knight, K.B., Clauset, A., 2016. The evolution of primate body size: left-skewness, maximum size, and Cope's rule. Pre-print. https://doi.org/10.1101/092866

Tsegai, Z.J., Kivell, T.L., Gross, T., Nguyen, N.H., Pahr, D.H., Smaers, J.B., Skinner, M.M., 2013. Trabecular bone structure correlates with hand posture and use in hominoids. PLoS ONE 8, e78781. https://doi.org/10.1371/journal.pone.0078781

Tsegai, Z.J., Skinner, M.M., Gee, A.H., Pahr, D.H., Treece, G.M., Hublin, J.J., Kivell, T.L., 2017. Trabecular and cortical bone structure of the talus and distal tibia in *Pan* and *Homo*. Am J Phys Anthropol 163(4), 784–805.

Tsegai, Z.J., Skinner, M.M., Pahr, D.H., Hublin, J.-J., Kivell, T.L., 2018. Ontogeny and variability of trabecular bone in the chimpanzee humerus, femur and tibia. Am J Phys Anthropol 167, 713–736. https://doi.org/10.1002/ajpa.23696

Uchiyama, T., Tanizawa, T., Muramatsu, H., Endo, N., Takahashi, H.E., Hara, T., 1999. Three-dimensional microstructural analysis of human trabecular bone in relation to its mechanical properties. Bone 25(4), 487–491.

Upham, N.S., Esselstyn, J.A., Jetz, W., 2019. Inferring the mammal tree: species-level sets of phylogenies for questions in ecology, evolution, and conservation. PLoS Biol 17, e3000494. https://doi.org/10.1371/journal.pbio.3000494

Veneziano, A., Irish, J. D., Meloro, C., Stringer, C., & De Groote, I. 2019. The functional significance of dental and mandibular reduction in *Homo*: A catarrhine perspective. Am. J. Primatol., 81(3), e22953.

Veneziano, A., Cazenave, M., Alfieri, F., Panetta, D., Marchi, D., 2021. Novel strategies for the characterization of cancellous bone morphology: Virtual isolation and analysis. Am J Phys Anthropol 175(4), 920-930 https://doi.org/10.1002/ajpa.24272

Veracini, C., 2009. Habitat Use and Ranging Behavior of the Silvery Marmoset (*Mico argentatus*) at Caxiuanã National Forest (eastern Brazilian Amazonia)., In: The Smallest Anthropoids: The Marmoset/Callimico Radiation. Ford S. M., Porter L.M., Davis L.C, Springer (eds), pp. 221–240.

Walmsley, T., 1918. The reduction of the mammalian fibula. J Anat 52, 326–331.

Wang, H., Sherry Liu, X., Zhou, B., Wang, J., Ji, B., Huang, Y., Hwang, K-C & Edward Guo, X. 2013. Accuracy of individual trabecula segmentation based plate and rod finite element models in idealized trabecular bone microstructure. Journal of biomechanical engineering, 135(4), 044502.

White, T.D., Black, M.T., Folkens, P.A., 2011. Human Osteology, 3rd Edition. Academic Press. San Diego.

Wickham, H., 2016. ggplot2: Elegant Graphics for Data Analysis. Springer-Verlag New York.

Wund, M.A., 2012. Assessing the impacts of phenotypic plasticity on evolution. Integr Comp Biol 52(1), 5–15. https://doi.org/10.1093/icb/ics050.

Yeni, Y.N., Zinno, M.J., Yerramshetty, J.S., Zauel, R., Fyhrie, D.P., 2011. Variability of trabecular microstructure is age-, gender-, race- and anatomic sitedependent and affects stiffness and stress distribution properties of human vertebral cancellous bone. Bone 49, 886–894.

You, K., Shung, D., 2022. Rdimtools: An R package for dimension reduction and intrinsic dimension estimation. Software Impacts 14(1), 100414.

Youlatos, D., 2008. Locomotion and Positional Behavior of Spider Monkeys., In: Spider Monkeys. Behavior, Ecology and Evolution of the Genus *Ateles*. Campbell C.J. (ed), Cambridge Studies in Biological and Evolutionary Anthropology 55.

Youlatos, D., Gasc, J.P., 2011. Gait and Kinematics of Arboreal Quadrupedal Walking of Free-ranging Red Howlers (*Alouatta seniculus*) in French Guiana, In: Primate Locomotion. Linking Field and Laboratory Research. D'Aout K., Vereecke E.E. (eds), Springer. New York.

~~Zhou, B., Liu, X. S., Wang, J., Lu, X. L., Fields, A. J., & Guo, X. E. 2014. Dependence of mechanical properties of trabecular bone on plate–rod microstructure determined by individual trabecula segmentation (ITS). Journal of biomechanics, 47(3), 702-708.~~

Figure captions

Fig. 1. Primate species studied in this work. The three factors potentially associated with their distal fibular trabecular architecture that were addressed in this work, are summarized: 1. phylogenetic relationships, shown through the time-calibrated tree; 2. locomotor habits, detailed with the color legend; 3. body mass, through the proxy used in this work, shown with bar plots. See Methods for details.

Fig. 2. The steps performed to orient all the fibulae in a standard position are exemplified on the distal fibula of *Cercopithecus mitis* UniFl-SPEC 3011. In both **A** (anterior view) and **B** (distal view) PAF, i.e. proximal part of the fibulotalar articulation of the distal fibula, is oriented to be parallel to the coronal plane (shown with a blue line in 2A and 2B). **C.** The bone is then oriented so that the two axes of PAF (visually recognized and highlighted in red, due to the quasi-regular shape of the articular facet) lie in the sagittal (shown in orange) and the transverse (shown in green) planes. DAF, i.e. distal part of the fibulotalar

articulation of the distal fibula, is shown but was not studied in this work. **D.** The Region of Interest (ROI) ultimately analyzed is here shown in the context of the entire distal epiphysis. A sub-region of the distal fibula corresponding to the PAF cortical bone + trabecular bone was cropped (highlighted in aqua green, also shown in Fig. 3A) and from it a ROI representing only the PAF trabecular bone was extracted (highlighted in purple, also shown in Fig. 3B).

Fig. 3. Isolation of the whole articular trabecular architecture, exemplified on the distal fibula of *Cercopithecus mitis* UniFl-SPEC 3011. A. The oriented sub-stack corresponding to the isolated PAF. PAF is shown in red and its proximal and distal limits, used to isolate PAF, are highlighted. B. Exploiting the 'indianaBones' R package, the trabecular bone is isolated and used to compute BoneJ parameters. C. The trabecular network of B. is skeletonized in Amira. The skeleton is used to compute the topological indices of 'indianaBones'.

Fig. 4. A. Boxplots highlighting the univariate pattern of variation of BV/TV from the distal fibular trabecular architecture. Terrestrial taxa are shown in blue, semi-arboreal in green and arboreal in purple, and taxa yielding the maximum and minimum value for each category of the Degree of Arboreality are indicated. **B.** The BV/TV values for the studied species are mapped on the phylogeny used in this work, with ancestral states reconstructed. Here, the color legend instead indicates the variable values. ~~**B**~~**C.** Boxplots highlighting the univariate pattern of variation of size-corrected BS/TV from the distal fibular trabecular architecture. Terrestrial taxa are shown in blue, semi-arboreal in green and arboreal in red, and taxa yielding the maximum and minimum value for each category of the Degree of Arboreality are indicated. ~~**C**~~**D.** The size-corrected BS/TV values for the studied species are mapped on the phylogeny used in this work, with ancestral states reconstructed. Here, the color legend instead indicates the variable values.

Fig. 5. Multivariate patterns of variation in distal fibular trabecular architecture. **A, B** and **C.** Upper panels: phylomorphospaces built with PC1-PC2 (**A**), PC1-PC3 (**B**) and PC2-PC3 (**C**) resulting from a PCA on all the studied trabecular traits (using size-corrected values in case of variables significantly related to body mass, as detailed in Table 3). Abbreviations: *Cj* for *Callithrix jacchus*, *Hs* for *Homo sapiens*, *Pt* for *Pan troglodytes*, *Oc* for *Otolemur crassicaudatus*. Bottom panels: variable loading plots summarizing how single traits contribute to species distribution on the corresponding morphospaces in the upper panels. In **A**, **B** and **C**: Degree of arboreality categories are shown with colors: arboreal in purple, semi-arboreal in green, terrestrial in blue. Abbreviations for variables in the loading plots: DA (degree of anisotropy), BV/TV (bone volume fraction), BS/TV (bone surface density), Tb.Th (trabecular thickness), $NodDen_{Aver}$ (average node density), $NodDen_{Med}$ (median node density), $TrabLen_{Aver}$ (average trabecular length), $TrabTort_{Aver}$ (average trabecular tortuosity), $TrabTort_{Med}$ (median trabecular tortuosity), FD (fractal dimension). **D.** Boxplot highlighting the univariate pattern of variation of PC2 (used to build the bivariate scatterplots in **A** and **C**). Terrestrial taxa are shown in blue, semi-arboreal in green and arboreal in red. The position of *Homo sapiens*, outlying other terrestrial taxa, is shown.

The relationship between primate distal fibula trabecular architecture and degree of arboreality, phylogeny and size

Alfieri F.[1,2,3,4], Veneziano A.[5], Panetta D.[6], Salvadori P.A.[6], Amson E.[7], Marchi D.[8,9]

1. Institute of Ecology and Evolution, Universität Bern, Bern, Switzerland
2. Department of Earth Sciences, University of Cambridge, Cambridge, UK
3. Institut für Biologie, Humboldt Universität zu Berlin, Berlin, Germany
4. Museum Für Naturkunde, Leibniz-Institut Für Evolutions- Und Biodiversitätsforschung, Berlin, Germany
5. Departament d'Enginyeria Mecànica, Universitat Rovira i Virgili, Tarragona, Spain.
6. Institute of Clinical Physiology, IFC-CNR, Pisa, Italy,
7. Staatliches Museum für Naturkunde, Stuttgart, Germany.
8. Department of Biology, Università di Pisa, Pisa, Italy.
9. Centre for the Exploration of the Deep Human Journey, University of the Witwatersrand, Johannesburg, South Africa.

Corresponding author: Fabio Alfieri, email: fabio.alfieri@unibe.ch and fabio_alfieri@yahoo.it

Supplementary material

Additional methods

Extraction of the topological indices of complexity

For each trabecular skeleton imported in R, we extracted the following datasets:

- Node Density ('skelDensity' function, 'indianaBones R package, Veneziano et al. 2021), unit: nodes per mm^3, termed NodDen, is returned as a 3D distribution of values corresponding to the trabecular volume. From this matrix, we computed average ($NodDen_{Aver}$) and median ($NodDen_{Med}$) values.
- Trabecular Length ('skelLength', function, 'indianaBones R package), unitless, termed TrabLen, is returned as a 3D distribution of values corresponding to the trabecular volume. From this matrix, we computed average values ($TrabLen_{Aver}$)
- Trabecular Tortuosity ('skelTortuosity' function, 'indianaBones R package), unitless, termed TrabTort, is returned as a 3D distribution of values corresponding to the trabecular volume. From this matrix, we computed average ($TrabTort_{Aver}$) and median values ($TrabTort_{Med}$)
- Fractal Dimension, unitless, termed FD, is represented by a value corresponding to the 'estdim' item, deriving from the 'est.boxcount' function ('Rdimtools' package, You and Shung 2022)

Additional results

		Ateles paniscus	*Cercopithecus mitis*	*Colobus guereza*	*Homo sapiens*
DA	**Mean**	0,41	0,2355	0,3855	0,523
	SD	0,066468037	0,053033009	0,147785317	0,057266919
	CV	0,162117164	0,225193242	0,383360097	0,109496977
Tb.Th	**Mean**	0,2335	0,2465	0,2615	0,2446
	SD	0,028991378	0,055861436	0,055861436	0,034092521
	CV	0,124160077	0,2266184	0,213619257	0,139380708
BV/TV	**Mean**	0,303670043	0,404825635	0,409740277	0,29728171
	SD	0,020845874	0,026904958	0,043890686	0,074895289
	CV	0,068646463	0,066460608	0,107118311	0,251933726
BS/TV	**Mean**	3,535940993	4,498408087	4,097106185	2,241101202
	SD	0,18733188	0,434174239	0,360551972	0,677985798
	CV	0,052979357	0,096517308	0,088001618	0,302523508
$NodDen_{Aver}$	**Mean**	0,002162819	0,016509235	0,003174778	0,000202589
	SD	0,000466742	0,004277054	0,000587006	3,36301E-05
	CV	0,215802522	0,259070398	0,184896763	0,166001208
$NodDen_{Med}$	**Mean**	0,002133644	0,015902645	0,00313306	0,000195014
	SD	0,000446296	0,004086497	0,000587984	3,6981E-05
	CV	0,209170849	0,256969635	0,187670747	0,189632788
$TrabLen_{Aver}$	**Mean**	0,343610972	0,328193961	0,320826513	0,403325357
	SD	0,014019287	0,045619767	0,027345511	0,017005238
	CV	0,040799883	0,139002457	0,085234573	0,042162581
$TrabTort_{Aver}$	**Mean**	1,100034231	1,111598961	1,11645701	1,081448361
	SD	0,016340938	0,013202172	0,02367794	0,004719293
	CV	0,014854936	0,01187674	0,021208107	0,004363864
$TrabTort_{Med}$	**Mean**	1,053929561	1,056767123	1,060701548	1,048028197
	SD	0,006011882	0,004482764	0,008282433	0,001784651
	CV	0,005704254	0,00424196	0,007808448	0,001702866
FD	**Mean**	2,284168728	2,166133666	2,334246513	2,540686634
	SD	0,08112744	0,033079592	0,069801618	0,024839923
	CV	0,035517271	0,015271261	0,029903276	0,009776854

Table S2. For the four species with sample size >1 (i.e. *Ateles paniscus*, *Cercopithecus mitis*, *Colobus guereza* and *Homo sapiens*) for each trabecular variable we computed mean, standard deviation (SD) and coefficient of variation (CV=SD/Mean).

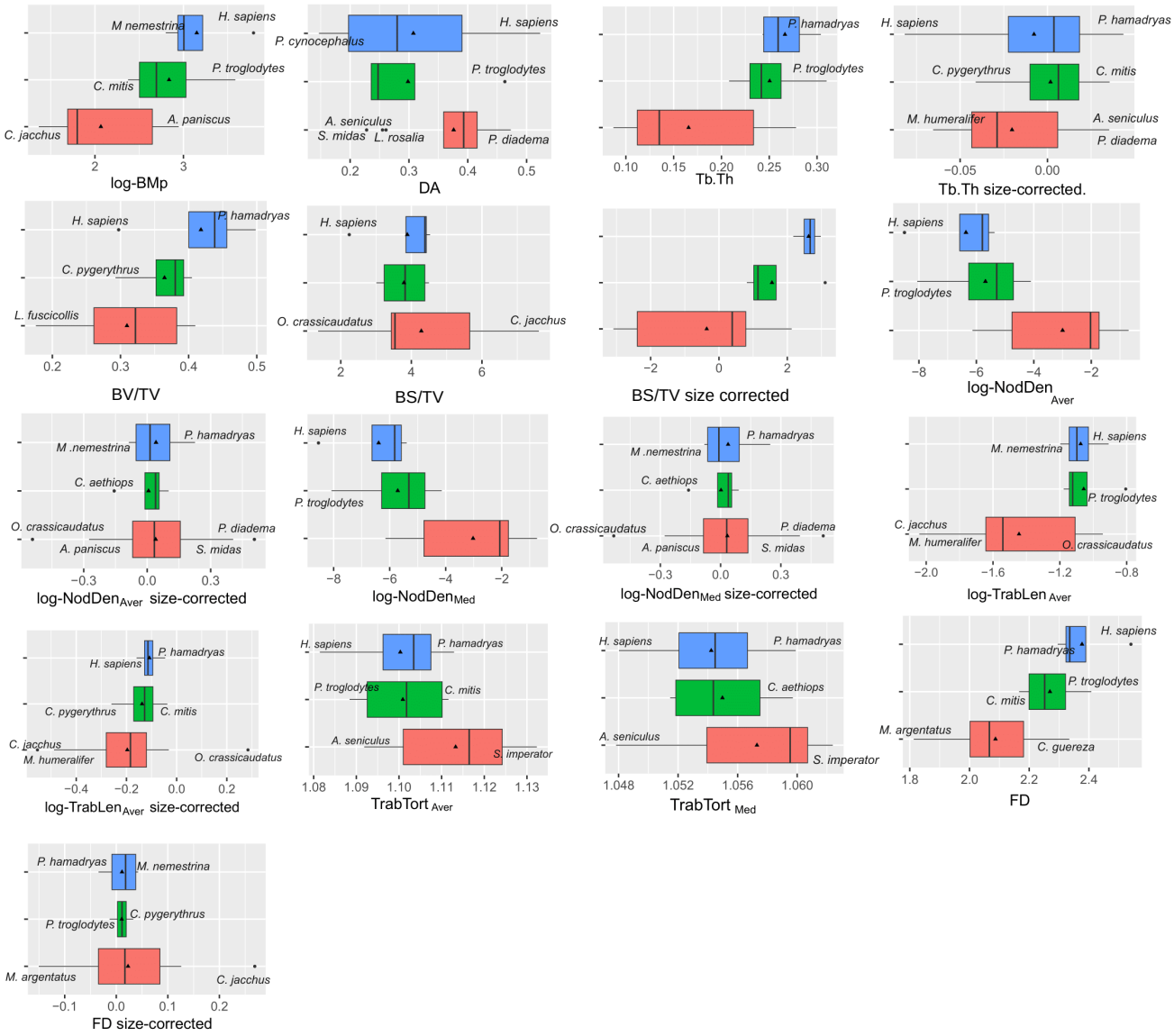

Fig. S1. Boxplots showing, for the primate species here studied, the variation of body mass (accounted for through the proxy log-BMp) and distal fibula trabecular traits, in relation to locomotion, i.e. degree of arboreality (terrestrial in blue, semi-arboreal in green, arboreal in red). For trabecular variables that are significantly correlated with log-BMp (see Table 3), additional boxplots with size-corrected values were generated (see details in the main text). In all the boxplots, species yielding outlying and extreme values are labelled.

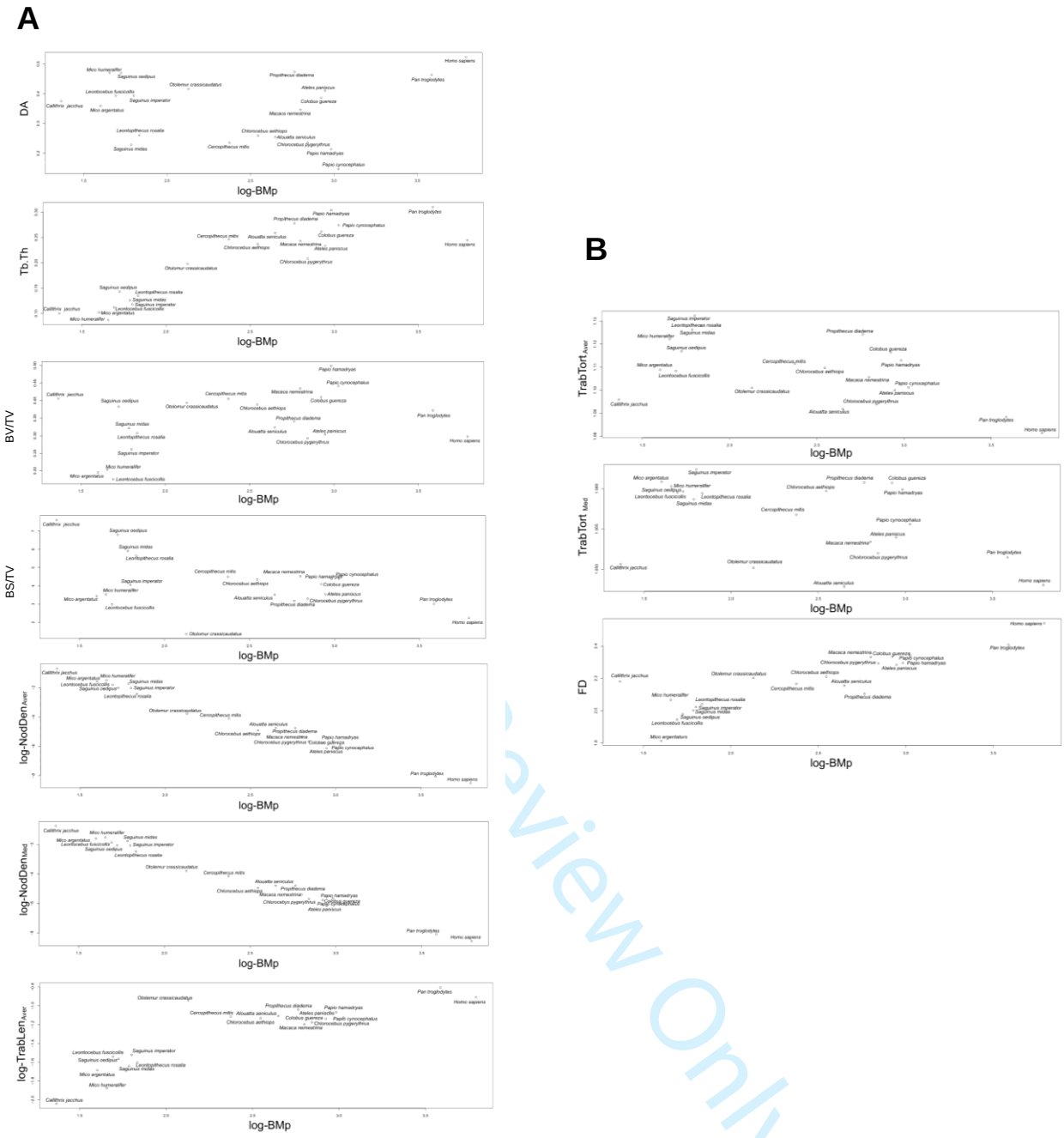

Fig. S2A, B. Through bivariate scatterplots 'variable *vs.* log-BMp' (i.e. the body mass proxy here employed) it is shown how, for each distal fibula trabecular trait, the values yielded by the analyzed primate species relate to body mass.

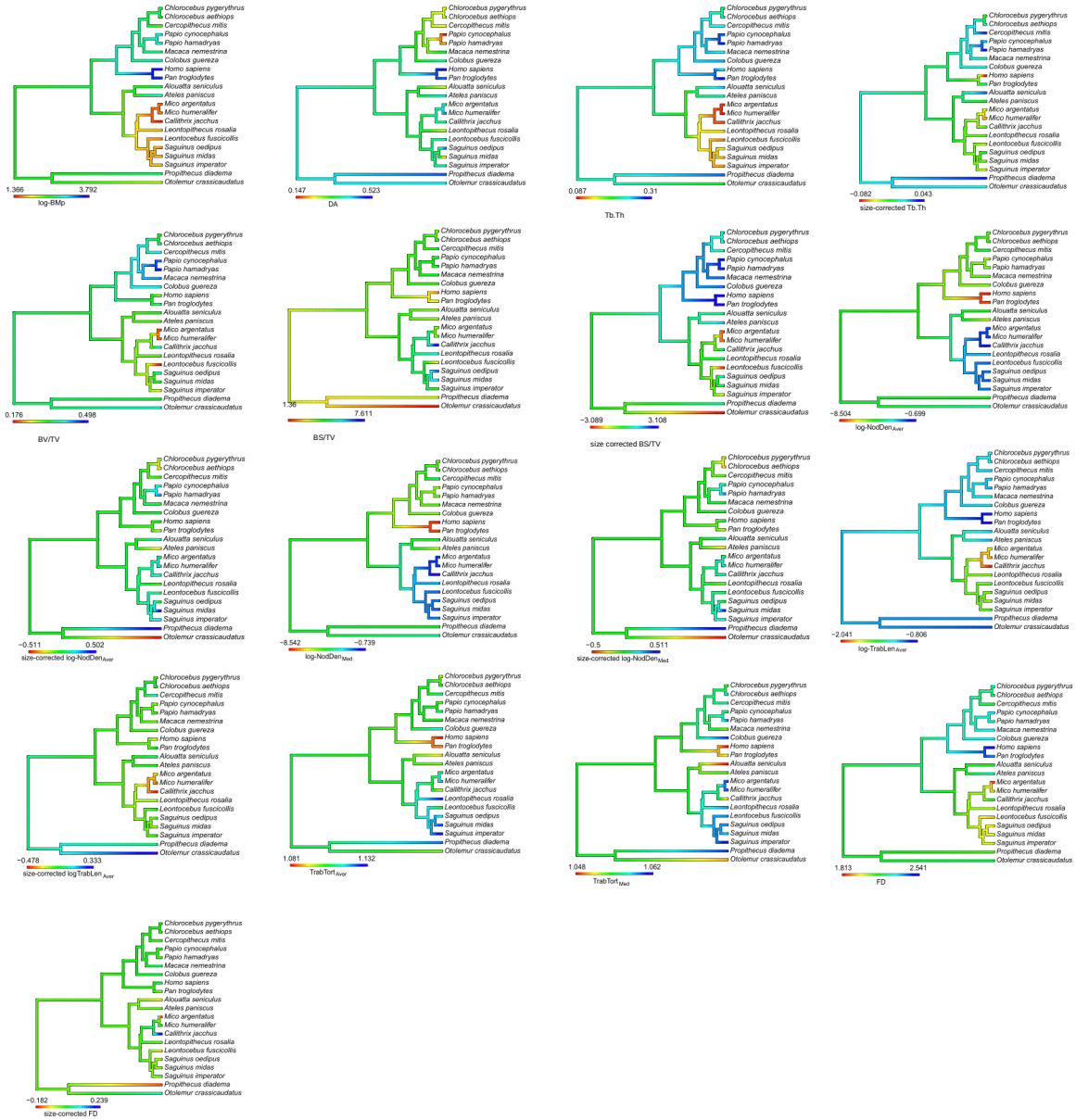

Fig. S3. The phylogenetic signal present in the distribution of body mass (i.e. log-BMp) and distal fibula trabecular traits' values, is visualized mapping primate species values on the time-calibrated phylogeny used in this work (see details in the main text).

	Standard deviation	Proportion of Variance	Cumulative Proportion
PC1	2.254744	0.50839	0.50839
PC2	1.355543	0.18375	0.69214
PC3	1.295712	0.16789	0.86002
PC4	0.863086	0.07449	0.93452
PC5	0.458556	0.02103	0.95554
PC6	0.4487	0.02013	0.97568
PC7	0.387401	0.01501	0.99068
PC8	0.256222	0.00656	0.99725
PC9	0.165674	0.00274	0.99999
PC10	0.00801	0.00001	1

Table S3. Summary statistics of the PCs generated through PCA on the trabecular variables. The first 4 PCs, explaining more than 90% of the total variance, i.e. 93%, were used to run a multivariate generalized least square regression against degree of arboreality, with logBMproxy as a covariate, to estimate locomotor, body mass and phylogenetic effects on primate distal fibula trabecular structure, analyzed multivariately.

	Standard deviation	Proportion of Variance	Cumulative Proportion
PC1	1.832475	0.3358	0.3358
PC2	1.65416	0.27362	0.60942
PC3	1.252008	0.15675	0.76617
PC4	0.910586	0.08292	0.84909
PC5	0.87788	0.07707	0.92616
PC6	0.697867	0.0487	0.97486
PC7	0.329092	0.01083	0.98569
PC8	0.302833	0.00917	0.99486
PC9	0.226327	0.00512	0.99998
PC10	0.013265	0.00002	1

Table S4. Summary statistics of the PCs generated through PCA on the trabecular variables which were preliminarily size-corrected (see details in the main text) only if they resulted to be significantly related to logBMproxy through univariate PGLS regressions (Table 3). The first 4 PCs, cumulatively explaining the 85% of the total variance, were used to build bivariate phylo-morphospaces, allowing to visualize potential locomotor effects without the major influence of body mass.

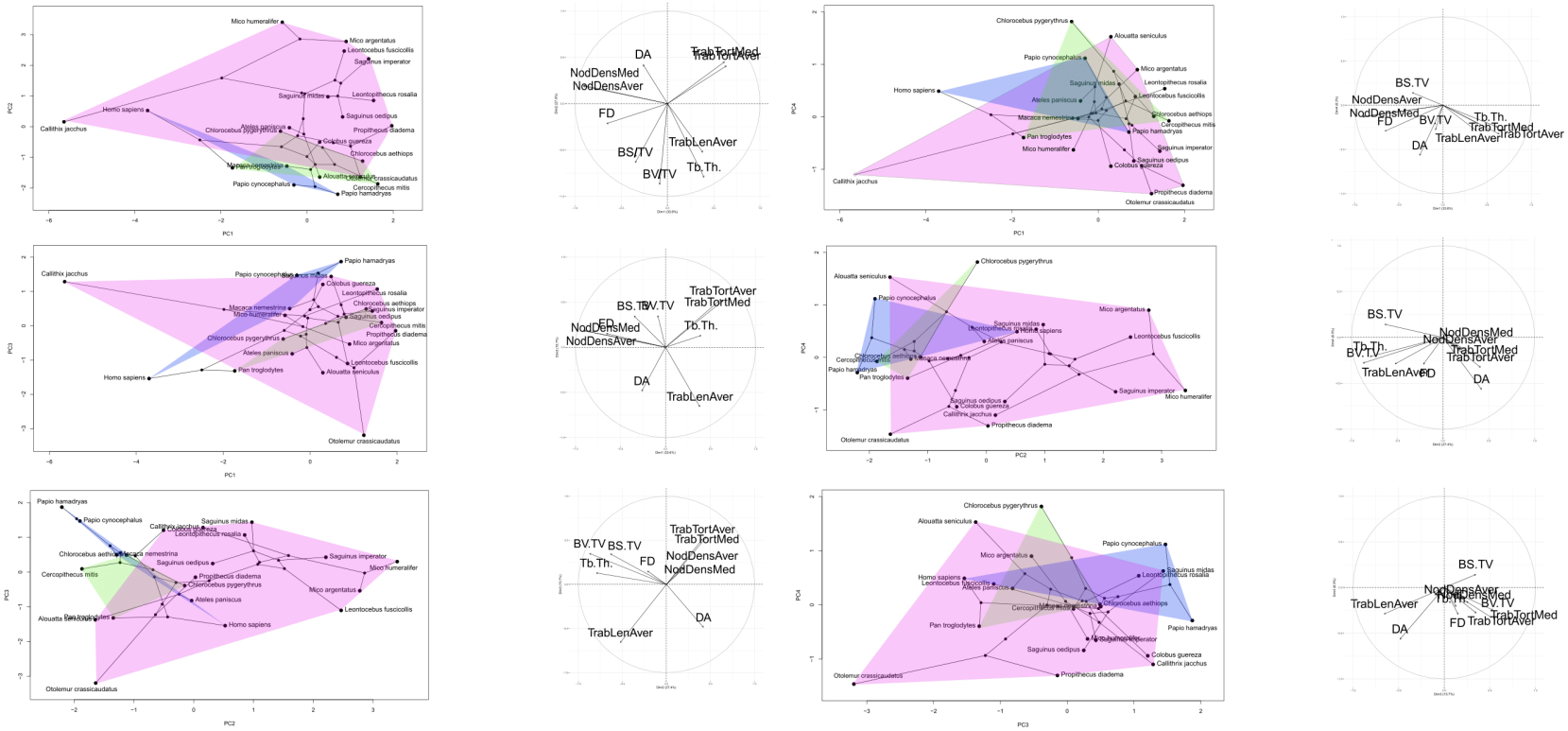

Fig. S4. Multivariate patterns of variation in distal fibular trabecular architecture. The left plots (in each of the six quadrants) represent phylomorphospaces built with PC1-PC2 (upper left quadrant), PC1-PC3 (middle left quadrant), PC2-PC3 (bottom left quadrant), PC1-PC4 (upper right quadrant), PC2-PC4 (middle right quadrant) and PC3-PC4 (bottom right quadrant) resulting from a PCA on all the studied trabecular traits (using size-corrected values in case of variables significantly related to body mass, as detailed in Table 3). The right plots (in each of the six quadrants) represent the variable loading plots summarizing how single traits contribute to species distribution on the corresponding morphospaces. Degree of arboreality categories are shown with colors: arboreal in purple, semi-arboreal in green, terrestrial in blue. Abbreviations for variables in the loading plots: DA (degree of anisotropy), BV/TV (bone volume fraction), BS/TV (bone surface density), Tb.Th (trabecular thickness), $NodDen_{Aver}$ (average node density), $NodDen_{Med}$ (median node density), $TrabLen_{Aver}$ (average trabecular length), $TrabTort_{Aver}$ (average trabecular tortuosity), $TrabTort_{Med}$ (median trabecular tortuosity), FD (fractal dimension).

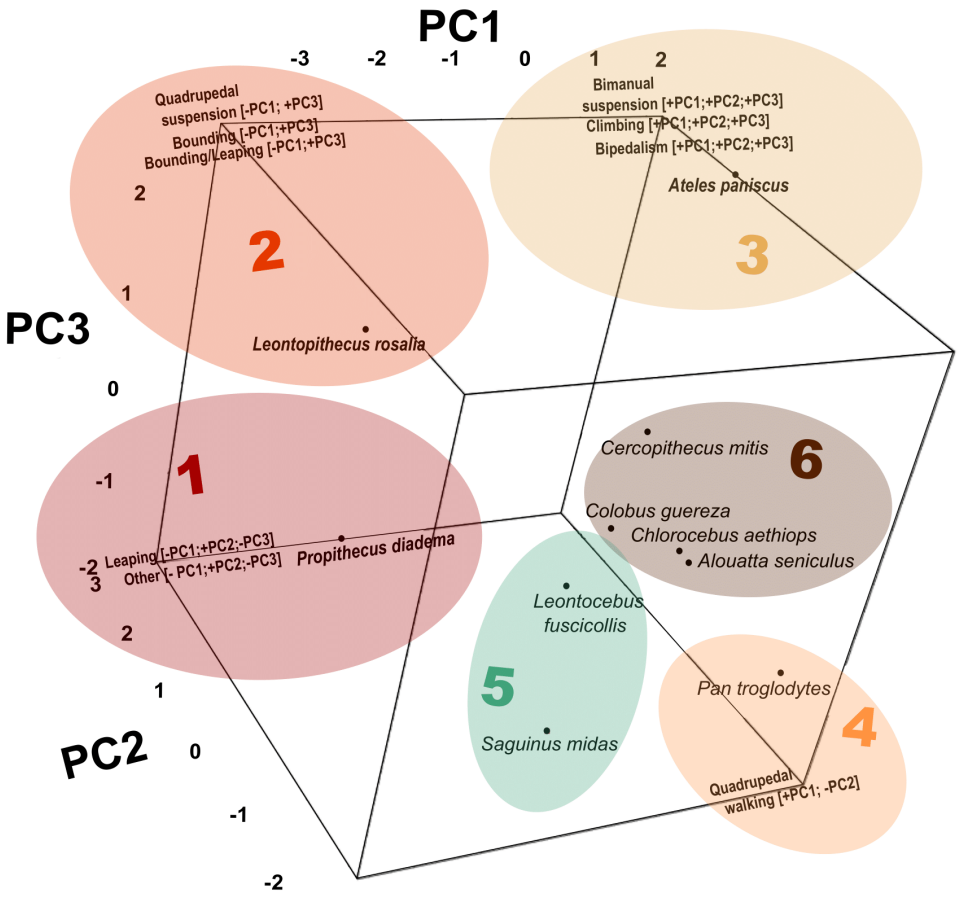

Fig. S5. 3D plot built with PCs deriving from a PCA run on locomotor behavioral data collected from Granatosky (2018), processed and transformed as detailed in the main text. We visually identified six regions corresponding to preponderant locomotor behaviors, region 1: dominant leaping, region 2: dominant quadrupedal suspension/bounding, region 3: dominant bimanual suspension/climbing, region 4: dominant quadrupedal walking, region 5: unspecialized category with less quadrupedal walking; region 6; unspecialized category with higher frequency of quadrupedal walking.

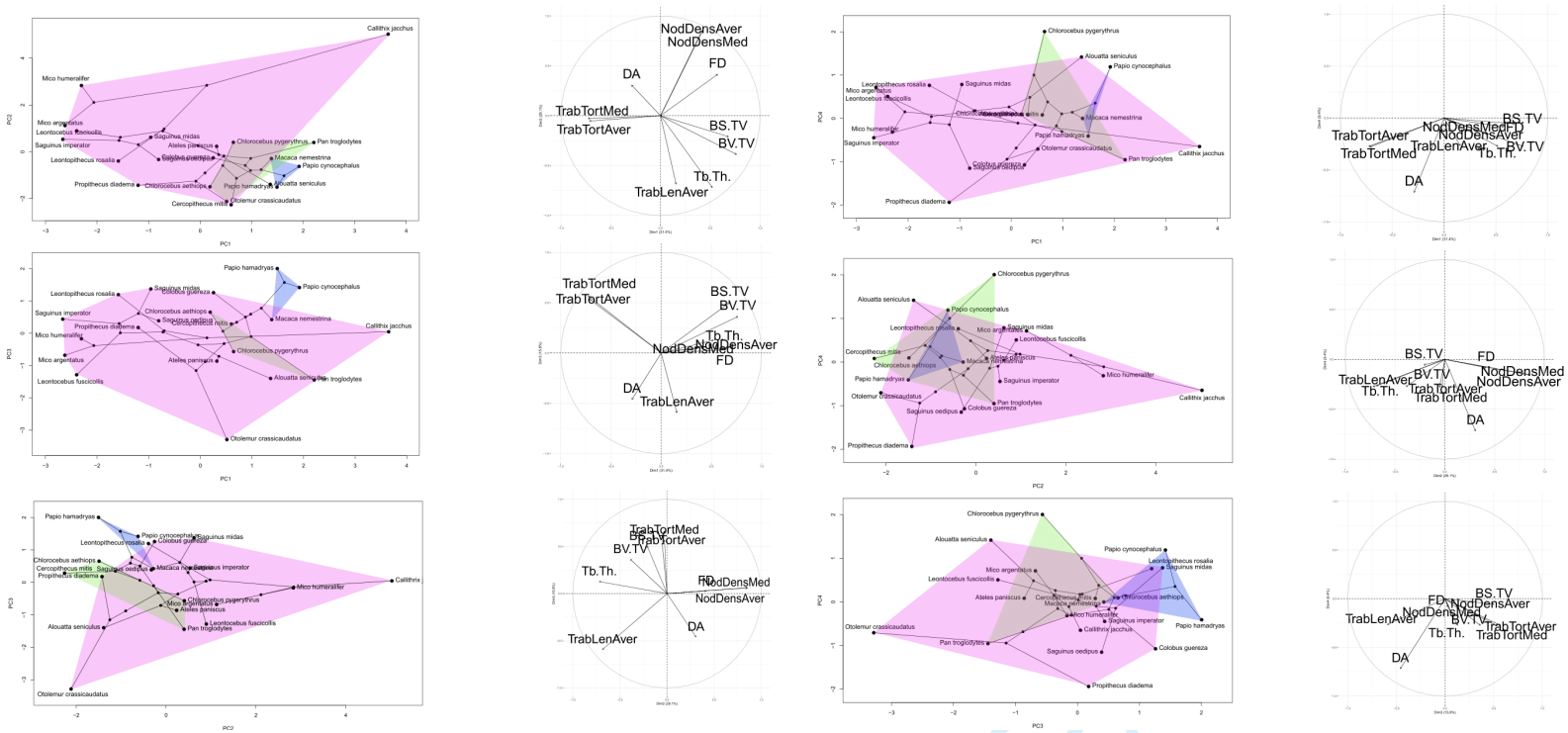

Fig. S6. Multivariate patterns of variation in distal fibular trabecular architecture after the exclusion of *H. sapiens*. The left plots (in each of the six quadrants) represent phylomorphospaces built with PC1-PC2 (upper left quadrant), PC1-PC3 (middle left quadrant), PC2-PC3 (bottom left quadrant), PC1-PC4 (upper right quadrant), PC2-PC4 (middle right quadrant) and PC3-PC4 (bottom right quadrant) resulting from a PCA on all the studied trabecular traits (using size-corrected values in case of variables significantly related to body mass, as detailed in Table 3). The right plots (in each of the six quadrants) represent the variable loading plots summarizing how single traits contribute to species distribution on the corresponding morphospaces. Degree of arboreality categories are shown with colors: arboreal in purple, semi-arboreal in green, terrestrial in blue. Abbreviations for variables in the loading plots: DA (degree of anisotropy), BV/TV (bone volume fraction), BS/TV (bone surface density), Tb.Th (trabecular thickness), $NodDen_{Aver}$ (average node density), $NodDen_{Med}$ (median node density), $TrabLen_{Aver}$ (average trabecular length), $TrabTort_{Aver}$ (average trabecular tortuosity), $TrabTort_{Med}$ (median trabecular tortuosity), FD (fractal dimension).

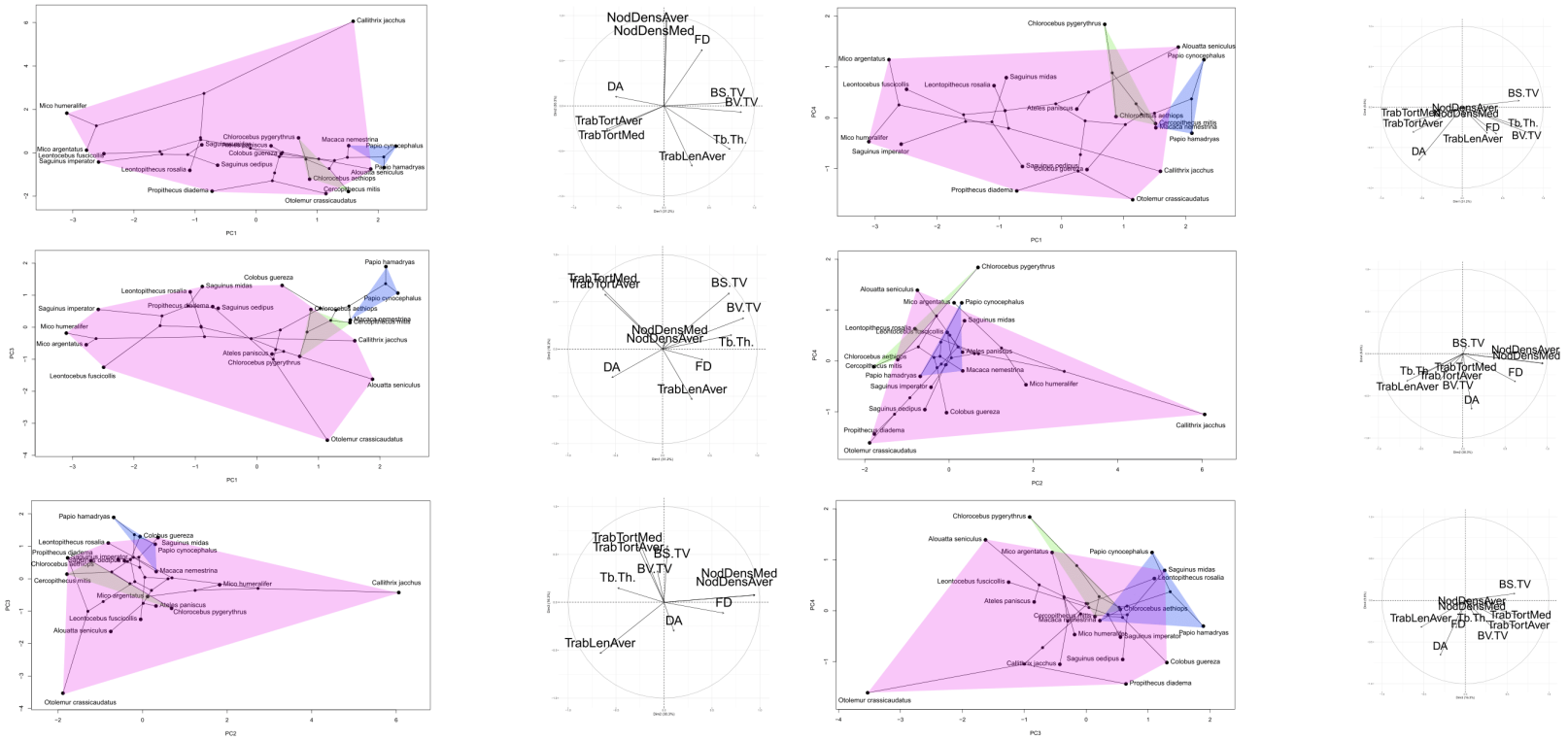

Fig. S7. Multivariate patterns of variation in distal fibular trabecular architecture after the exclusion of *H. sapiens* and *P. troglodytes*. The left plots (in each of the six quadrants) represent phylomorphospaces built with PC1-PC2 (upper left quadrant), PC1-PC3 (middle left quadrant), PC2-PC3 (bottom left quadrant), PC1-PC4 (upper right quadrant), PC2-PC4 (middle right quadrant) and PC3-PC4 (bottom right quadrant) resulting from a PCA on all the studied trabecular traits (using size-corrected values in case of variables significantly related to body mass, as detailed in Table 3). The right plots (in each of the six quadrants) represent the variable loading plots summarizing how single traits contribute to species distribution on the corresponding morphospaces. Degree of arboreality categories are shown with colors: arboreal in purple, semi-arboreal in green, terrestrial in blue. Abbreviations for variables in the loading plots: DA (degree of anisotropy), BV/TV (bone volume fraction), BS/TV (bone surface density), Tb.Th (trabecular thickness), $NodDen_{Aver}$ (average node density), $NodDen_{Med}$ (median node density), $TrabLen_{Aver}$ (average trabecular length), $TrabTort_{Aver}$ (average trabecular tortuosity), $TrabTort_{Med}$ (median trabecular tortuosity), FD (fractal dimension).

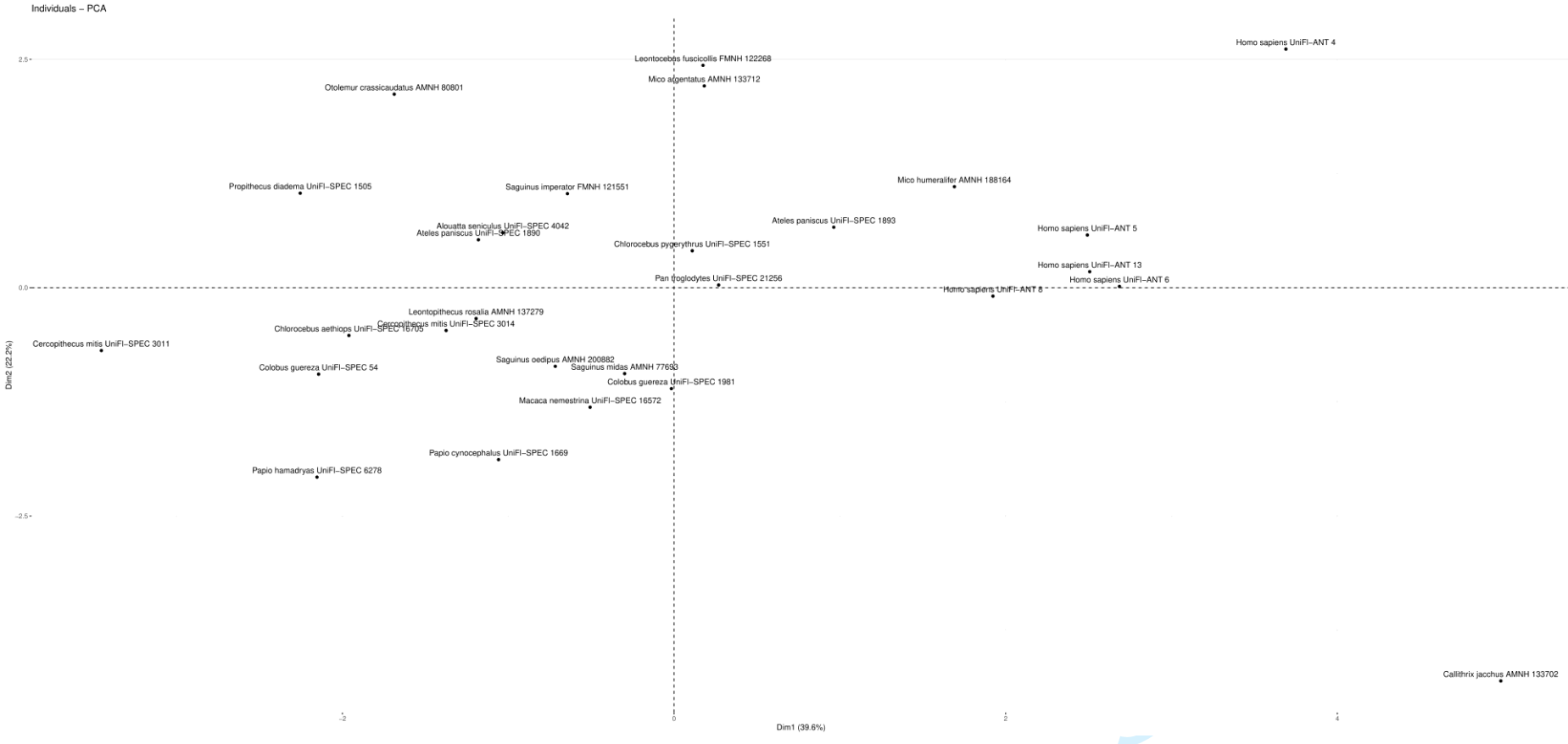

Fig. S8. Bivariate scatterplot built with the first two PCs deriving from a PCA having as observations distal fibula trabecular data for the single specimens, instead of averaged values for taxa.

Supplementary Note 1

For a subset of the studied taxa (n=10, 7 of which were classified as 'arboreal' in this work) we collected quantitative data on locomotor behaviors from Granatosky (2018) (data for the remaining taxa of our sample are not present in Granatosky 2018). The collected data, provided as percentages in the original work, were transformed through an arcsine square root transformation (common procedure in the analysis of proportional ecological data, in order to minimize variance and normalize the distribution, Monclús-Gonzalo et al., 2023; Sokal and Rohlf, 1995). Then, data from multiple observations for the same species were averaged, obtaining a single value for each behavior for each taxon, and a PCA was run, building a PC1-PC3 (cumulatively explaining 64.2% of the total variance) 3D scatterplot based on behavioral data, i.e. an 'ethospace' (Fig. S5). This plot confirmed that *A. paniscus* and *P. diadema* occupy extreme positions in the explored range of locomotor diversity, corresponding to regions related to predominant leaping (for *P. diadema*, region 1 in Fig. S5) and bimanual suspension/climbing (for *A. paniscus*, region 3 in Fig. S5). Other potential clusters may be represented by: species with predominant quadrupedal suspension/bounding (the taxon closer to this condition is *L. rosalia*, region 2 in Fig. S5), species with predominant quadrupedal walking as *P. troglodytes* (region 4 in Fig. S5) and two potential clusters of quite unspecialized species with arboreal habits (one of which shows less quadrupedal walking, including *L. fuscicollis* and *S. midas* and shown with region 5 in Fig. S5, compared to the other, including e.g. *A. seniculus* or *C. guereza*, and shown with region 6 in Fig. S5). A straightforward assessment of potential relationships between these differences and major trabecular features of primate distal fibula is checking if taxa with more derived and discrepant locomotor behaviors (e.g. leapers, bimanual suspensory) occupy distinct and peripheral regions of the morphospace, contrasting taxa with more similar behaviors instead expected to occupy the central regions of the scatterplot (following e.g. Ryan and Shaw, 2012). Exploring the morphological variability found in this work, it is clear that no patterns related to the frequency of specific locomotor behaviors arose. For instance, *P. diadema* and the other strepsirrhine leaper *O. crassicaudatus*, are close each other in some plots but also close to taxa with quite distinct locomotor

behaviors (e.g. unspecialized *C. mitis* and *A. seniculus* or the prevalently terrestrial quadrupedal *P. hamadryas* in PC1-PC2 plot, Fig. 5), or they occupy different areas of the morphospaces (e.g. PC2-PC3 plot, Fig. 5). Also, *A. paniscus*, expected to occupy another peripheral position of the morphospace due to hindlimb lower activities deriving from its prevalent bimanual suspensory habits, is instead often occupying central regions of the plot, e.g. often close to *C. pygerythrus* (PC1-PC2, PC2-PC3 and PC1-PC3 plots, Fig. 5) that, in turn, is a relatively unspecialized taxon (since it largely mirrors its sister taxon *C. aethiops*, Fleagle, 2013) (Fig. S5).

Supplementary Note 2

The exclusion of *H. sapiens* causes the morphospace area occupied by the remaining terrestrial taxa (*Papio* spp., + *M. nemestrina*) to be smaller. It, in turn causes terrestrial taxa to be discriminated from all the other primates with minor overlap (in PC1-PC2 and PC1-PC3 plots, Fig. S6). However, it should be noted that this condition may be related to phylogeny, since the exclusion of *H. sapiens* causes the terrestrial taxa to be represented by a clade in the phylogeny (Fig. 1) with the impossibility to disentangle locomotor and phylogenetic effects. In both PC1-PC2 and PC1-PC3 plots, terrestrial taxa tend to be discriminated from other primates for high BV/TV and BS/TV (and also high Tb.Th only in the PC1-PC2 plot) (Fig. S6). Since these patterns go against our expectations (Table 2 and main text), the presence of a phylogenetic effect seems more likely. The same occurs to semi-arboreal taxa after the exclusion of *P. troglodytes* (besides *H. sapiens*, Fig. S7), since the remaining taxa in the category form the clade (*Chlorocebus* spp. + *C. mitis*) (Fig. 1). Although it is here impossible to disentangle locomotor from phylogenetic effects, it is interesting that a gradient from terrestrial taxa (higher PC1 and PC3 scores) to arboreal taxa (lower PC1 and PC3 scores) is yielded by this new PCA. However, it is again driven by high BV/TV and BS/TV in terrestrial taxa (hence, contrasting biomechanical expectations). Strikingly, terrestrial taxa are set apart also for their lower DA values, which clearly contrasts the biomechanical properties associated with this parameter (expected to be higher in terrestrial environments, where loadings are more directionally stereotyped, e.g. Alfieri et al., 2022; Amson et al., 2017) (Fig. S7). The exclusion of *H. sapiens* and *P. troglodytes* does not affect the overall

apparent absence of relationships between the frequency of different locomotor behaviors and distal fibula trabecular structure (see above and main text). Indeed, a taxon with derived behavior such as *A. paniscus* (Fig. S5) occupies non-peripheral positions of the morphospace, often close to unspecialized taxa as *C. guereza* and/or *C. pygerythrus* (PC1-PC2, PC1-PC3, PC2-PC3 in both Fig. S6 and Fig. S7). Likewise, *P. diadema*, a specialized leaper (Fig. S5), frequently clusters close to unspecialized taxa (e.g. *C. aethiops* in PC1-PC2, PC1-PC3 plot, Fig. S6; and in PC2-PC3 plot, Fig. S7) or far from another leaper as *O. crassicaudatus* that, in turn, clusters close to unspecialized taxa (e.g. *C. aethiops* and *C. mitis* in PC1-PC2 plot, Fig. S7). We recognize that future works may address potential relationships between distal fibula trabecular structure and finer locomotor categorizations (as those arising from Fig. S5) building proper samples and running inferential statistical tests with larger sample sizes. Nevertheless, we interpret the trends discussed above as indicative of the fact that distal fibula trabecular bone may be associated neither with DOA, as defined in this work, nor with other locomotor aspects as leaping or lower hindlimb reliance in suspensory species. The only potential exception arising from this work is represented by the possible effect related to hominin bipedalism (see discussion above).

Supplementary Note 3

Not accounting for intraspecific variability is a common problem in phylogenetically informed analyses (see Garamszegi, 2014 for a discussion of potential solutions). Indeed, the introduction of phylogenetic data in comparative analyses (started with the work of Felsenstein, 1985) had several implications for zoological/anthropological comparative studies, including the fact that statistical observations are now represented by taxa, instead of specimens/individuals. It is a requirement of many statistical toolkits (e.g. those provided by the R packages mentioned in the Materials and Methods, in the main text) needed to apply phylogenetic comparative methods. Including multiple specimens for a single species (as we did for four taxa, Table 1), may represent a partial solution but, noticeably, even in this case before performing statistical analyses as PGLS or phylogenetic ANOVA, data for all the specimens belonging to a single species should be averaged and minimized to a single value per trait per taxon. Keeping in mind this limitation, it should also be noticed that one of the main problems

deriving from not taking intraspecific variability into account is the underestimation of potential overlap among species that, in turn, may inflate interspecific differences, e.g. causing significant *p*-values in phylogenetic ANOVAs, resulting in false-positives. Since we did not find confirmation for most of the expected differences related to locomotor aspects, we assume that accounting for intraspecific variability would have not changed the main result of this work, i.e. distal fibula trabecular structure does not relate to DOA. To observe the intraspecific variability for the four taxa for which we sampled more than one individual (*A. paniscus*, *C. mitis*, *C. guereza* and *H. sapiens*), we built a bivariate scatterplot with PC1-PC2 from a PCA having the observations represented by single specimens, instead of taxa (Fig. S8). Moreover, for these four taxa we summarized standard deviation (SD) and coefficient of variation (CV=SD/mean) for each trait (Table S2). On the morphospace, *C. mitis*, *C. guereza* and *A. paniscus* show a low to moderate intraspecific variability, since the specimens belonging to the same species show very similar PC2 scores while the variation along PC1 is wider. Specifically, the specimens belonging to *C. mitis* and *C. guereza* fall in the same quadrant, while the specimens belonging to *A. paniscus* fall in two different quadrants due to the PC1 scores variability. A low variability is shown by *H. sapiens*, since four out of five specimens lie in the same restricted region of the morphospace, with a single specimen instead likely representing an outlier (Fig. S8). The traits for the four species show an average CV of 0.119.

References:

Alfieri, F., Botton-Divet, L., Nyakatura, J.A., Amson, E., 2022. Integrative approach uncovers new patterns of ecomorphological convergence in slow arboreal xenarthrans. J Mamm Evol. 29(2), 283-312 https://doi.org/10.1007/s10914-021-09590-5

Amson, E., Arnold, P., van Heteren, A.H., Canoville, A., Nyakatura, J.A., 2017. Trabecular architecture in the forelimb epiphyses of extant xenarthrans (Mammalia). Front Zool 14, 52. https://doi.org/10.1186/s12983-017-0241-x

Felsenstein, J., 1985. Phylogenies and the comparative method. Am. Nat. 125(1), 1–15. https://doi.org/https ://doi.org/10.1086/284325

Garamszegi, L.Z., 2014. Uncertainties Due to Within-Species Variation in Comparative Studies: Measurement Errors and Statistical Weights, in: Modern Phylogenetic Comparative Methods and Their Application in Evolutionary Biology: Concepts and Practice. Garamszegi L.Z. (ed), Springer, pp. 157–199.

Granatosky, M. C. 2018. A review of locomotor diversity in mammals with analyses exploring the influence of substrate use, body mass and intermembral index in primates. J. Zool 306:207–216.

Monclús-Gonzalo, O., Alba, D.M., Duhamel, A., Fabre, A.C., Marigó, J., 2023. Early euprimates already had a diverse locomotor repertoire: Evidence from ankle bone morphology. J Hum Evol 181, 103395.

Ryan, T.M., Shaw, C.N., 2012. Unique suites of trabecular bone features characterize locomotor behavior in human and non-human anthropoid primates. PLoS ONE 7, e41037. https://doi.org/10.1371/journal.pone.0041037

Sokal, R., Rohlf, F., 1995. Biometry: The Principles and Practice of Statistics in Biological Research 3rd ed., Freeman, New York. ed.

Veneziano, A., M. Cazenave, F. Alfieri, D. Panetta, and D. Marchi. 2021. Novel strategies for the characterization of cancellous bone morphology: Virtual isolation and analysis. Am J Phys Anthropol 175(4), 920-930 https://doi.org/10.1002/ajpa.24272

You, K., and D. Shung. 2022. Rdimtools: An R package for dimension reduction and intrinsic dimension estimation. Software Impacts 14(1):100414.

Referee: 1

Comments to the Author

I have no additional comments on the manuscript. As in my previous review, I do still think many of measures of trabecular structure likely reflect genetic and developmental processes, and not mechanical loading. However, the authors have provided extensive explanation of why they think these variables are indicators of the mechanical environment.

Referee: 2

Comments to the Author

Thank you for thoughtfully considering reviewer comments and suggestions again. I acknowledge and appreciate your responses.

The revisions incorporated in this version of the manuscript are more effective in conveying the authors' due diligence for contextualizing their work in relevant literature. Specifically, important assumptions have been made clearer for the readers in how the authors justify the theoretical loading model (L390-419) and the interpretive value of the topological variables (L196-289). I look forward to future work by the authors as they continue to evaluate more morphological results in this line of investigation. I also encourage the authors to continue evaluating the underlying assumptions of the loading model too. There has been substantial relevant experimental work published since the formulation of the loading model by Marchi (2007), and it is helpful for readers that the current manuscript begins to acknowledge the complexity that exists in how bones of the primate leg are presumably loaded (L416-419).

We thank both the Referees for the positive feedbacks and the precious suggestions provided during the entire peer-review process. This manuscript is greatly improved thanks to them

Regarding the presentation of new results in the Discussion section (e.g., the "supplementary analysis" beginning on L998; and also L1106-1123), it could be worth considering the supplementary information section for these results rather than moving them to the Results section. This would not impact how the current version of the Results section is organized, and it would still permit discussing the implications of these results in the Discussion section. It could also shorten the length of the main text.

The long discussion section in Potential limitations, concerning additional supplementary analyses was largely moved to Supplementary Information (creating three Supplementary Notes, one for each of the issues discussed there), following the Referee's suggestion. In the Discussion, we just let a short section (divided in three small paragraphs, L. 1016-1047), summarizing the three issues and summarizing the main finding derived from the supplementary analyses

Figure 4 caption: Please correct typos in panel labels (e.g., "B" appears twice, and "D" is omitted).

We thank the Referee for noticing it, we edited accordingly.

The manuscript is clearly written, but it would still benefit from proof-reading for language. I have not noted all instances of awkward phrasing. Examples of typos and grammatical issues include:

We thank the Referee for suggesting some changes to fix grammatical issues. The edits suggested below were performted accordingly. This, together with the precious full language edit provided by the Editor should improve the language of the entire MS.

L840: For grammatical reasons, change to "Furthermore, it is clear that there is a residual …"

L960: feature

L1023: For grammatical reasons, change to “what was found”